Modeling of a compliant force distribution mechanism

For a deforming hydrostatic bearing

by

N.J. van Willigen

as fulfillment of the requirement to obtain the degree of

Master of Science
in Mechanical Engineering

at the Delft University of Technology,
to be defended publicly on Thursday September 26, 2019 at 14:00.

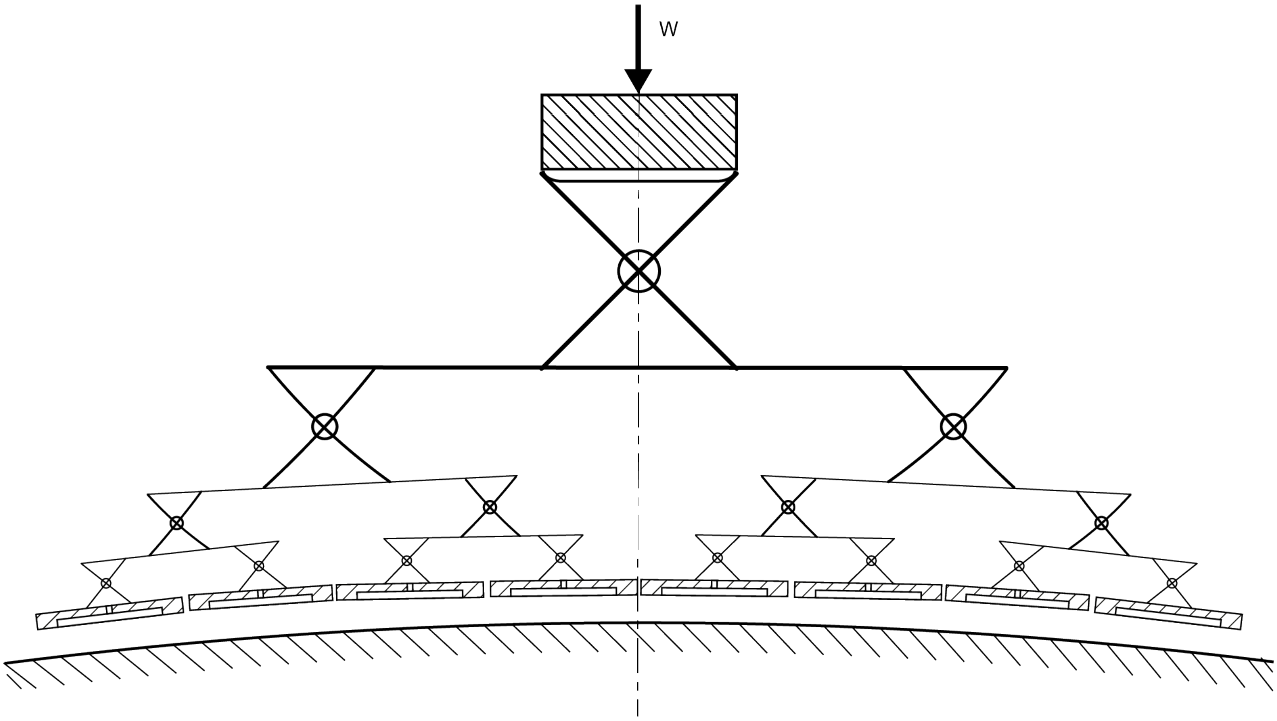

Student number:	4112067	
Project duration:	November 15, 2017 – September 26, 2019	
Thesis committee:	Dr. ir. R.A.J. Ostayen,	supervisor
	Ir. J.P.A. Nijssen,	daily supervisor
	Prof. Dr. Ir. J.L. Herder	committee
	Dr. Ir. M. Langelaar	committee

List of Definitions

Term	**Definition**
Axial loading	Loading perpendicular to the bearing surface
Axial stiffness	Resistance to axial displacement, of either deformation or loss in flight height, due to axial forces
Bearing load capacity	Maximum load a hydrostatic bearing can carry while maintaining a given film thickness.
Bearing land	Bearing material which would make physical contact with the guiding surface if there would be no hydrostatic film
Bearing recess	Enclosure in bearing land much larger than fluid film thickness such that fluid pressure can equally distribute in the recess
Bearing tilt	Change of the in-plane angle with respect to the guiding surface
Deformation factor	Axial deformation a single slipper can endure without losing full film lubrication or risking mechanical failure
Film stiffness	Describes the relationship between fluid pressure and film thickness
Flight Height	Distance between bearing surfaces, as separated by hydraulic fluid
Full film lubrication	The lubrication film fully separates two solid surfaces such that there is no mechanical contact possible between them. Therefore friction levels are reduced to a point dominated by lubricant viscosity
Guiding surface	Surface opposing the bearing surface
Guiding surface curvature	The inverse of the radius of a circle that would be tangent to a point on a smooth wavy guiding surface profile
Hydrostatic tilt-stiffness	Relationship between tilt of a hydrostatic bearing slipper and applied moment
Hydrostatic bearing slipper	Single bearing element with a individual fluid supply
Hydraulic fluid	Fluid used for lubrication and separation of bearing surfaces
Large deformation	Deformation which is larger than 10% of the element's length
In-Plane	Plane tangent to bearing surfaces
Nominal film thickness	Expected average film thickness for a given load capacity
Out-of-Plane	Plane perpendicular to bearing surfaces
Relative waviness amplitude	Amplitude of sinusoidal wave describing the guiding surface scaled such that the amplitude has no dimension and is a fraction of wavelength
Rotational stiffness	Resistance to change of flexure angle in response to a moment, in this report used for mechanical stiffness of the structure
Supply Pressure	Pressure provided to the hydrostatic bearing by an external pump
Tilt stiffness	Resistance to change of slipper angle in response to a moment, in this report used for stiffness due to hydraulic pressure
Waviness	Smooth periodic changes in height of the guiding surface surface
Waviness Amplitude	Maximum periodic axial distance of the guiding surface as measured from the average height
Waviness Profile	Sine wave or other periodic function used to describe the waviness
Whiffletree	A force distribution mechanism using pivots and linkages

List of Symbols

Parameter	Definition	Unit
A	Bearing surface area	m
A	Guiding surface waviness amplitude	m
A_o	Orifice area	m^2
$\bar{A}$	Bearing shape factor	-
b	Bearing width (out-of-plane length)	m
$\bar{B}$	Bearing flow factor	-
C_o	Orifice discharge coefficient	-
d	Linearised slipper spacing	m
η	Dynamic viscosity	$\mathrm{m^2\,s^{-1}}$
E	Young's Modulus	$\mathrm{kg\,m^{-1}\,s^{-2}}$
ϕ	Bearing angle	rad
ϕ_1	Angle of first slipper with x-axis	rad
ϕ_{12}	Angle of first level coupling element	rad
ϕ_{ax}	Angle of highest level coupling element	rad
f	Bearing footprint as percentage of wavelength	-
F_{ax}	Axial bearing load	N
F_n	Normal bearing load	N
h_0	Nominal film height	m
h	Film thickness	m
I	Second moment of Inertia	m^4
K_θ	Rotational stiffness flexure	$\mathrm{N\,m\,rad^{-1}}$
K_ϕ	Tilt stiffness slipper	$\mathrm{N\,m\,rad^{-1}}$
λ	Guiding surface wavelength	m
L	Slipper length	m
L_s	Cross-flexure spring element length	m
L_f	Actual slipper spacing	m
N	Number of slippers	-
M	Moment on bearing due to tilt	$\mathrm{N\,rad^{-1}}$
P_a	Atmospheric Pressure	$\mathrm{N\,m^{-2}}$
P_s	Supply Pressure	$\mathrm{N\,m^{-2}}$
P_r	Recess Pressure	Pa
ρ	Density of lubricant	$\mathrm{kg\,m^{-3}}$
r	Stroke of bearing mechanism	m
R	Arm length pivot	m
σ	Stress level flexure	$\mathrm{kg\,m^{-1}\,s^{-2}}$
s	Scaling to wavelength factor	$\mathrm{m^{-1}}$
θ	Flexure angle	rad
θ_1	Angle of flexure of first slipper	rad
θ_{12}	Angle of flexure of first coupling element	rad
θ_{ax}	Flexure angle connecting bearing to load	rad
t	Flexure spring element thickness	m
v	Axial deformation factor	-
W	Work done by bearing	$\mathrm{kg\,m^2\,s^{-2}}$
x	x-position on guiding surface	m
x_1	x-position of the middle of the first slipper	m
x_{12}	the middle x-position between slippers 1 and 2	m
y	y-position on guiding surface	m
y_1	y-position of the middle of the first slipper	m
y_{12}	y-position of the middle of the first slipper	m

Preface

Children are always under the impression that their fathers can create and repair anything. I was no different. My dad taught me about the art of tinkering and was tinkering about for as long as I can remember. This is what has sparked my interest in engineering, taking things apart and see how they work. this scattered my interest over all fields of physics. And I consider tinkering an art, the ingenuity of mankind becomes visible and tangible through the beauty of improvising. Even more important to me, one can help others while doing so. I hope that I too can bring the impression that everything is create-able or repairable, and most of all be a help for others. Whether that is in my personal surroundings or on a community-wide scale does not matter to me, as long as I can be of assistance to others.

This is why I was very interested in this project. The possibility to use my interests of a wide range of physics into a single element seemed perfect. It would allow new applications and had potential to be used in the wind turbines. Helping to create cheaper sustainable energy is like a good way to help society. While this project did not end with these results, others may do so in the future, for me it was another learning experience. My time here in delft helped me find out what I wanted to do. I am grateful that I had the time to make mistakes here in Delft, the opportunity to explore what type of person I would like to become and to learn so very much. My choice for mechanical engineering in Delft was never well grounded, but I am so glad that I chose to study here. I can look back on an amazing time at this university.

Jan van Willigen
Delft, September 16, 2019

Summary

Hydrostatic bearings are a type of fluid bearing that use an external pump to provide a hydraulic film on which the bearing can slide. This full film lubrication prevents mechanical contact between the guiding surface and the bearing. Because of this, hydrostatic bearings are well known for having low friction and low wear. The working principle of the hydrostatic bearing is illustrated in figure 1.

The load capacity of a hydrostatic bearing is dependent on the pressure in the hydraulic film and bearing land area. The relation between fluid pressure and film height, and thus load capacity and film height is referred to as film stiffness. As a high loading capacity is wanted in many hydrostatic bearing applications the film stiffness is high. The design of the hydrostatic bearing itself is therefore also very stiff.

If the guiding surface is not parallel to the bearing land, the hydraulic film would not be well defined. Large gaps could cause a large pressure drops and contact might occur, thus resulting in a loss of full film lubrication, causing wear. Since the bearing is very stiff, it is unable to deform to take the shape of the guiding surface. Thus, well defined film thickness is lost where the guiding surface is not parallel with the bearing land. This can be due to machining imperfections, however there are applications where the guiding surface has a large waviness; a varying curvature in the direction of the guiding surface. Because of the potential loss of full film lubrication hydrostatic bearings are not considered a feasible option for these applications. If a hydrostatic bearings would be able to deform to take the shape of the guiding surface the film would remain parallel and full film lubrication would be maintained. This would make hydrostatic bearing a feasible option in applications with a wavy guiding surface.

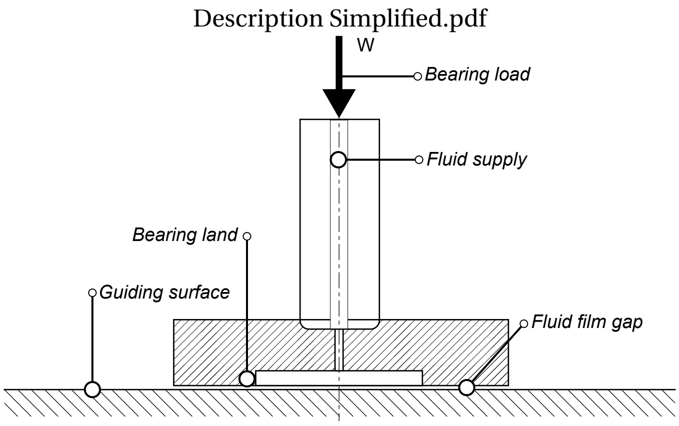

Figure 1: Working principles of single slipper hydrostatic recess bearing.

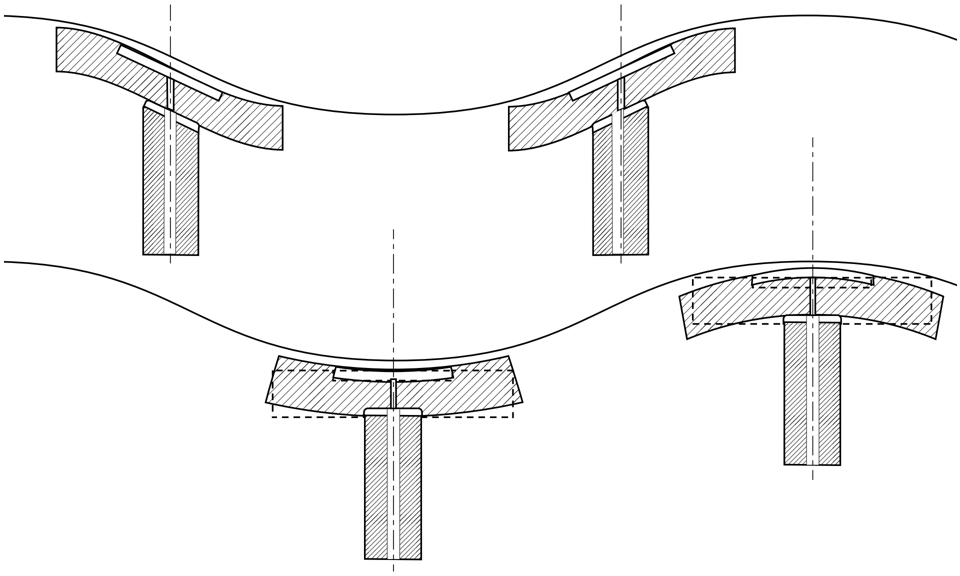

Figure 2: Four positions of a slipper hydrostatic bearing deforming to wavy guiding surface. It is seen at the point of maximum concave and convex curvature as-well as two asymmetrically deformation modes.

This is the focus of this thesis; to design and model a hydrostatic bearing capable of deforming to a wavy guiding surface, such that full film lubrication is maintained for all variations of the curvature of the guiding surface. Aiming to design a hydrostatic bearing that is able to deform to a guiding surface with varying curvature, while having similar loading conditions than a stiff hydrostatic bearing.

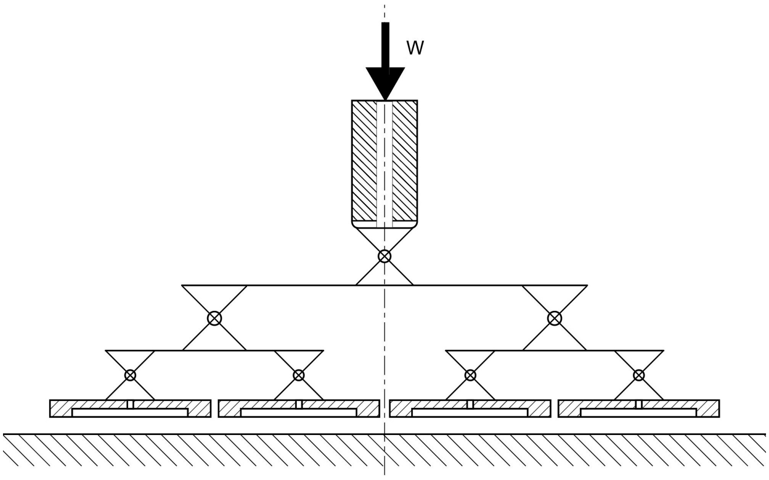

Figure 3: Impression of a whiffletree based distribution of four slippers.

This is achieved through the use of a compliant whiffletree to distribute the loads of multiple deformable hydrostatic slippers. These hydrostatic slippers are capable of deforming on their own, but are limited as their deformation is not sufficient to account for the complete deformation required to take the shape of the guiding surface. The same pivots used in the whiffletree will allow for tilt of the hydrostatic slippers. This will result in a lower maximum deformation required by the hydrostatic slipper. The maximum deformation of a hydrostatic slipper is limited by internal stresses, caused by the compressive forces and strain on the material.

The kinematics are set up to model the motion of the whiffletree in order to make predictions on maximum angles the slippers, and thus the pivots, will have to make. The model of slipper deformation in combinations with whiffletree kinematics gives a design tool for how many slippers are required for certain wavy guiding surface under given loading conditions.

The research includes a collection of models describing the deformation of the slipper, whiffletree kinematics, tilt of a hydrostatic bearing and a linear flexure. These models can be used as a design tool for a concept of a large deforming hydrostatic bearing using a whiffletree based compliant force distribution mechanism.

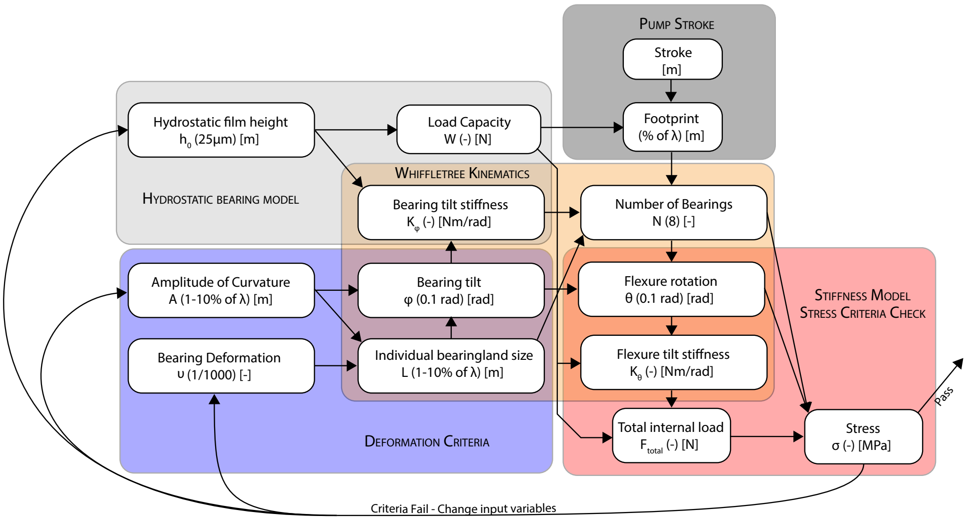
Pump Stroke
Stroke [m]
Footprint (% of λ) [m]
Hydrostatic film height h0 (25μm) [m]
Load Capacity W (-) [N]
Hydrostatic bearing model
Whiffletree Kinematics
Bearing tilt stiffness Kφ (-) [Nm/rad]
Number of Bearings N (8) [-]
Amplitude of Curvature A (1-10% of λ) [m]
Bearing tilt φ (0.1 rad) [rad]
Flexure rotation θ (0.1 rad) [rad]
Stiffness Model
Stress Criteria Check
Bearing Deformation υ (1/1000) [-]
Individual bearingland size L (1-10% of λ) [m]
Flexure tilt stiffness Kθ (-) [Nm/rad]
Pass
Deformation Criteria
Total internal load Ftotal (-) [N]
Stress σ (-) [MPa]
Criteria Fail - Change input variables

Figure 4: Visual overview of models and relationships used in this research, each of the colored blocks represents a model.

In this case study cross flexures are used as pivot points and multi-recess orifice bearings for the individual slippers. These implementations result in constraints on the model and introduce failure criteria, such that in the end a trade-off must be made between loading capacity and deformability of the hydrostatic bearing model.

Contents

Introduction

Background information

Global energy demands are ever growing. The effects of anthropogenic carbon emissions drive the need for sustainable energy sources. Offshore wind energy poses a solution[11]. High installation and maintenance cost reduce commercial viability. Delft Offshore Turbines is one of many looking for a feasible option in the offshore wind energy, they propose to connect a cluster of wind turbines to a single centralised generator through fluid power transmission. Removing the need for a generator in each turbine will decrease structural, installation and maintenance costs and therefore increase commercial feasibility[17].

In this project a hydraulic radial pump would be connected to the turbine rotor to generate a high pressure flow[18]. In this pump the bearing on the interface between the plunger and running track has stress levels that would be to high for which conventional roller bearings[45]. Hydrostatic bearings are proposed as an alternative, due to their low wear, low friction and high loading capacity. However, hydrostatic bearings on a running track with varying curvature, such as required in this type of radial pump, introduces new problems.

This application was the initial spark which ignited the interest in deforming hydrostatic bearings for these type of application.

The potential of hydrostatic bearings

The interest in hydrostatic bearings comes from the ability to fully separate two solid surfaces, referred to as full film lubrication[26]. The full film lubrication of a hydrostatic bearing is what gives the hydrostatic bearing its characteristics. Low wear, low friction and high loading capacity are key aspects to grant precision and long lifetime to machine tools. For these reasons they are attractive to implement in various applications. Figure 1.1 shows an example of two surfaces separated by a full film.

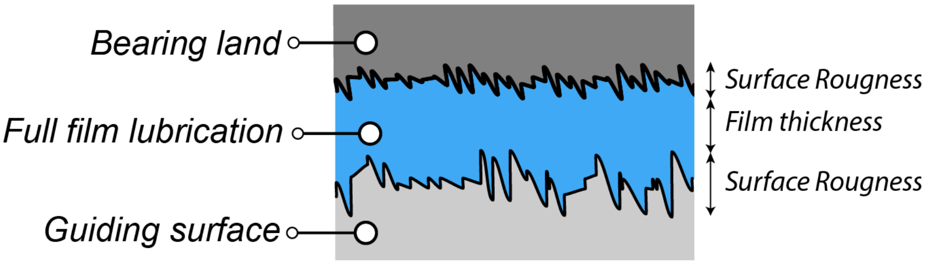

Figure 1.1: Two bearing surfaces separated by full film lubrication. The film thickness is large in respect to the surface roughness of the bearing surfaces. Assuring that solid-to-solid contact does not occur, allowing for minimal wear and low friction.

Hydrostatic bearing fundamentals

The hydraulic fluid is pumped in between the bearing land and the guiding surface through an external pump. Separating two surfaces of one-another through full film lubrication using an external pump is the working principle of a hydrostatic bearing. This principle can be seen in figure 1.2.

The load capacity of a hydrostatic bearing is dependent on the pressure in the hydraulic film and bearing land area. The film pressure depends on the supply pressure and film thickness. As load increases the film thickness becomes thinner, in turn increasing the pressure in the fluid. This continues until an equilibrium between the load and film pressure has been established. The relation between fluid pressure and film height, and thus load capacity and film height, is referred to as film stiffness. This relationship is typically depicted by a specific curve, an example of such a curve can be seen in figure 1.3.

The film pressure can be calculated for a specific bearing type with known geometry and for a given film height. This results from solving the Reynolds's equation, the mass balance for inlet and outlet flows [54]. For a parallel bearing the supply pressure decreases to atmospheric pressure, and the rate of change is determined by the film height. For a recess bearing as seen in figure 1.2, the recess pressure is inversely proportional to the film thickness, h.

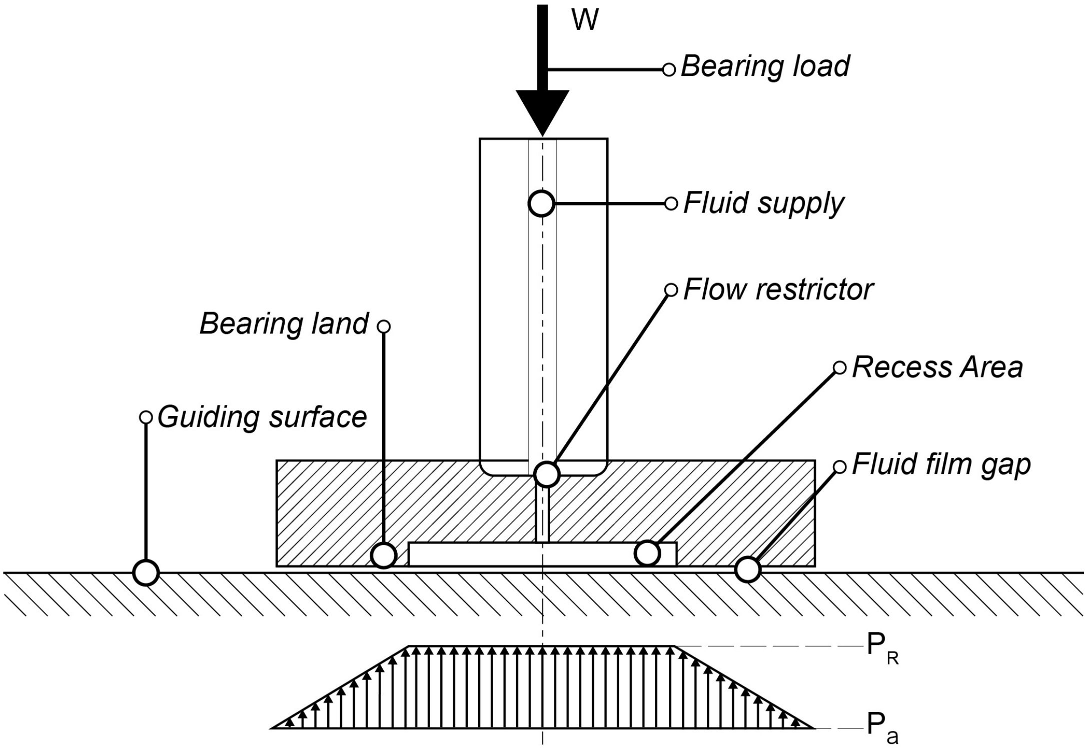

Figure 1.2: Working principles of single slipper hydrostatic recess bearing. The hydraulic pressure is well defined as the bearing land and guiding surface are parallel. The hydraulic pressure counteracts the axial load W the bearing carries. The pressure within the recess chamber is constant and pressure linearly decreases to atmospheric pressure throughout the fluid film gap.

With the hydraulic film pressure known, normal load on the bearing can be calculated. For the bearing seen within the figure the load capacity of the bearing is given by equation (1.1).

$$F_\text{n} = P_r \bar{A} A \tag{1.1}$$

Where A is the total bearing surface area and $\bar{A}$ is the shape factor, a geometry dependent parameter, equal to the fraction of effective area. The normal load should be transferred independent on the shape or position of the guiding surface.

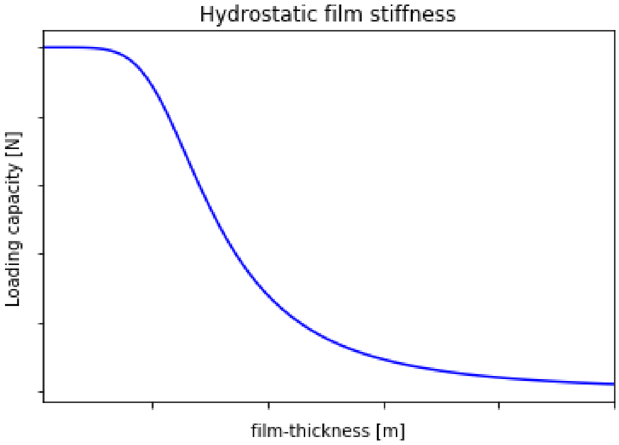

Figure 1.3: An example of a film stiffness curve for a hydrostatic bearing.

When the load on bearing becomes so large that the film thickness becomes smaller than surface roughness full film lubrication can not be maintained. The bearing transfers the load normal to the guiding surface while the bearing translates over the guiding surface. This is done with low friction and minimal wear, hydrostatic bearings are therefore further investigated for their implementation in applications with wavy guiding surfaces.

State of the Art

The performance of a hydrostatic bearing depends on its ability to maintain a lubrication film separation between two solid surfaces. Current applications of hydrostatic bearing are often as planar bearings for linear guiding as seen in figure 2.1a or annular bearing as in figure 2.1b. Fully hydrostatic turning machines have been available since the 80's [6]. These involve surfaces with a constant curvature, like planes in linear guide or circles in shafts. For any point of on these surfaces the bearing surface can be parallel to the guiding surface without deforming. As loading conditions do not become excessive the film thickness will remain well above the range of any surface imperfections. The full film lubrication can then be well developed and the hydrostatic potential can be fully utilized.

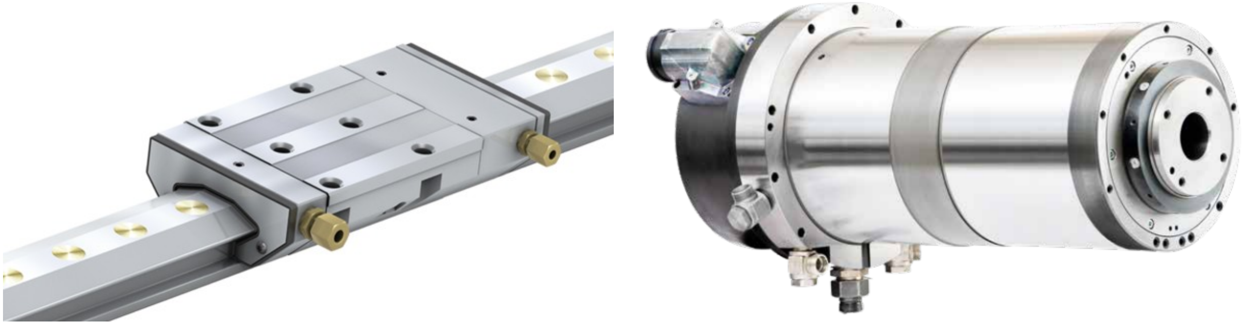

(a) A hydrostatic linear guide system [7]

(b) Hydrostatic spindle for machining lathes [8]

Figure 2.1: Examples of off-the-shelf hydrostatic bearing products as found in product catalogs

However, if the guiding surface is not parallel to the hydrostatic bearing it might be possible that full film lubrication can not be maintained as the fluid supply can not indefinitely pressurize a larger and larger flow required to separate the two surfaces. This non-parallel guiding surface might be due to imperfections in machining of the guiding surface, by excessive deformation of either the guiding surface or the hydrostatic bearing, or by design. A radial hydraulic pump would be an example of a system where a guiding surface with varying curvature, the background information introduces the need for a hydrostatic bearing for this application. A typical hydrostatic bearing is not capable of following these wavy guiding surfaces. As it requires a different shape of the bearing in order for it to have a parallel film for every position of the hydrostatic bearing on the guiding surface. From the wide range of literature available on hydrostatic bearings, the literature study focuses on deformable hydrostatic bearings, a list of the main keywords used to investigate these is found in table 2.1.

Deformable hydrostatic bearings in literature

Since the idea of hydrostatic bearings appeared in 1852[23] they have found their way into precision machines. They have been investigated to implement in cryogenic turbo-pumps in rocket engines [52], large pads in hydro power units [35], and have increasing growth in precision machining tools [54]. This is a potential explanation for increasing interest in literature in recent years [36].

However, while scientific interest in hydrostatic bearings has been growing in the past decades, no literature is found on hydrostatic able to follow a large wavy guiding surface. Also no research has been found on hydrostatic bearings used to follow surfaces with a specifically designed waviness or irregularities much larger than the film height. Therefore, the scope of the literature study widened in the search for deformable bearings. Bearings that aim to maintain full film lubrication using deformations have been found [65][20], even though these bearings only undergo small deformations they grant insight for larger deforming concepts. Therefore, small deforming bearing are taken into account in the literature overview, as found in appendix D. The literature papers are organized by the cause which introduced the change in film height for their application.

In figure 2.2 an example of a hydrostatic thrust bearing with a nominal flight height of 100 µm while surface waviness is measured at 300 µm. It is used on a surface with irregularities larger than it's nominal flight height and full film lubrication can not be maintained[66]. It has a rubber support to account for tilting of the bearing and in order to follow the surface waviness of the running track. The bearing can deform and the bearing can maintain full film lubrication. Under nominal loading conditions this rubber is compressed 50 µm.

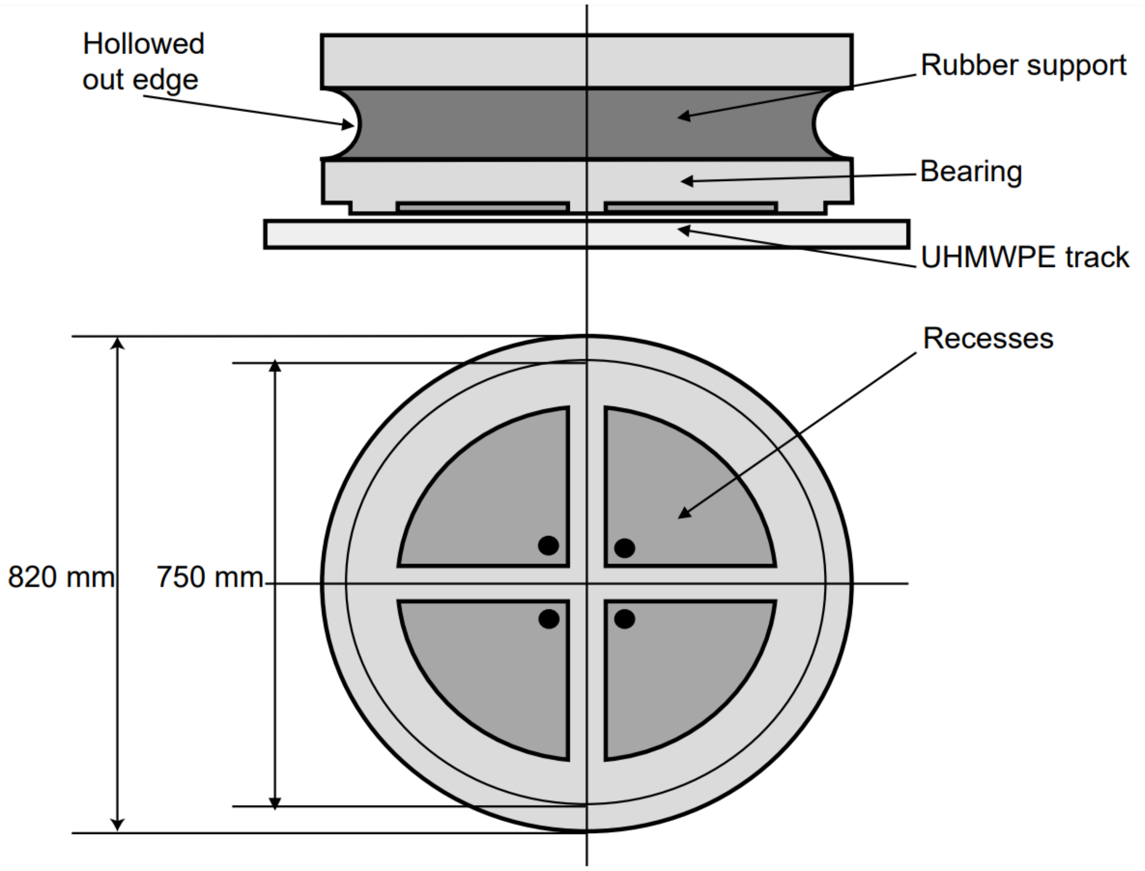

Figure 2.2: Hydro-foot with rubber support used in the prince Willem-Alexander lock gates

A tilting pad bearing is seen in figure 2.3, the bearing pad is lubricated through a oil inlet however it is not a hydrostatic bearing[35]. This particular bearing is a hydrodynamic bearing, meaning the fluid film is pressurized by the high speed of the journal as it forms a wedge between the bearing surfaces[29]. Hydrodynamic bearings have no full film lubrication during start up and even with spring supports to compensate for tilt and oil lubrication for cooling there still is friction and wear, eventually leading to mechanical failure[33]. The pressure development can be seen in figure 2.4. Thrust bearings using spring supports do not tilt on a pivot, but tilt due to deflection of the springs[47][10]. Like the rubber support from figure 2.2 the bearing has an elastic support behind the bearing surface, even though this is not a continuous deforming elastic media it still allows for deformations.

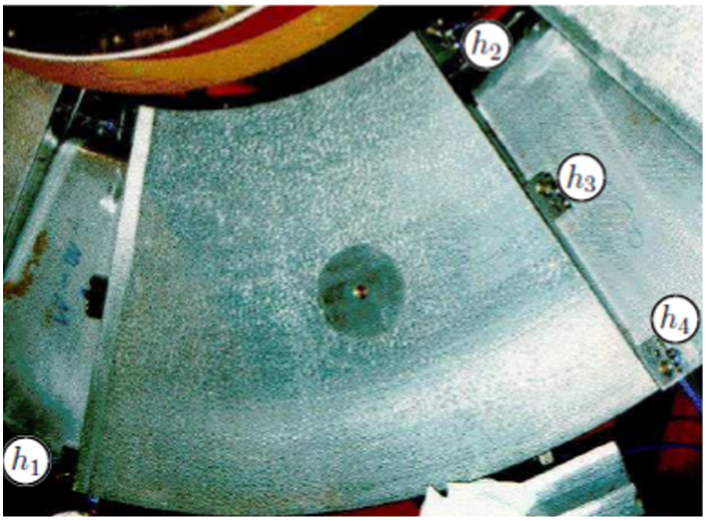

Figure 2.3: A tilting pad thrust bearing, with hydrostatic recess. Hydrostatic lubrication is used to decrease temperature and friction however no full film lubrication is achieved [29]

Figure 2.5 shows a gas lubricated compliant bearing developed for oil-free high-performance turbo-machinery. It uses a combination of centered flexures for radial stiffness and flexure pivots to allow for rotational compliance[20].

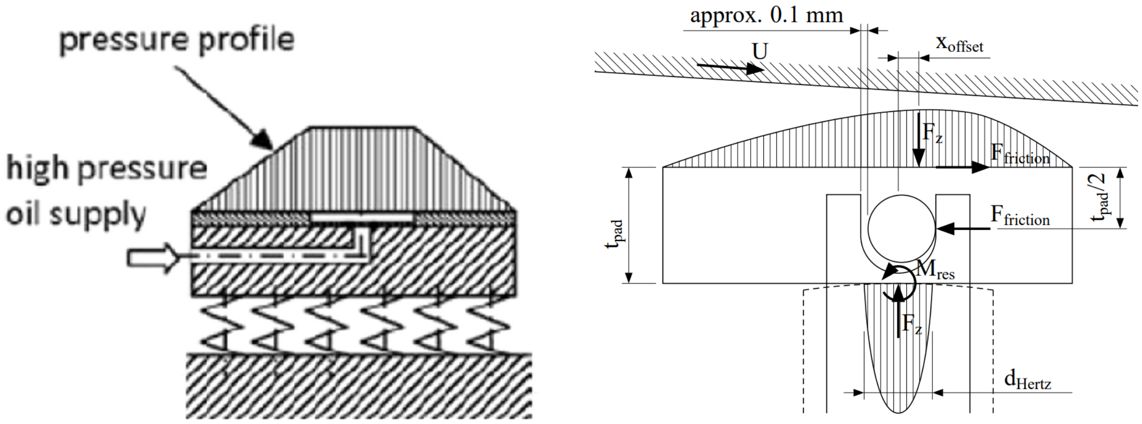

Figure 2.4: Schematic drawing of tilting pad bearings and accompanying pressure distributions

It is described as a hybrid bearing, meaning it utilizes the principle of hydrostatic pressurization of the fluid film as well as pressurization due to wedging of the fluid film. It also uses flexures instead of a rolling contact pivot as seen in figure 2.4 this removes a hertz contact point. As this is not affected by wear, it might be a more suitable pivot for long term use. This specific bearing has been designed to maximize load carrying capacity while maintaining compliance to compensate for misalignment and variations in rotor geometry.

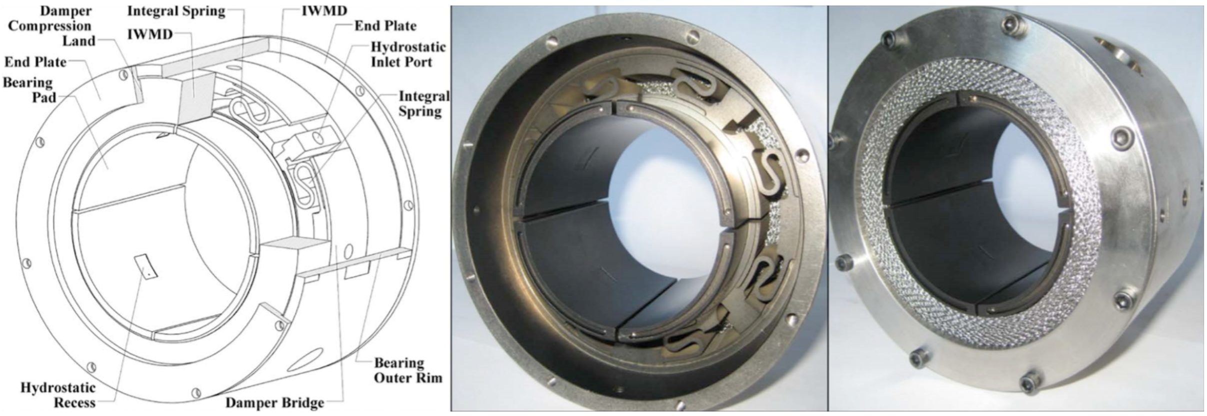

Figure 2.5: Compliant hybrid journal bearing with a integral wire mass damper using flexures, compliant pivots and integral springs.

With these examples the main principles in state of the art deformable hydrostatic bearings have been presented. To summarize these are; elastic continua as bearing support to compensate for guiding surface waviness, pivots and compliant flexure elements that allow pad tilting and spring supports providing radial, normal or tilt stiffness. As the bearings that undergo small deformations use either elastic deforming bearing slippers or elastic bearing supports and mechanical structures, to allow the bearing to deform, these principles are further investigated. The

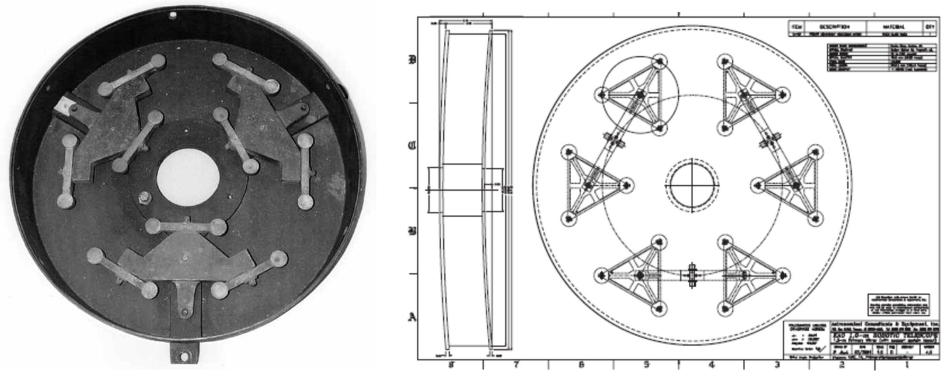

(a) Whiffletree based mirror support from 1835[15]

(b) Schematic of a whiffletree like primary mirror support system[50]

Figure 2.6: Examples of off-the-shelf hydrostatic bearing products as found in product catalogs

literature overview can be defined by the keywords found in tables 2.1 and 2.2, while the actual overview is found in the appendix D.

Table 2.1: Keywords used to investigate deforming hydrostatic bearings, combinations of these keywords have also been used

Keywords related to large deformation

Elastic	Deforming	Flexible	Deformable
Bearing stiffness	Bending	Flexures	Compliant
Tilting	Compliance	Controllable	Compensating

Keywords related to hydrostatic bearings

Fluid bearing	Hybrid bearing	Hydrostatic	Hydrodynamic

Keywords related to variations in guiding surface

Eccentricity	Misalignment	Geometric imperfections	Surface roughness

Keywords related to bearing geometry

Multi-recess	Bearing pad	Shape variation	Bearing geometry
Bearing support	Pad support	Number of recess	Tilt-compensation

Researchers additionally investigated

B.H. Ertas	A.H. Slocum	W.B. Rowe	R.A.J. van Ostayen

Elastic bearing slippers could be combined with linkage mechanisms like a rocker-bogie to distribute loads and/or increase range of motion. The combination of deforming bearings and force distribution mechanisms is also investigated. As support structures are available in an abundance of fields, a separate literature review has been done in the field of support structures, of which the keywords can be found in the table 2.2. Figures 2.6a and 2.6b show whiffletrees as a force distribution mechanism. Whiffletrees have been used since ancient times in agricultural societies but have made their way into telescopes as a good way to control load acting upon the mirrors[15]. They are still being developed for telescopes today [50][4].

Table 2.2: Keywords used to investigate large deforming mechanical mechanisms

Keywords related to elasticity

Elastic	Deforming	Flexible	Adjustable
Stiffness	Bending	Flexures	Compliant
Yielding	Compliance	Controllable	Compensating
Linkage	Four-bar linkage	Five-bar linkage	Pivots

Keywords related to mechanical support mechanisms

Rocker-Bogie	Suspension	Whipple-tree	Parallel robots
Passive robots	Passive linkage system	Robotic mechanisms	Force balance

Keywords related to kinematics

Kinematic supports	Passive motion following	Kinematic synthesis	Passive kinematics
Motion analysis	Body-guidance synthesis	Rigid body synthesis	Suspension analysis

Books additionally investigated

Compliant Mechanisms [37]	Flexures [63]	Handbook for Compliant Mechanisms [32]

Conclusion

From literature it can be concluded that a large deforming hydrostatic bearing does not yet exist. As proposed in the introduction there is a range of applications will be available for deformable hydrostatic bearings, as they would be competitors to ball bearings. Therefore, it will be an challenging research topic as the possibilities and limitations are not yet known. The existing principles of small deforming elastic hydrostatic slippers and whiffletree force distribution mechanism are taken as inspiration to model the concept of largely deforming hydrostatic bearing upon. Using the principle of pivoting flexure elements to compensate for tilting and using multiple hydrostatic slippers to distribute loads.

Problem definition

When the guiding surface has a varying curvature, the bearing must deform to have a similar shape. This will allow the film to maintain parallel. In order for the bearing to deform it must be compliant, however if it were to be compliant the bearing could deform under loading conditions where the guiding surface has a constant curvature. High axial loading capacity is often a criteria why hydrostatic bearings are proposed, therefor this property must be safeguarded.

This is the design challenge. To design a hydrostatic bearing able to deform to a wavy guiding surface, this means it has a varying curvature in the direction of the running track, while maintaining high axial loading conditions.

Now it has been established that the design must be stiff in axial direction and rotationally compliant. However, how stiff and how compliant must the structure be? As the full film lubrication can be achieved if the bearing and guiding surface are the same shape, this is part of the design objective. To keep the bearing land and guiding track parallel. An example of a deformable hydrostatic bearing that deforms to have it's bearing surface parallel to a wavy guiding surface can be seen in figure 3.1.

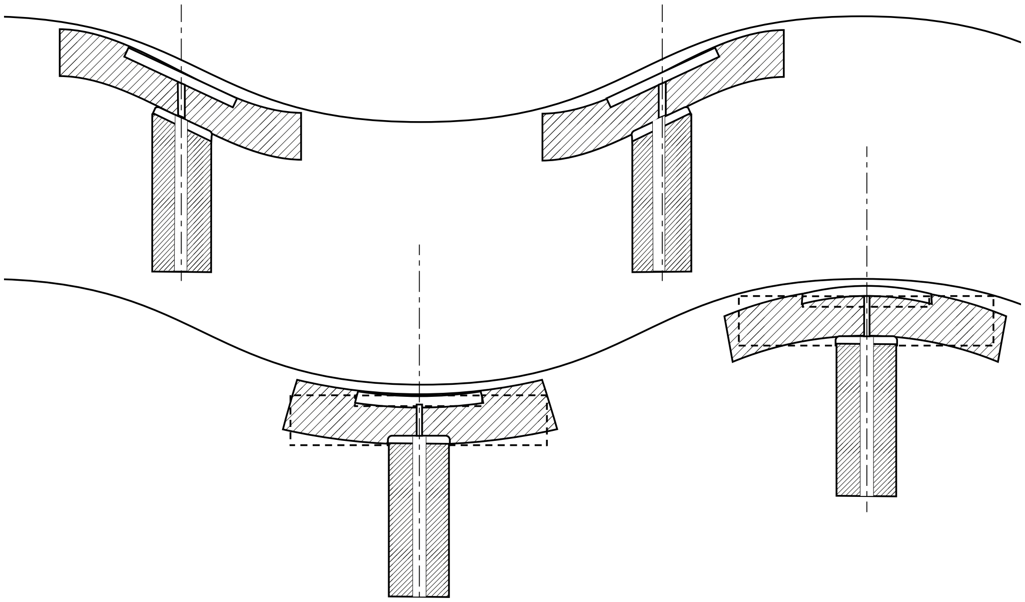

Figure 3.1: A single hydrostatic slipper deforming to a guiding surface with varying curvature in the direction of the running track.

The pressure profile of a hydrostatic bearing will generate a force normal to the guiding surface. If small deformations are compensated for by the deformation of the bearing land through an elastic deformable continuum than a curvature might be simplified to a straight path under an angle. The resultant force for each bearing pad can thus be related to this angle and the size of the bearing pad.

The amount of deformation needed depends on the curvature of the guiding surface and on the size of the bearing pad. A smaller bearing pad covers a smaller portion of the guiding surface as it resembles a straight line more closely and therefor requires less deformation of the bearing pad.

Research Objective

The goal of this thesis is to gather knowledge through modeling in order to make decisions on design choices. This will be the foundation from which large deformable hydrostatic bearings can be designed. To investigate the feasibility of large deformable hydrostatic bearings. To explore multiple concepts and model the motion of a deformable bearing on a wavy guiding surface.

This is all encapsulated by the goal to;

> *Design and model a hydrostatic bearing for large deformations and high loading conditions using a mechanical support structure*

In order to achieve this goal the following research questions have been set-up;

- How large of a waviness can be followed using elastic hydrostatic slippers?
- Can compliant mechanisms be combined with elastic slippers to improve overall compliance?
- What are the kinematics of a whiffletree-like structure on a wavy guiding surface
- Can multiple deformable hydrostatic slippers be combined in a force distribution mechanism to improve waviness following capabilities?

Organization of this thesis

Figure 3.2 gives an overview on how the chapters are connected. Chapter 4.1 is written in a paper style format and can be read as a stand alone document. However, it is recommended to first read first four chapters as they are introductory to those unfamiliar to hydrostatic bearings and introduce a modeling principle used later on. The modeling of this problem is started in chapter 4. With this one should have a proper understanding such that the paper can be read, which expands on the modeling principles. After the paper, chapter 6 elaborates the models and explains it's further use and limitations. While the actual scripts and user manuals for the model can be found in appendix C. These will lead to the answers to the research questions in chapter 8, where they are evaluated and discussed. Following this some recommendations are given for future research and this thesis closes with a general conclusion.

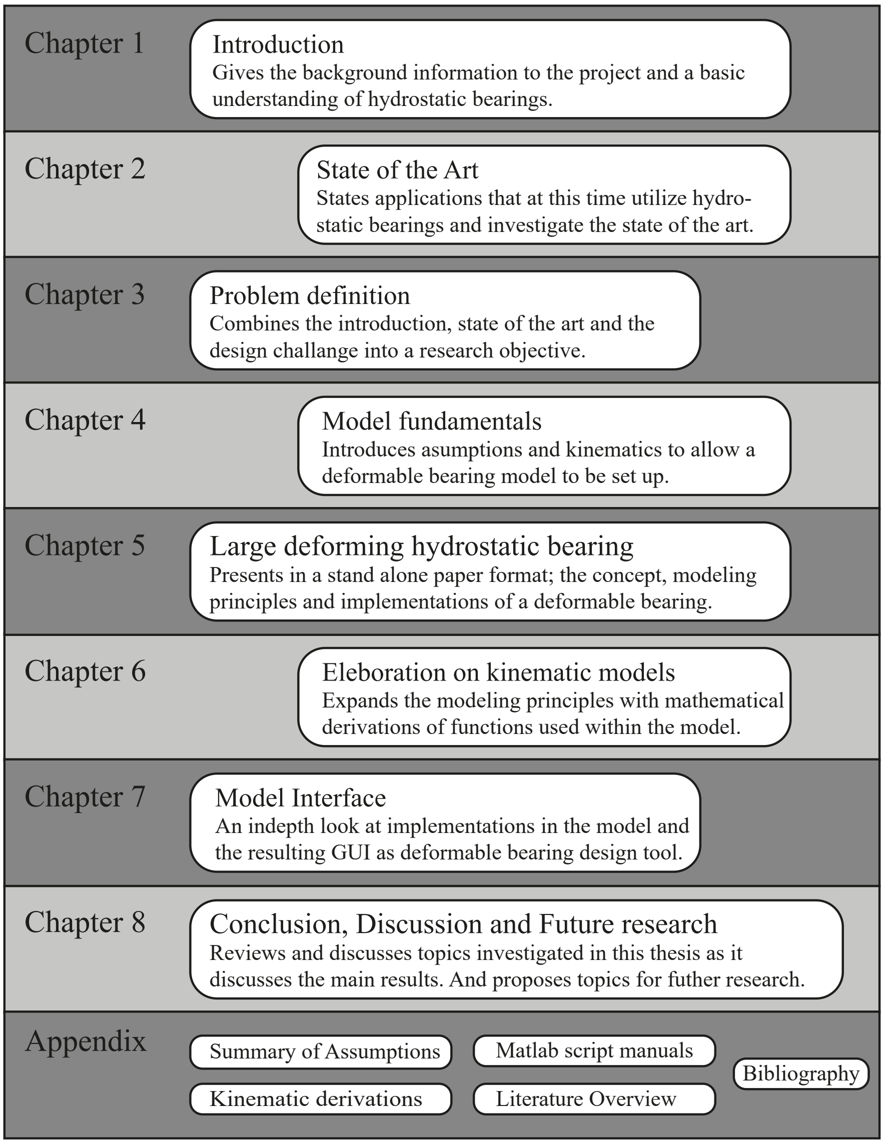

Chapter 1	Introduction Gives the background information to the project and a basic understanding of hydrostatic bearings.
Chapter 2	State of the Art States applications that at this time utilize hydrostatic bearings and investigate the state of the art.
Chapter 3	Problem definition Combines the introduction, state of the art and the design challange into a research objective.
Chapter 4	Model fundamentals Introduces asumptions and kinematics to allow a deformable bearing model to be set up.
Chapter 5	Large deforming hydrostatic bearing Presents in a stand alone paper format; the concept, modeling principles and implementations of a deformable bearing.
Chapter 6	Eleboration on kinematic models Expands the modeling principles with mathematical derivations of functions used within the model.
Chapter 7	Model Interface An indepth look at implementations in the model and the resulting GUI as deformable bearing design tool.
Chapter 8	Conclusion, Discussion and Future research Reviews and discusses topics investigated in this thesis as it discusses the main results. And proposes topics for futher research.
Appendix	Summary of Assumptions Matlab script manuals Bibliography Kinematic derivations Literature Overview

Figure 3.2: Visual representation of contents presented in this work.

Model Fundamentals

For a description of a deformable bearing, the model starts with a description of the guiding surface. Figure 3.1 shows a single slipper over a wavy guiding surface. This figure has implemented the idea that the curvature can be described by a periodic sinus wave. This has been chosen to model the guiding surface as the deforming hydrostatic bearing aims to be used in applications with a guiding surface with periodic varying curvature. While some are linear wavy sinusoidal running tracks others are more complex. Examples of such systems can be seen in figure 4.1.

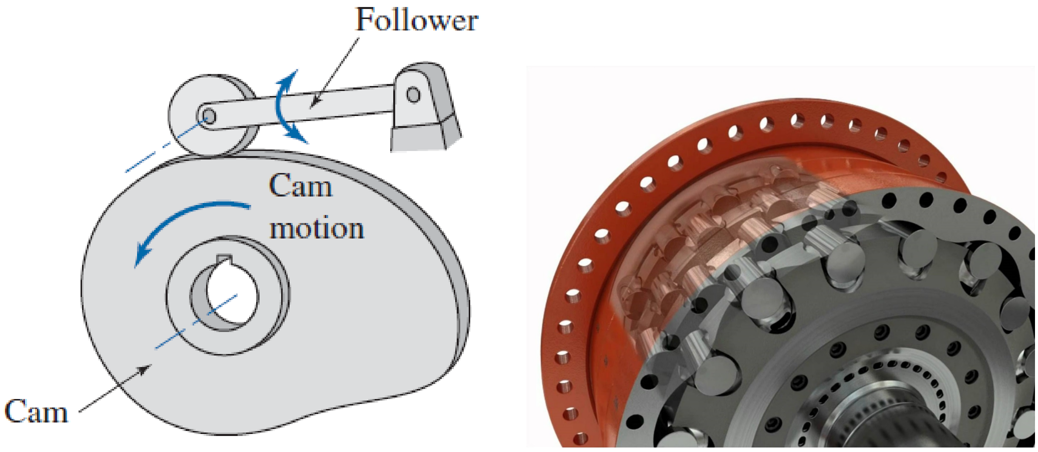

(a) Generic cam and cam-follower

(b) Hägglunds hydraulic drive[5]

Figure 4.1: Example applications with solid-to-solid contact surfaces with roller bearings and varying curvature of the guiding surface.

Looking at the guiding surface from the perspective of the bearing, the guiding surface has a periodic change in curvature. A waviness amplitude, stroke or curvature function can be set up as a function changing over time, position or rotation of the guiding surface. The result will always be a continuous periodic function, figure 4.2 shows one way to set up a function on the guiding surface. As a periodic function it could then be deconstructed into a sum of sinusoids, using Fourier series. Therefore even if the guiding surface is not a linear sine wave, a sin wave can be used to model the guiding surface, as seen in figure 3.1.

Kinematic set-up

Using a sine wave as description for the guiding surface a model of the deformable slipper can be set up. First a single slipper is placed on the guiding surface, as a pivot has been introduced it can be placed tangent to the guiding surface. Separated by a hydraulic film of tens to hundreds of micrometres thick. It has been assumed that the dimensions of the guiding surface are much larger than this fluid film gap. And as the bearing is relatively small compared to the wavelength, the angle of the slipper with the horizontal, ϕ, is equal to the tangent with the guiding

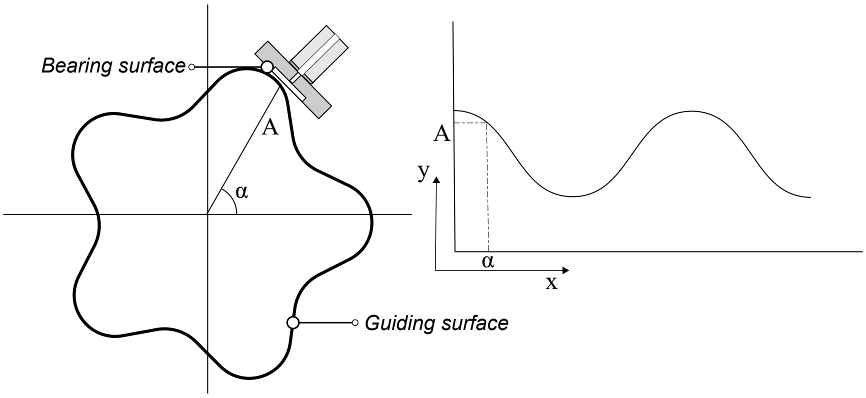

Figure 4.2: Describing the guiding surface as a function of the cam lift for a arbitrary guiding surface with varying curvature

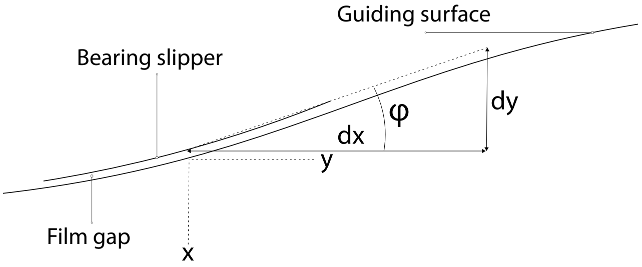

Figure 4.3: Hydrostatic slipper placed on a guiding surface. Tangent line with the guiding surface defines slipper angle ϕ.

surface. And as the guiding surface was described by a sine wave, equation (4.4) defines this angle. This definition can be seen in figure 4.3.

$$\phi = \arctan\left(\frac{dy}{dx}\right) \tag{4.1}$$

$$s = \frac{2\pi}{\lambda} \tag{4.2}$$

$$y = sA\sin(sx) \tag{4.3}$$

$$\phi = \arctan(sA\cos(sx)) \tag{4.4}$$

Here, x is denoted the position of the guiding surface, normalized by a scaling factor to 2π. This scaling factor, s, is defined in equation (4.2). It is introduced to have universal equations independent of guiding surface length. This gives us the equation for y, as given by equation (4.3). The amplitude of the sinus, A is defined as the waviness amplitude of the guiding surface, as seen in figure 4.4. Scaling A with the factor s will make it dimensionless and therefore if it is scaled with this factor s, A is called the Relative Waviness Amplitude. The bearing is expected to have an elastic support structure able to deform a fraction of it's length as seen in figure 4.4. This fraction will from now on be called the axial deformation factor or noted as υ. From literature it was concluded that an elastic bearing support is possible to achieve with to maintain full film lubrication $\upsilon = \frac{1}{1000}$ [65]. Meaning the deformation of a bearing slipper with length L in axial direction is $\frac{1}{1000}$L.

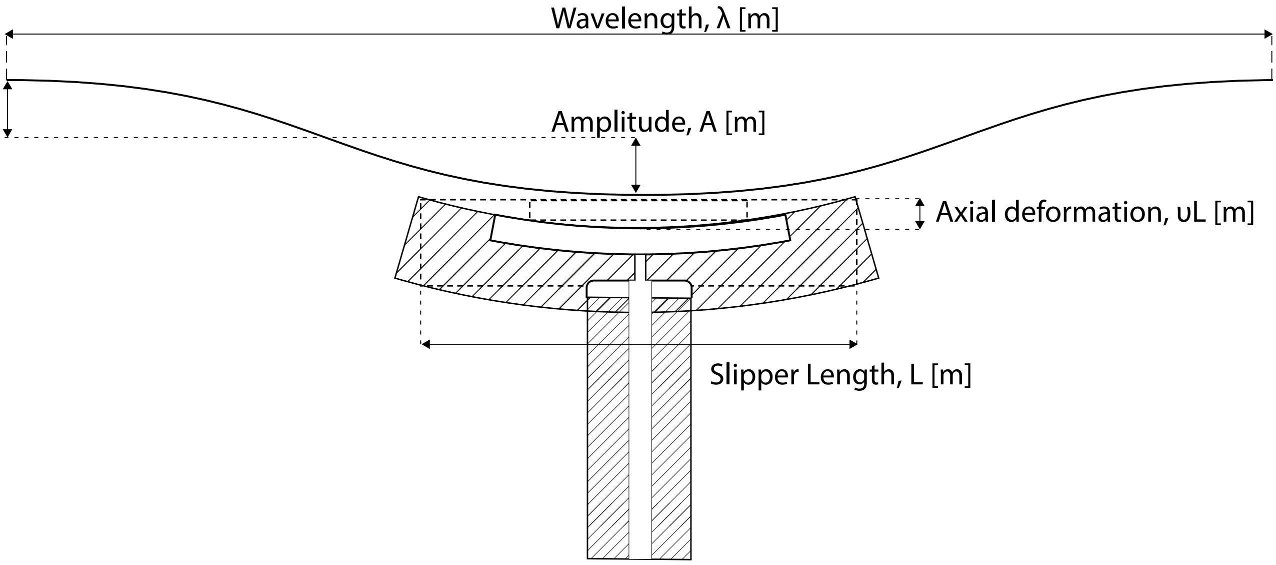

Figure 4.4: Elaboration on variables and dimensions used to describe slipper and the corresponding wavy guiding surface.

Whiffletree-based deforming hydrostatic bearing
Modeling and design of a compliant force distribution mechanism

N.J. van Willigen*, J.P.A. Nijssen *, R.A.J. van Ostayen *
*Department of Precision and Microsystems Engineering, Delft University of Technology, Delft, The Netherlands

***Abstract*—Hydrostatic bearings are well known for having low friction and low wear in combination with high loading capacity. Traditionally, the running surfaces for a hydrostatic bearing are plane, rigid and smooth, ensuring a parallel lubricating film in the full range of movement. In this paper, we consider a new type of compliant, hydrostatic bearing where the running surfaces have a surface waviness with a large amplitude resulting in a varying curvature for the hydrostatic bearing to follow in its range of movement. Design choices and subsequent modeling of these types of bearings are presented in this work. The introduced bearing concept is based on a compliant whiffletree mechanism able to distribute load over multiple hydrostatic slippers. This increases deformability of the complete bearing system. In a case study the limitations of a large deforming hydrostatic bearing are modeled to understand the impacts on performance and implications.**

***Index Terms*—Hydrostatic bearings, Compliant Mechanism, Deformable slipper, Flexures, Whiffletree.**

I. Introduction

Hydrostatic bearings are accepted as good candidates to replace rolling bearings due to their minimal wear and friction[1]. Hydrostatic bearings are typically designed with rigid, non-compliant bearing surfaces in order to obtain a high load carrying capacity, which is often required for their applications. This causes current hydrostatic bearings to lose functionality when used on a guiding surface with varying curvature or large waviness. As the high stiffness prevents the hydrostatic bearing to deform and follow the shape of the guiding surface. If rigid hydrostatic bearings are present in these kind of systems, this results in loss of full film lubrication, leading to mechanical contact. State of the art hydrostatic bearings only consider small guiding surface irregularities, in the order of magnitude of surface roughness or anomalies caused by eccentricity[2][3], if considered at all. Over the past decades there has been an increasing interest in hydrostatic bearings. However, little research has been done in the field of large deformable hydrostatic bearings[4]. Where large deforming hydrostatic bearing are defined as bearing used on the running track with continuous variations which are orders of magnitude larger than surface roughness and the nominal lubrication film thickness. To compensate for these variations a few consider an elastic bearing support within the bearing[2][5]. However, these are used to for small deformations. Therefore, hydrostatic bearings are currently not considered as design alternatives to roller bearings in applications where waviness of the guiding surface is involved.

At present, on the running track of large doors, cranes and conveyors, rolling or sliding bearings are primarily used. The same goes for machining; only a few manufactures consider hydrostatic bearings an option for guiding tracks of lathes, cutting and milling machines. The guiding surfaces of these applications are often not wavy by design but by machining imperfections[6]. For these applications hydrostatic bearing guiding surfaces already provide higher accuracy in components with relatively low machining accuracy due to the error averaging effect of the support film. Also, the elastic deformations of the guiding surfaces due to high loading can lead to a varying curvature[2]. Thus the guiding surface can not always be assumed to be infinitely stiff. The existence of a deformable hydrostatic bearing could allow for less wear in these application and thus longer lifetime, lowering the need for maintenance.

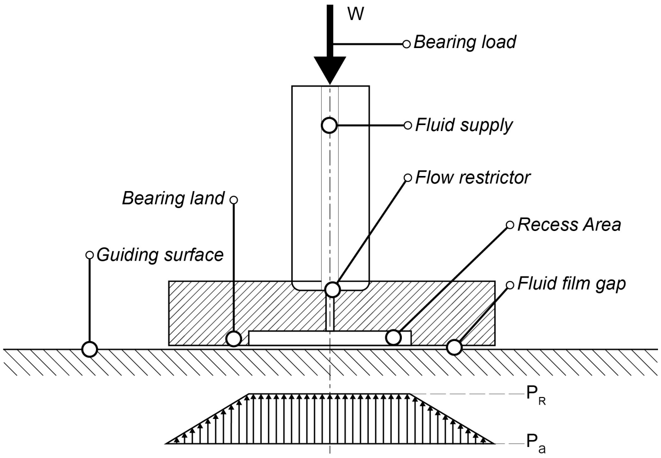

Fig. 1: Working principles of single slipper hydrostatic recess bearing. The hydraulic pressure is uniformly defined as the bearing land and guiding surface are parallel. The hydraulic pressure counteracts the axial load W the bearing carries. The hydraulic pressure is visualized below the bearing, with the pressure decreasing to atmospheric pressure throughout the fluid film gap.

In addition, full film lubricated systems offer even more advantages in submerged applications. An example of such a wet application environment is the use of hydrostatic bearings in a hydraulic pump as the interface between the running surface and the plunger[7]. Certain pumps, such as radial pumps or axial piston pumps, could be designed to have a running surface with a varying curvature. If the bearings were made compliant they would be able to follow this shape. However, deformation in the normal direction would occur due to the load. Mechanical failure of the bearing due to this compression limits the load capacity of the bearing.

Therefore, a hydrostatic bearing needs to be developed that is able to follow the curvature of the guiding surface, while maintaining high normal stiffness. The development of such a bearing would increase the number of possible applications significantly.

This paper will present the concept and modeling of a large deforming hydrostatic bearing concept. This bearing concept maintains high loading capacity in the presence of waviness in the direction of the running track using a compliant force distribution mechanism.

Section II describes the principle of a deformable hydrostatic bearing slipper. ection III presents a concept of a large deforming hydrostatic bearing by connecting multiple deformable slippers. For this whiffletree-based concept the kinematics are set up as well. Section IV concludes the modeling part by introducing additional constraints as a result of physical limitations. Sections V and VI present available implementations of the bearing slippers and joints respectively. Finally, a complete case study is discussed in section VII. To conclude, the limitations of this design are presented.

II. Deformable hydrostatic bearings

The working principle of a hydrostatic bearing has been illustrated in figure 1. In this figure a single slipper (or hydrofoot) is seen. This work considers the variation in curvature is only the direction of motion of the bearing, this allows the hydrostatic bearings to be simplified to 2D for now. In figure 1 the pressure drop over the bearing land is described as a linear decrease, this assumption holds if the guiding surface and bearing land are parallel [8]. So for a given load, a uniform film with height h, is present between the track surface and bearing land area. This film transfers the axial load on the bearing to the guiding surface while allowing the motion of the bearing as translates over the guiding surface. The normal load on a recess bearing is given by equation (1), which holds if if the bearing and guiding surface are parallel [1].

$$F_{\mathrm{n}} = P_r \bar{A} A \tag{1}$$

Where A is the total bearing surface area and Ā is the shape factor, a geometry dependent parameter, equal to the fraction of effective area. The recess pressure, P_r is dependent on the fluid film-thickness and bearing geometry parameters. With variations in curvature or waviness of the running track much larger than the fluid film-thickness and the surface roughness the bearing land surface will have to adjust to the profile of the guiding surface for all positions on the track. If this does not happen, the film thickness must compensate for this to prevent mechanical contact and a parallel film can not be maintained, such that the loading capacity can not be well defined. As the normal load acting upon the bearing should be transferred independent on the shape or position of the guiding surface.

The bearing slipper should deform to match the shape of the guiding surface, as seen in figure 2. The normal pressure forms the slipper towards the shape of the guiding surface through elastic deformation. The elastic compression of the guiding surface due to the load the bearing is applying upon it, is not taken into account. The running track is considered to be a rigid wavy guiding surface which is very stiff compared to the bearing. In order for the slipper to be able to follow guiding surfaces with larger variations in curvature, the slipper compliance must be increased. However, more compliance will introduce more strain on the slipper, increasing the risk of mechanical failure. To reduce internal stresses, the bearing slipper design and support structure can be altered. Research is being done on the design of bearing slippers such that these can allow large deformations while maintaining high loading capacity[7][9][10]. The deformable slipper is a key part in the design of large deformable hydrostatic bearings.

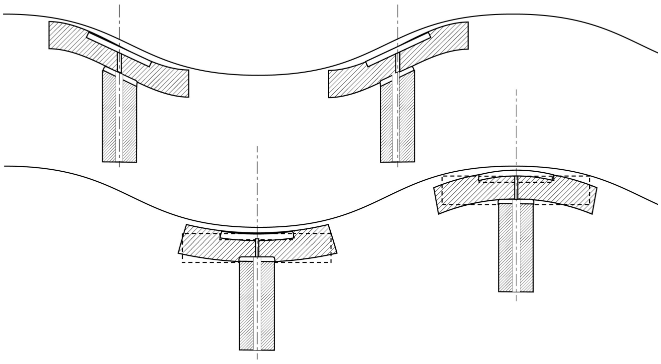

Fig. 2: Representation of single slipper hydrostatic bearing deforming to prevent contact and achieve a parallel film while following a guiding surface with large waviness.

In this work, large deformation is defined as the deformation corresponding to the deformation required to follow a valley-to-peak waviness magnitude of the guiding track equal to ten percent or more of the track length. This, is a comparable metric to the one used in large deforming compliant mechanisms[11].

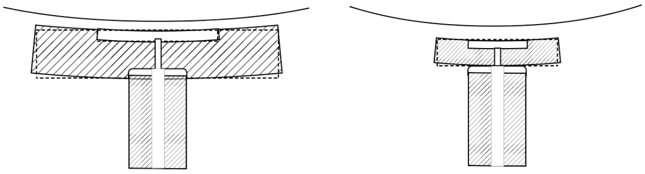

Fig. 3: Two bearings parallel to their guiding surfaces, this visualization shows that the smaller slipper on the right can maintain parallel on a guiding surface with larger waviness, than the larger slipper on the left.

For slippers with in-plane length much smaller than half a wavelength of the waviness of the guiding surface, the maximum required axial displacement will be smaller on this point of maximum curvature. Because the deformation on the point of maximum curvature requires symmetrical deformation of the bearings, the absolute deformation is lower. In order to determine the magnitude of axial displacement required by a single slipper, placed on the location of maximum curvature, the compliance of a single slipper must be investigated.

The largest required displacement of the bearing slipper is when the bearing is located on the point of smallest curvature of the guiding surface. On this point curvature goes from positive to negative and as seen in figure 2, the slippers will also undergo asymmetrical deformation to follow this guiding surface. A pivot that would allow for rotation of slipper will move the point of maximum displacement to the point where the absolute curvature is largest. This pivot would be able to account for the deformation of the tilt and therefore decrease the maximum required deformation. Slipper length is defined as the in-plane length of an un-deformed slipper. And wavelength is defined as the distance between two extremities on the guiding surface. These definitions can be seen in figure 4.

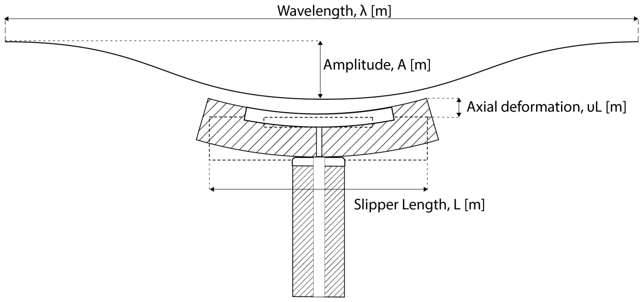

Fig. 4: Elaboration on variables and dimensions used to describe slipper and the corresponding wavy guiding surface

Using smaller bearing slippers would allow the bearing to follow tracks with a higher waviness amplitude, which can be seen in figure 3. This reduces load capacity, as equation (1) notes load capacity is proportional to bearing land area. To compensate for the lose of load capacity multiple individual slippers could be linked together to form one larger hydrostatic bearing. Using the previously introduced pivots it could tilt the individual slippers similar to a hydrostatic bearing with multiple recess chambers. As the forces would have to be distributed equal as in a whiffletree, this is the basis for the bearing mechanism presented in the next section, and is visualised in figure 6.

As a pivot on a slipper will significantly decrease the need of individual deformation of a single slipper, pivots are attached to the slippers. Pivots with a rotational stiffness much smaller than the tilt stiffness of the slippers are desired. Low rotational stiffness for the pivots is therefore presented in more detail in section V.

Bearing slippers have been modeled in the past as elastic bending elements that bend a fraction of their length in the axial direction, as elastic supports helped to achieve this. Theoretical modeling of elasto-hydrodynamic lubrication have been analysed in-depth[2][10][12]. Slipper deformation is modeled it is done through deformation as a fraction of the bearing length [9][13]. This modeling principle is applied in this paper; the maximum bearing deformation is given as a fraction of the slipper length. The amount of bending of the bearing should be at least equal to the axial curving of the guiding surface in order to maintain parallel film. This is referred to the deformation criteria. Failing this criteria would result in the loss of a parallel hydraulic film. Using a sine wave to describe the continuous varying curvature of the guiding surface. This models the convex and concave curving of the guiding surface, for which the respective deformation criteria are given by equations (2) and (3).

$$A - \upsilon L \leqslant A \sin(x + \frac{1}{2}L) \tag{2}$$

$$-A + \upsilon L \geqslant A \sin(x + \frac{1}{2}L) \tag{3}$$

Here A is the relative waviness amplitude, υ the relative deformation factor and L is the individual slipper length. An assumption on υ is made based on previous research on elastic supports[9]. The factor chosen, $\frac{1}{1000}L$, will allow the bearing slipper to deform without making mechanical contact. The horizontal position of the deforming slipper on the guiding surface is given by x. Note that the waviness is relative to a 2π wavelength, thus slipper length, waviness and the position on the guiding surface are fractions of the wavelength.

Due to equations (2) and (3) being symmetric, if one is satisfied, the other is as well. This allows us to combine the equations for convex and concave into one equation. The deformation criteria is therefore given by equation (4).

$$A \sin(x) \mp \upsilon L \leqslant \pm A \sin(x + \frac{1}{2}L) \tag{4}$$

Following this criteria it can be seen what the maximum amplitude is that can be followed by a slipper of specific length and deformation fraction. This can be seen in figure 5.

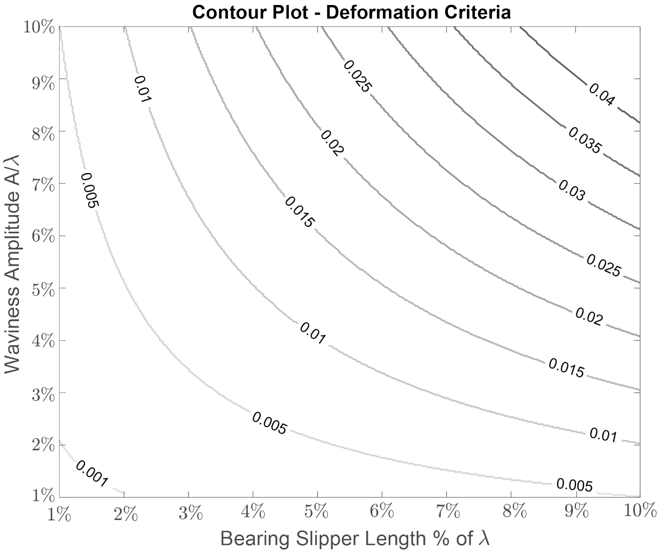

Fig. 5: Contour plot with varying slipper compliance. It shows the maximum running track waviness a slipper can follow for a given slipper length and slipper deformation factor. The waviness and slipper length are expressed relative to guiding surface wavelength. The contour lines give the axial deformation factor, the fraction of a slipper's length it can deform.

The contour plot in figure 5 shows it is possible to follow more wavy running tracks when the slipper is smaller. This is what was expected from figure 3. As was also expected, more compliant slippers are able follow guiding tracks with larger waviness. Thus all slippers must be very complaint. However, the deformation factor, υ, can not simply be increased. As mechanical failure, due to compression, must be investigated for more compliant slippers.

The effect of bearing compression can be complex but the main issue is the internal stress due to strain. A material with a lower Young's Modulus will be able to deform easier and therefore allow for a more compliant slipper. The possibility to increase compliance of a slipper without leading to mechanical failure is a research topic worked upon[10]. The focus of this paper is not investigating slipper deformation or development of compliant slippers. Therefore υ is used for axial deformation as in input parameter in the model.

III. Compliant distribution mechanism

Slipper size can be decreased to allow for wavier guiding tracks to be followed in exchange for lower load capacity. If multiple slippers are connected the load capacity is increased. This requires a mechanism that allows all slippers to follow the guiding surface while transferring the load. Thus a mechanism is wanted that can deform and distribute loads with high axial stiffness. These prerequisites are met by a whiffletree; a classical mechanism to distribute loads over multiple elements.

In a whiffletree the critical components are the pivot points, which have to transfer the axial load. If the pivot points are contact bearings, these will be subjugated to wear. The large deformable hydrostatic bearing is interesting because of its low wear, therefore introducing contact bearings is unwanted. Compliant pivots such as flexures are investigated as an alternative, since they do not experience wear through contact.

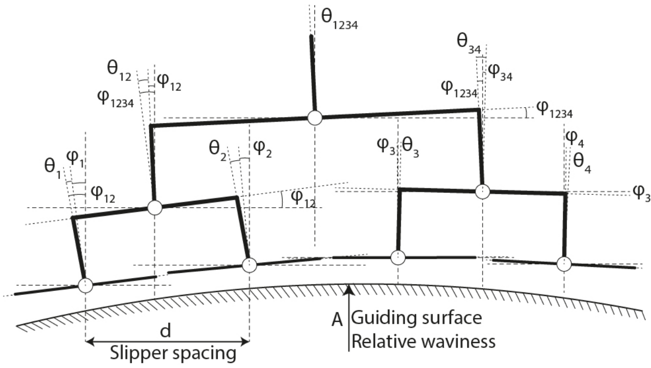

Fig. 6: Four slippers connected through a whiffletree-based mechanism. For illustrative purposes the pivot points are on the bottom of the connecting elements. The angles θ define the pivot angles. ϕ describe the angle of the slipper relative to the horizontal. Higher levels of ϕ, as ϕ_{12}, define the angle of the transverse connecting elements. The angles depend on the position of bearing on the curve, the amplitude of guiding surface and the distance between two slippers.

A geometric symmetrical whiffletree is used to model the behaviour of the individual elements and the pivots. A symmetrical whiffletree has been chosen as it would require less unique elements, making it easier to design and to be understood. An example of such a whiffletree based mechanism can be seen in figure 6. The position of one slipper to the next is fixed by the mechanism, so its position in space is given by equation (5).

$$\begin{aligned} L_f^2 &= (x_2 - x_1)^2 + (y_2 - y_1)^2 \\ &= (x_2 - x_1)^2 + A^2(\sin(x_2) - \sin(x_1))^2 \end{aligned} \tag{5}$$

Here, L_f is the length between the two slippers and x_i, y_i respectively the x and y position of a slipper on the guiding surface, normalized to a single wavelength. The slipper follows the guiding track $y_i = A\sin(x_i)$, where A is the relative waviness of the running track. Index i notes the slipper number. Equation (5) shows that the relation for the position of two connected slippers is non-linear. There is therefore no explicit solution for the position of the second slipper relative to the first. If we make a simplification that the relative waviness amplitude between the two slippers is small, then the position of x_2 van be defined as $x_2 = x_1 + L$. This introduces an error but allows for a kinematic description.

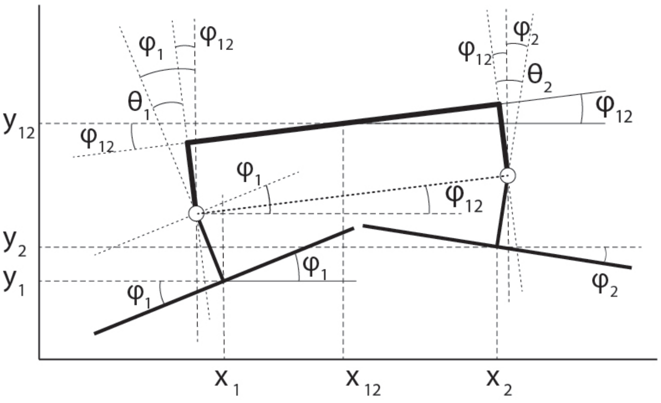

Fig. 7: Two slippers connected to each other through perpendicular rigid beam elements. The pivot points are found in the middle of the vertical elements. This is one cell (or branch) of a symmetrical whiffletree

A single cell (or branch) of this whiffletree is seen in figure 7. From this geometry the kinematic description is further defined. The angles of connecting elements are directly coupled to the position the two slippers and influencing the angles of the pivot points. The assumption has been made that the length of the transverse connecting elements are equal to the length of an individual slipper. The axial connecting elements are equal to half this length. These are design parameters which later be optimized and depend on the type of pivot joint. The angles are thus defined as:

$$\phi_1 = \arctan(A\cos(x_1)) \tag{6}$$

$$\phi_{12} = \arctan \frac{x_1 - \frac{L}{4}\sin(\phi_1) - x_2 - \frac{L}{4}\sin(\phi_2)}{y_2 + \frac{L}{4}\cos(\phi_2) - y_1 + \frac{L}{4}\cos(\phi_1)} \tag{7}$$

$$\theta_1 = \phi_1 - \phi_{12} \tag{8}$$

The position of the slipper is used to define the slipper angle. The slipper must be under this angle to remain parallel to the guiding surface. This angle is then used to calculate the angle of the pivot points. These pivot angles are the difference between the angle of the slipper and the angle of the connecting element. This can later be expanded to other slippers and to all whiffletree branches, as all cells can be connected like the two slipper cell from figure 7. This cell will be connected to a second cell with two other slippers. The pivot connecting the element that connects the entire mechanism to the axial load should provide the remaining angular rotation.

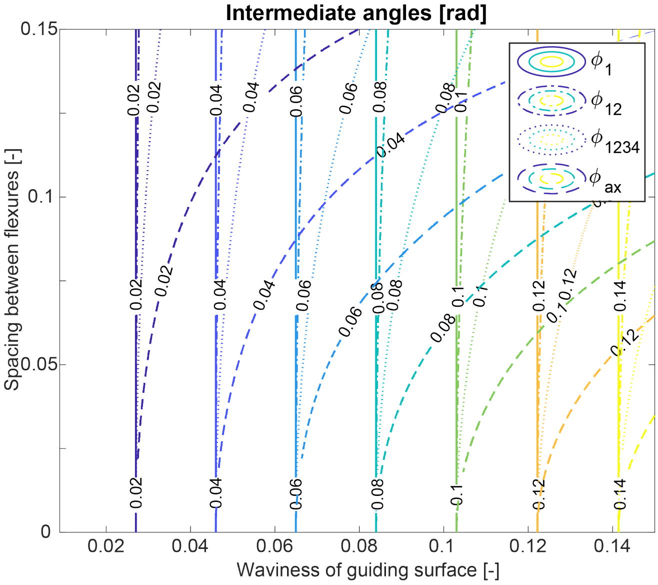

Fig. 8: Angles of intermediate bodies as a function of waviness amplitude and distance between the slippers for an eight slipper whiffletree mechanism.

As seen in figure 6, for all positions of the bearing system on the guiding surface, the angles of the slippers and the connecting elements are defined. While a description of all angles is known, interest lies only in the maximum angles. To understand the relationship between slipper length, waviness and the maximum angles an eight slipper whiffletree is modeled. This number has been chosen as it can clearly show the effects of having a large number of slippers while remaining easily interpreted. In figure 8 a contour plot shows the maximum angles of ϕ.

The angles of the level connected to the slipper is given by ϕ_1 analog to figure 6 and 7. For small distances between the bearings, the angles of all intermediate bodies ϕ_i are equal to A. Similarly, it can be seen that for a small bearing all angles of the intermediate bodies are equal to one another. Finally, the maximum angle grows to be as large as the maximum waviness and only decreases if the distance between slippers increases.

The angles of the intermediate bodies are dummy variables. Only used to calculate the pivot angles and to give insight on where the underlying structure and patterns of pivot angles come from. Figure 9 shows the pivot angles are clearly the difference between multiple whiffletree levels, which can only be seen seeing it side by side with figure 8. In the first level the pivot of this cell is denoted as θ_1, that connects two bearing slippers to one intermediate body as seen in figure 7. The uppermost level connects the entire bearing to the axial load, therefore it must provide for remaining rotation. This angles is denoted as θ_{ax}. The maximum angle of this last level pivot clearly shows a decrease when the maximum angles of the lower level pivot angles increases.

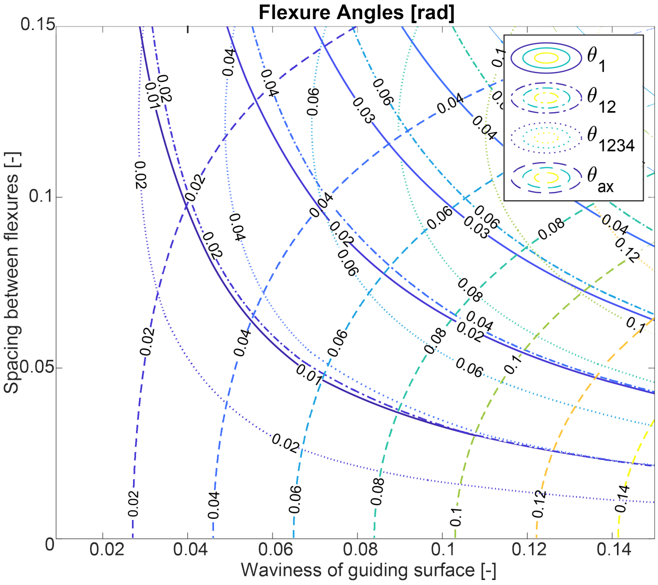

Fig. 9: The maximum pivot angles as function of waviness amplitude and distance between the slippers for an eight slipper whiffletree mechanism.

IV. Constraints and limitations

The complete model consists of multiple models of physical behaviour which cannot be altered. Only the input values and the constraints can be changed. The collection of models that combine into a description of the deforming hydrostatic bearing can be seen in figure 10. Each of these coloured blocks is either a piece of modeled physics presented before, or a model constraint.

The purple block represents the deformation criteria model as defined in section II. The input variables of relative waviness amplitude and axial bearing deformation give us the maximum bearing slipper size that can be placed on a certain guiding surface. This maximum length is used as input for other models.

The hydrostatic bearing model for a single slipper relates load capacity and bearing tilt stiffness to film height, which is the input. Film thickness influences recess pressure, and slipper length is determined by the deformation criteria, for which relative waviness amplitude and deformation factor are required.

And slipper length leads to the maximum pivot angles for a whiffletree on a wavy guide surface. This is given by the kinematics described in equations (6)-(8).

So within the model all parameters are connected and influence each other. With the input parameters known, the

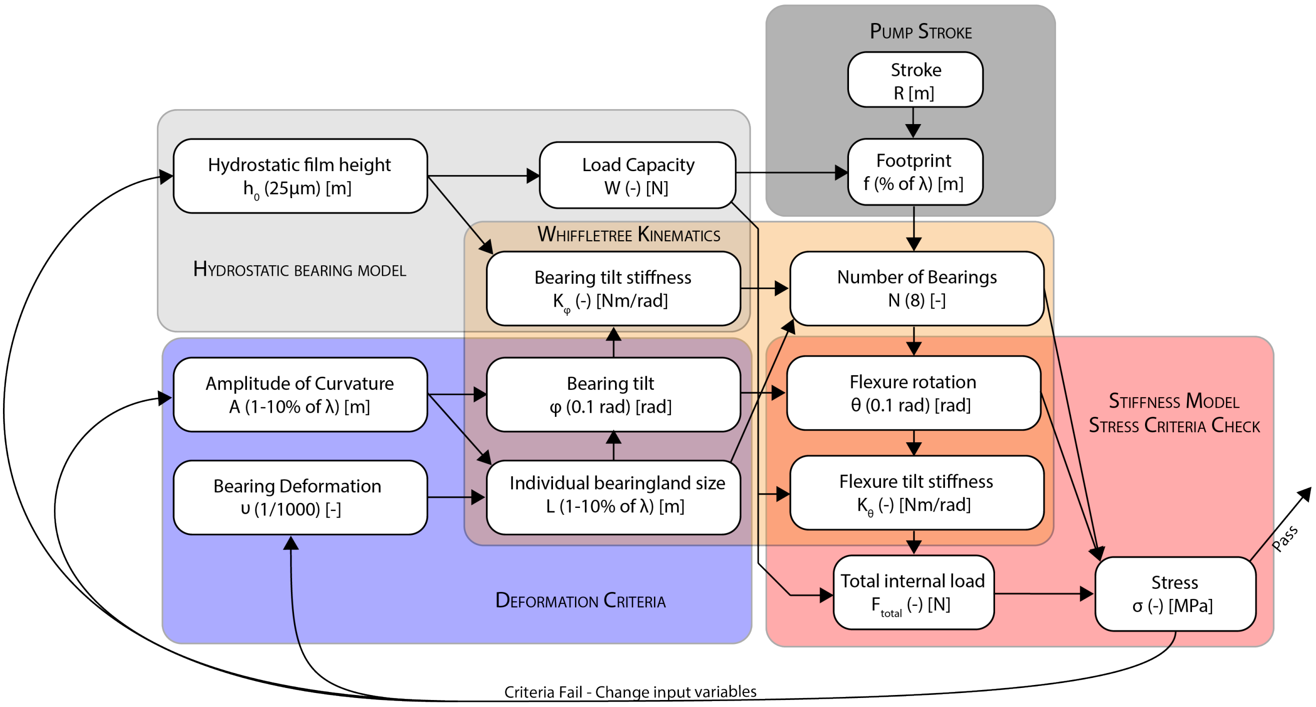

Fig. 10: Overview of models and relationships used, each of the colored blocks are a model explained in a section of this paper.

system requires constraints and limitations. The final step in the model is to check the stress levels. These are dependent on the type of pivot and slipper implementation. Therefore a case study for a large deforming hydrostatic bearing, implementing cross flexures and multi-recess orifice bearings system, will be presented.

The complete model can be seen as an optimization where e.g. the axial load can be maximized, while having the following constraints:

1) Rotational stiffness joints much lower than tilt stiffness of single slipper to maintain parallel film
2) Deformation criteria must be met in order to to maintain parallel film between slipper and guiding surface
3) Pivot stress levels under endurance limit of pivot material to prevent mechanical failure
4) Footprint of bearing must be constraint

A. Footprint Constraint

The footprint relation is the only constraint that is not within any of the aforementioned models.This is caused by the dependancy on the application. A large footprint increases load capacity. A small footprint however increases axial displacement, which is desired in for example pumps. This constraint is thus dependent on the designer and the desired application.

For a bearing perfectly following the guiding surface, its stroke could be determined through equations (9)-(11). Assuming a symmetric guiding surface, the stroke is given the following set of equations:

$$r_{\text{Stroke}} = y_{\text{max,tot}} - y_{\text{min,tot}} \tag{9}$$

$$y_{\text{max,tot}} = \frac{1}{(\frac{\pi}{2}+\frac{f}{2})-(\frac{\pi}{2}-\frac{f}{2})}\int_{\frac{\pi}{2}+\frac{f}{2}}^{\frac{\pi}{2}-\frac{f}{2}} A\sin(x)\mathrm{d}x \tag{10}$$

$$= \frac{A}{f}\sin(\frac{f}{2}) \tag{11}$$

This can give an extra constraint on the footprint, in these equations denoted as f; the summation of all relative slipper lengths. The optimization process could optimize for work done instead of maximizing load capacity. Depending on the application the model could provide or optimize for other parameters. Equations (12) and (13) show the relationship and equation (14) concludes for footprints smaller than a single wavelength, the work done is maximum at about $\sim$ 64% guiding surface coverage.

$$\text{W} = r_{\text{Stroke}} \cdot F_{\text{axial}} \tag{12}$$

$$y_{\text{max,tot}} = -y_{\text{min,tot}} \tag{13}$$

$$\text{W} \propto 2\frac{A}{f}\sin(\frac{f}{2})P_r f b \bar{A}$$

$$\text{W} \propto Af\sin(\frac{f}{2}) \tag{14}$$

In equation (14) b is defined as the slipper width, which has been set to be equal as half of the slipper length. Therefore f and b both depend on slipper length.

V. Compliant pivot implementation

The pivots must transfer all load from the lower levels up to the highest level. The load on to the bearing must be transferred through the pivots, the intermediate bodies and down to the individual hydrostatic slippers. The bearing thus requires a high axial stiffness. It has been noted that these pivots require a rotational stiffness which is much lower than the tilt stiffness of the slippers in order to prevent mechanical contact. The maximum rotation these pivots will have to make are found in figure 9. These are relatively small rotations under large loads which will lead to hertz stresses, which lead to wear. Therefore, reintroducing rolling contact to the bearing system is unwanted because it negates all the advantages of replacing a conventional roller bearing with a hydrostatic bearing. Compliant joints are investigated as an option for low wear, low rotational stiffness and high axial stiffness.

From previous studies it was concluded that cross flexures meet these requirements[14]. Notch flexures would not be able to make the rotation that is expected. Complex variations like the butterfly hinges[15] or Flex-16[16] flexures use the working principle of a cross flexure. Many compliant pivoting elements have been developed yet the cross flexure stands out as one of the first and most understood [17]. Therefore cross flexures have been chosen to implement as pivot as it could be studied analytically, while these models are not present in literature for its complex counterparts. Figure 11 shows how cross flexures as pivots might be implemented. An approximation for stress levels for simple cross flexures has be found in literature[18], as seen in equation (15).

$$\sigma = \frac{Et}{2L_s}\theta + \frac{F_x}{tb_s} \tag{15}$$

Here the stress σ is calculated for the outer edge of the flexure using the flexure angle, denoted as θ. E is the Young's Modulus of the flexure material, t stands for the thickness of the flexure, F_x is the axial load on the flexure and L_s is the length of the flexure spring element. For a standard cross flexure the flexure elements are positioned under a 45° angle. Therefore, this length will be taken as $\sqrt{2}$ times the length of the element it supports. The flexure width is defined by the parameter b_s. The flexure is a as wide as the bearing allows it, which is equal to the width of the connecting element. As the flexure width wants to be as large as possible it is chosen half of slipper width, and the slipper width is taken as half of the slipper's length.

To distribute stresses more evenly over all flexures, it is recommended to choose a configuration for which not all of the rotation is done by just one of the flexures. Ideally all flexures make an equally large maximum rotation. It is likely to choose a configuration where the pivot points at the slipper end hold only a small rotation compared to the rotation of the pivot at the axial end. This will cause a larger stress concentration in the uppermost pivot, as seen in figure 9.

Up to this point, the stiffness has been assumed to be much smaller than the tilt-stiffness of the bearing. Equation (16) describes rotational stiffness for a cross flexure.

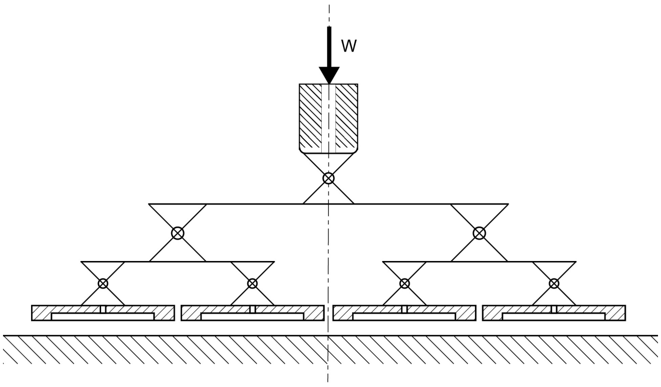

Fig. 11: Impression of hydrostatic bearing with whiffletree based distribution of four slippers using compliant cross flexure elements as pivots.

$$K_\theta = \frac{EI_{\text{total}}}{L_s} \tag{16}$$

In this equation I_{total} is the total moment of inertia of the flexure elements on which the moment is applied and L_s is the length of cross flexure spring elements.

These two equations are constraints on the entire bearing system, as tilt stiffness from figure 14 will be compared with the outcome of equation (16). Material properties will be compared to the outcome of stress equation (15).

The final step in the model is to check the stress levels. The stress levels of the flexures should be below the flexure material's endurance limit, the fatigue stress a material can handle for 10^6 cycles[8].

VI. Hydrostatic slipper implementation

The pivot's rotational stiffness must be much lower than the tilt stiffness of the slippers below it. As the tilt stiffness of the bearing is yet unknown this first has to be modeled. Therefore a hydrostatic slipper is set up to model load capacity, and with it, tilt stiffness.

The tilt stiffness of the bearing is modeled for a single slipper, assuming a multi-recess bearing with orifice flow restrictor. A multi-recess bearing, as seen in figure 12, has tilt stiffness achieved through individual fluid inlets. These individual flow restrictors give each recess a film stiffness independent of the other chambers[19].

The tilting of the slipper causes a film height difference between two sides of the slipper, as illustrated in figure 12. This inequality in film height causes a pressure difference over the bearing land of the slipper, and therefore results in a moment on the bearing. This moment is dependent on film height. Studies have been done on the tilting of multi-pad bearings[12], however a simplified description should be sufficient for choosing a pivot type. Simplifying the slipper recesses as separate rigid bearings, as seen in figure 13, gives the moment and tilt stiffness as follows:

$$M_\phi = F_{\text{left}}r_{\text{left}} + F_{\text{right}}r_{\text{right}} \tag{17}$$

$$K_\phi = \frac{\partial M_\phi}{\partial \phi} \tag{18}$$

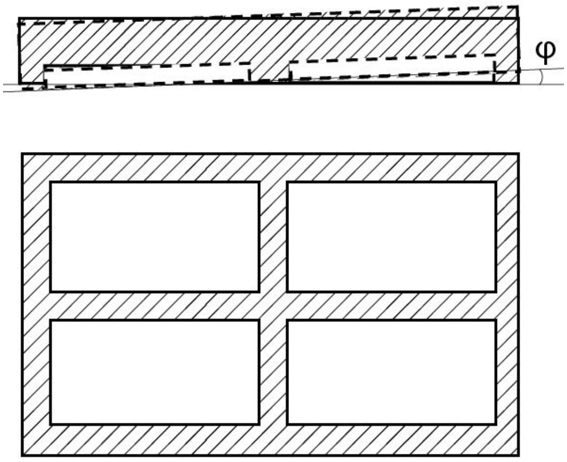

Fig. 12: A side section and bottom view of a multi-recess bearing tilting under an angle ϕ.

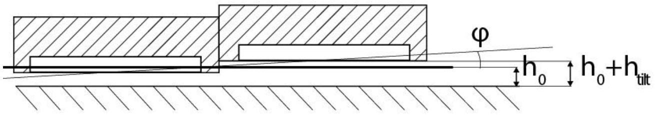

Fig. 13: A simplified model of bearing tilt of a multi-recess bearing. The original film height of the bearing without tilt would be $\mathrm{h_0}$, but due to tilt a difference of $\mathrm{h_{tilt}}$ is introduced.

In equation (17) r is the arm of the moment, as the recess bearing drawn is symmetric and only tilts over one axis. The distance on the left side is the exact opposite on that of the right. The force is a function of recess pressure, as known from equation (1). Equation (19) calculates the recess pressure for a multi-recess orifice bearing as defined by Rowe [1]. With this, the complete film stiffness is set up. In figure 14 the axial stiffness and tilt stiffness can be seen dependent on film height.

$$P_r = \frac{\sqrt{1 + 4P_s \frac{\rho}{2(C_o A_o)^2}(\frac{\bar{B}h^3}{\eta})^2}}{2\frac{\rho}{2(C_o A_o)^2}\frac{\bar{B}h^3}{\eta}} \tag{19}$$

In equation (19) the parameters are filled in to give an order of magnitude estimation. A supply pressure $[P_s]$ of $10\,\mathrm{bar}$ is used. The dynamic viscosity $[\eta]$ of water is $1.002\,\mathrm{MPa\,s}$. And for the orifice parameters C_o and A_o the values 0.55 and $1\,\mathrm{mm}^2$ are used respectively.

This model corresponds with the expectation that load capacity scales linear with bearing size and tilt stiffness is proportional to the bearings size, L, to the forth power. Figure 14 shows that even for large film thicknesses, $50\,\mathrm{\mu m}$, the tilt stiffnesses of the slippers are $500\,\mathrm{N\,m\,rad^{-1}}$ and $50\,\mathrm{MN\,m\,rad^{-1}}$ for the $10\,\mathrm{mm}$ and $100\,\mathrm{mm}$ slipper sizes respectively. Therefore these will be the values used to compare tilt stiffness with rotation stiffness of the pivots.

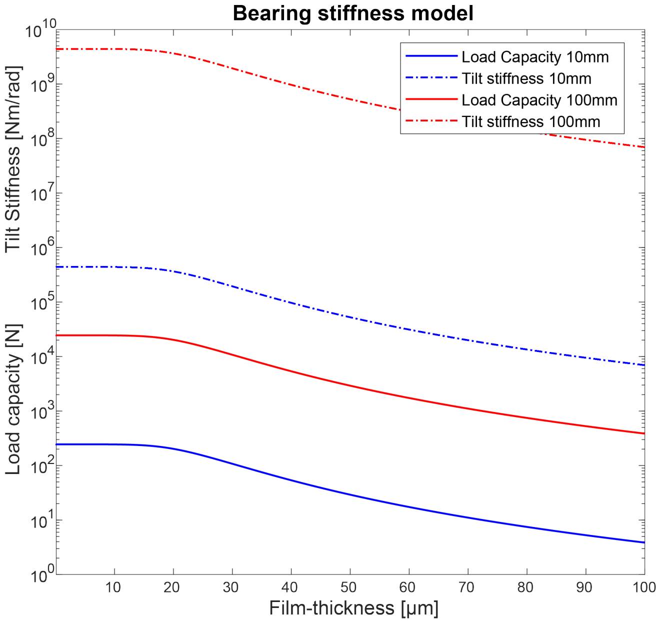

Fig. 14: Film Stiffness and tilt stiffness curve for rectangular multi recess bearings. With $\bar{A}$ of 0.78 and $\bar{B}$ of 2.23.

VII. Case Study and Results

Implementing multi-recess bearings as slipper and cross flexure as compliant joints grants us insight into a complete deforming hydrostatic bearing. For this example we are maximizing the load using a total of eight slippers. The eight slippers require four levels of cross flexures, as seen in figure 15. The load capacity is increase until it in combination with the stress due to bending is too large for the flexure. As mechanical failure is presumed to occur as it crosses the threshold for endurance limit of steel, in this case is defined as $270\,\mathrm{MPa}$[20]. A waviness amplitude of the guiding surface which has to be followed is chosen to be 2% of the wavelength. Assuming a wavelength of a meter this is a $40\,\mathrm{mm}$ peak/valley. With the deformation factor υ of 0.001 this gives a maximum single slipper size of $10\,\mathrm{mm}$ to maintain a parallel film.

Matching this design the maximum angle the flexure element has to make is $0.6°$. The flexures are made out of spring steel with a young's modulus of $200\,\mathrm{GPa}$ with a thickness of $1\,\mathrm{mm}$. The flexures are at a $45°$ angle from one another, and with flexure length equal to slipper length. For the $0.6°$ the functions for stress and stiffness found in literature can still be used, but these will become inaccurate for larger angles due to non-linearity. Filling the chosen flexure values into equation (16), gives a rotation stiffness of $16.66\,\mathrm{N\,m\,rad^{-1}}$. Which is lower than the tilt stiffness of $500\,\mathrm{N\,m\,rad^{-1}}$. However, the difference is only one order of magnitude so the film thickness might be influenced, it is recommended to decrease flexure stiffness if stress levels allow it.

For this configuration a film thickness of $95\,\mathrm{\mu m}$ is found, corresponding to a load capacity of single slipper of $6.7\,\mathrm{N}$. And for this film thickness the tilt stiffness of a multi-recess bearing is larger than the rotational stiffness found, as seen in figure 13. The model has now given us maximum loading

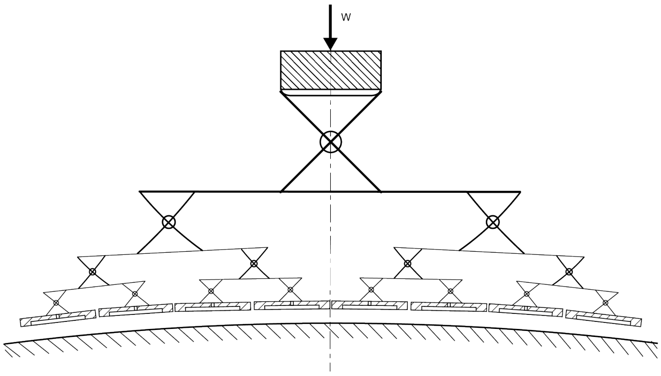

Fig. 15: Whiffletree-based distribution of eight deformable slippers. Note that dimensions as amplitude, slipper size and flexures size are not to scale with the case study and slippers are illustrated as single-recess bearings.

capacity, $53.72\,\mathrm{N}$, for an eight slipper whiffletree, with slippers of $20\,\mathrm{mm}$, which are capable of following a $20\,\mathrm{mm}$ amplitude wavy guiding tracks.

This is one possible design, from this one example it is impossible to make conclusion on whether altering a parameter will lead to failure or not. It was chosen to visualise this in a Matlab[21] Graphical User Interface, as seen in figure 16. The parameters are connected as visualised by figure 10 and utilises all modeling principles presented in this paper.

VIII. Conclusion

This work showed the use of a pivot to increase wavy guiding surface following capabilities of deformable hydrostatic slippers. The combination of these two topics within a whiffletree improved the working range of deforming hydrostatic bearings. The whiffletree concept is feasible for applications if the main goal is to have a waviness following hydrostatic bearing. However, as shown there are limitations to this concept. The load carrying capacities are not on par with the alternatives, as stress in both flexures and slipper is limiting.

The model shows an increase in slipper compliance is needed to further increase the maximum waviness the slippers can follow without decreasing their size. The other limitation is caused by stress limitations in the compliant pivot. In the case study, the stress levels in the compliant flexure exceed the maximum allowed endurance limit if either axial forces or waviness was further increased.

For a whiffletree-based design there is a trade-off between loading capacity and deformability. The priority in the case study was given to deformability to follow a certain waviness guiding surface, therefore the loading capacity is low. Choosing a higher loading capacity would have decreased the maximum waviness that could have been followed. And the design choice to maximize work per stroke can be made, here in it is wanted to increase both waviness and load capacity.

IX. Discussion

This trade-off can be further used to change parameters or design choices to optimize for either deformability or load capacity. In this section, recommendations for such design choices are presented. As figure 5 showed, if the individual slipper's compliance improves it is possible to further increase the capability to follow wavy guiding surfaces. And as stress levels in flexure prove to be problematic, these could be replaced by alternatives better able to handle large loads. Therefore further work is required on both individual slipper deformation and the creation of a compliant joint for high loading conditions.

Cross flexures in the case study are loaded in compression. However, the design could be adjusted to load the flexures in tension. This might decrease chance on mechanical failure. A design can also be chosen to adjust the rotation point, which might decrease the maximum pivot angle[22]. Cross flexure were chosen from literature but, alternatives are available[14]. Q-LIFT pivots could provide lower stress levels when the rotation is the dominant cause of stress[16]. If the axial loading is the main cause of stress then pivots such as compliant rolling contact elements could be implemented instead of a pure compliant flexure. These are far more capable of handling high loading capacity and maintain low rotational stiffness[23][24].

However the concept of the large deforming mechanism could also be changed. This design is based on the classical whiffletree, but with more research being done in mechanisms, it shows alternatives and promising enhancements. An alternative deforming distribution mechanism could be a zero potential energy system[25], that it could easily take all shapes, while maintaining axial stiffness[26]. A zero stiffness mechanism was considered but not worked out as current understanding on kinematics was insufficient and as overall limitations were yet unknown. The kinematics were investigated for a symmetrical whiffletree for which all slipper were continuously parallel to the guiding surface, yet it might be possible to have a bearing with some non-parallel slippers, but with the system as a whole still maintaining full film lubrication. In these cases non-asymmetrical whiffletrees might provide require less angular rotation, resulting in lower stress levels. For a symmetrical guiding surface there no advantages were seen to develop a non-symmetrical whiffletree concept and was therefore not investigated.

An alternative mechanism could be pressure vessels, using the hydraulics fluids providing the support film to pressurize chambers within the elastic bearing support. This could provide hydrostatic slippers with increased compliance[10]. And these might be used as pivots where the pressurized chambers could move fluid to tilt, while maintaining axial stiffness. Therefore the pressure vessel itself becomes a hydrostatic pivot with high axial stiffness and low rotational stiffness.

References

1 Rowe, W. B., *Hydrostatic, Aerostatic and Hybrid Bearing Design.* Elsevier, 2012. [Online]. Available: https://doi.org/10.1016/c2011-0-07331-3

2 van Ostayen, R. A., van Beek, A., and Ros, M., "A mathematical model of the hydro-support: an elasto-hydrostatic thrust bearing with mixed lubrication," *Tribology International*, vol. 37, no. 8, pp. 607–616, aug 2004. [Online]. Available: https://doi.org/10.1016/j.triboint.2004.01.008

3 Ertas, B. H., "Compliant hybrid journal bearings using integral wire mesh dampers," *Journal of Engineering for Gas Turbines*

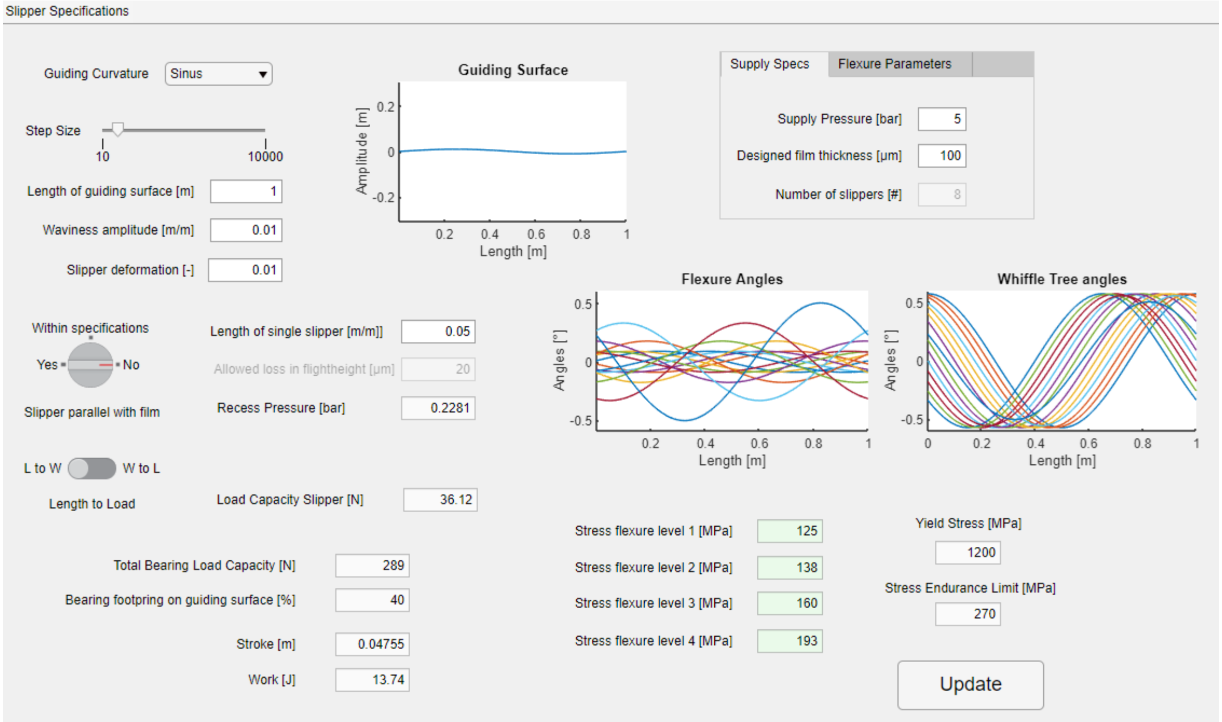

Slipper Specifications

Guiding Curvature: Sinus

Step Size

Length of guiding surface [m]: 1

Waviness amplitude [m/m]: 0.01

Slipper deformation [-]: 0.01

Within specifications: Yes No

Slipper parallel with film

L to W / W to L

Length to Load

Length of single slipper [m/m]]: 0.05

Allowed loss in flightheight [μm]: 20

Recess Pressure [bar]: 0.2281

Load Capacity Slipper [N]: 36.12

Total Bearing Load Capacity [N]: 289

Bearing footpring on guiding surface [%]: 40

Stroke [m]: 0.04755

Work [J]: 13.74

Supply Specs | Flexure Parameters

Supply Pressure [bar]: 5

Designed film thickness [μm]: 100

Number of slippers [#]: 8

Stress flexure level 1 [MPa]: 125

Stress flexure level 2 [MPa]: 138

Stress flexure level 3 [MPa]: 160

Stress flexure level 4 [MPa]: 193

Yield Stress [MPa]: 1200

Stress Endurance Limit [MPa]: 270

Fig. 16: Screenshot of the graphical user interface. With an automated set of variables that meet both stress and deformation criteria.

and Power, vol. 131, no. 2, p. 022503, 2009. [Online]. Available: https://doi.org/10.1115/1.2967476

4 Liu, Z., Wang, Y., Cai, L., Zhao, Y., Cheng, Q., and Dong, X., "A review of hydrostatic bearing system: Researches and applications," *Advances in Mechanical Engineering*, vol. 9, no. 10, p. 168781401773053, Oct. 2017. [Online]. Available: https://doi.org/10.1177/1687814017730536

5 Manring, N. D., Johnson, R. E., and Cherukuri, H. P., "The impact of linear deformations on stationary hydrostatic thrust bearings," *Journal of Tribology*, vol. 124, no. 4, p. 874, 2002. [Online]. Available: https://doi.org/10.1115/1.1482118

6 Qi, E., Fang, Z., Sun, T., Chen, J., Liu, C., and Wang, J., "A method for predicting hydrostatic guide error averaging effects based on three-dimensional profile error," *Tribology International*, vol. 95, pp. 279–289, Mar. 2016. [Online]. Available: https://doi.org/10.1016/j.triboint.2015.11.032

7 Nijssen, J., Diepeveen, N., and Kempenaar, A., "Development of an interface between a plunger and an eccentric running track for a low-speed seawater pump," 06 2018.

8 van Beek, A. and Delft, T. U., *Advanced Engineering Design: Lifetime Performance and Reliability*. TU Delft, 2006. [Online]. Available: https://books.google.nl/books?id=NKGDOAAACAAJ

9 van Beek, A. and Lepic, L., "Rubber supported hydrostatic thrust bearings with elastic bearing surfaces of infinite length," *Wear*, vol. 201, no. 1-2, pp. 45–50, dec 1996. [Online]. Available: https://doi.org/10.1016/s0043-1648(96)06987-6

10 Nijssen, J. and van Ostayen, R., "Open form pressure balancing for compliant hydrostatic thrust bearings," in *Advances in Mechanism and Machine Science*. Springer International Publishing, 2019, pp. 3965–3974. [Online]. Available: https://doi.org/10.1007/978-3-030-20131-9_395

11 Howell, L. L., Magleby, S. P., and Olsen, B. M., Eds., *Handbook of Compliant Mechanisms*. John Wiley & Sons Ltd, Feb. 2013. [Online]. Available: https://doi.org/10.1002/9781118516485

12 van Beek, A. and van Ostayen, R., "Analytical solution for tilted hydrostatic multi-pad thrust bearings of infinite length," *Tribology International*, vol. 30, no. 1, pp. 33–39, Jan. 1997. [Online]. Available: https://doi.org/10.1016/0301-679x(96)00019-9

13 Ashour, N., Athre, K., Nath, Y., and Biswas, S., "Distortion analysis of large thrust bearing on elastic support," *Wear*, vol. 147, no. 2, pp. 421–430, Jul. 1991. [Online]. Available: https://doi.org/10.1016/0043-1648(91)90196-2

14 Machekposhti, D. F., Tolou, N., and Herder, J. L., "A review on compliant joints and rigid-body constant velocity universal joints toward the design of compliant homokinetic couplings," *Journal of Mechanical Design*, vol. 137, no. 3, p. 032301, jan 2015. [Online]. Available: https://doi.org/10.1115/1.4029318

15 Pei, X., Yu, J., Zong, G., and Bi, S., "A family of butterfly flexural joints: Q-LITF pivots," *Journal of Mechanical Design*, vol. 134, no. 12, p. 121005, Nov. 2012. [Online]. Available: https://doi.org/10.1115/1.4007917

16 Fowler, R. M., Maselli, A., Pluimers, P., Magleby, S. P., and Howell, L. L., "Flex-16: A large-displacement monolithic compliant rotational hinge," *Mechanism and Machine Theory*, vol. 82, pp. 203–217, Dec. 2014. [Online]. Available: https://doi.org/10.1016/j.mechmachtheory.2014.08.008

17 Haringx, J. A., "The cross-spring pivot as a constructional element," *Flow, Turbulence and Combustion*, vol. 1, no. 1, Dec. 1949. [Online]. Available: https://doi.org/10.1007/bf02120338

18 Smith, S. T., *Flexures*. CRC Press, apr 2014. [Online]. Available: https://doi.org/10.1201/9781482282962

19 Bassani, R. and Piccigallo, B., Eds., *Hydrostatic Lubrication*, ser. Tribology Series. Elsevier, 1992. [Online]. Available: https://doi.org/10.1016/s0167-8922(08)x7005-1

20 "Engineering toolbox, (2011). steels - endurance limits and fatigue stress - accessed 19 april 2019." [Online]. Available: https://www.engineeringtoolbox.com/steel-endurance-limit-d_1781.html

21 "Matlab v. r2017a https://www.mathworks.com/products/matlab.html, mathworks, natick, massachusetts, united states."

22 *Janssen precision engineering*, 2018. [Online]. Available: https://www.janssenprecisionengineering.com/page/cross-flexure-or-cross-spring-pivot/

23 Cannon, J. R., Lusk, C. P., and Howell, L. L., "Compliant rolling-contact element mechanisms," in *Volume 7: 29th Mechanisms and Robotics Conference, Parts A and B*. ASME, 2005. [Online]. Available: https://doi.org/10.1115/detc2005-84073

24 Montierth, J. R., Todd, R. H., and Howell, L. L., "Analysis of elliptical rolling contact joints in compression," *Journal of Mechanical Design*, vol. 133, no. 3, p. 031001, 2011. [Online]. Available: https://doi.org/10.1115/1.4003499

25 Schenk, M. and Guest, S. D., "On zero stiffness," *Proceedings of the Institution of Mechanical Engineers, Part C: Journal of Mechanical Engineering Science*, vol. 228, no. 10, pp. 1701–1714, Nov. 2013. [Online]. Available: https://doi.org/10.1177/0954406213511903

26 Tarnai, T., "Zero stiffness elastic structures," *International Journal of Mechanical Sciences*, vol. 45, no. 3, pp. 425–431, Mar. 2003. [Online]. Available: https://doi.org/10.1016/s0020-7403(03)00063-8

Elaboration on kinematic models

In the previous chapter relations were given and set up, the following sections elaborate on the mathematical derivations such that design choices are better understood and recreating the results will become easier.

Derivation of Deformation Criteria

Chapter II introduced the deformation criteria based on the principle that a hydrostatic slipper could deform a fraction of it's length, a that this deformation would not lead to mechanical failure of the hydrostatic slipper. Using this deformation principle allows the modeling of deformations to be done as in figure 6.1.

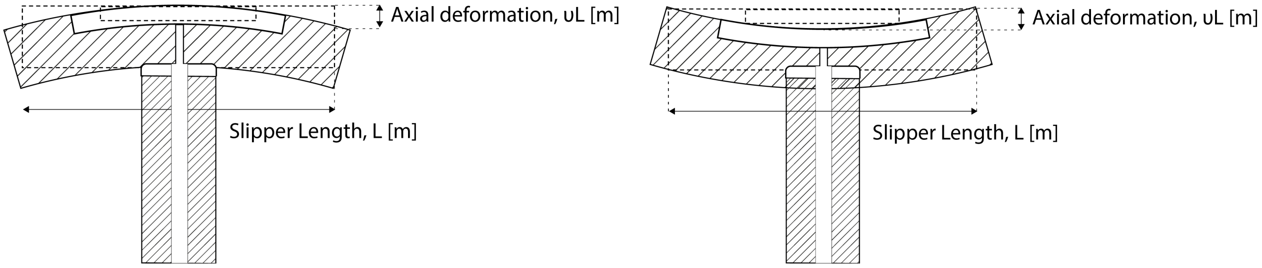

(a) A hydrostatic slipper deforming to a concave shape

(b) A hydrostatic slipper deforming to a convex shape

Figure 6.1: Hydrostatic bearing deformation is being modeled using the axial deformation factor υ for both convex and concave deformations

Combined with a sine curve as the guiding surface, the requirement to maintain parallel film can be defined. A parallel film is maintained if the bearing surface deforms an equal amount as the guiding surface. A simplified version of convex deformation from figure 6.1b is illustrated in figure 6.2. This clearly shows that axial deformation times the length should match the height difference on this point. This point is given by half a slipper length from the point of zero deformation. This leads to x_L being defined as in equation (6.1). Using the definition for the guiding surface from figure 4.3 and y-position of the middle of the bearing on guiding surface from equation (4.3), the left or right y-position of the bearing on the guiding surface is defined in equation (6.3).

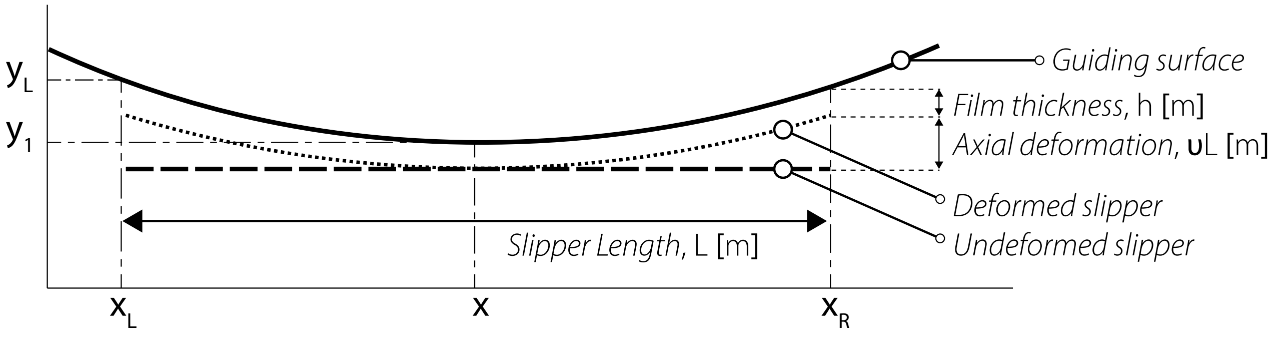

Figure 6.2: Representation of convex deforming bearing on wavy surface, on which the deformation criteria is based.

$$x_{\mathrm{L}} = x_1 - \frac{L}{2} \tag{6.1}$$

$$x_{\mathrm{R}} = x_1 + \frac{L}{2} \tag{6.2}$$

$$y_{\mathrm{L}} = sA \sin s x_{\mathrm{L}} \tag{6.3}$$

$$y_{\mathrm{R}} = sA \sin s x_{\mathrm{R}} \tag{6.4}$$

The scaling factor introduced in chapter 4 is applied. Note that from this point on wards this scaling is automatically implied. As stated, the bearing must deform equal to the guiding surface curving away, which is checked for the left and right-side most points of the bearing. As the curving away of the guiding surface is the most extreme as long as our slipper is less than a quarter of a wavelength. With the use of pivots, the undeformed bearings can be described by a tangent line position x_1. This is the middle of the bearing from which the tangent line is set up, as explained in chapter 4. This will allow us to set up the deformation criteria for both concave and convex curvature. Using the assumption that film thickness is negligible, y_1 is both the y-position of the guiding surface and the y-position of the middle of the bearing. The deformation cases for the peaks and valleys of the guiding surfaces are investigated. Here the deformation required will be largest, as proven in appendix C. On this position, the deformed bearing position is the bearing position, x_1 plus or minus vL. Equations (6.5) and (6.6) describe the deformed bearing positions for these symmetric positions.

$$y_{\text{LB}} = A\sin x_1 \pm vL \tag{6.5}$$

$$y_{\text{RB}} = A\sin x_1 \pm vL \tag{6.6}$$

In these equations the scaling factor s has already been applied, thus A is the Relative Waviness Amplitude, L is the length as a fraction of the wavelength and x_1 is the relative x-position. The subscripts LB and RB stand for Left-side Bearing and Right-side Bearing. y_{LB} gives the y-position of the left side of the slipper for maximum deformation. When positioning the bearing underneath the guiding surface as in figure 6.2 with a sine wave as the guiding surface, convex bending of the guiding surface will occur for $\pi \le x \le 2\pi$, similarly, concave deformation will occur for $0 \le x \le \pi$. For the convex bending y_{B}, the y-position of the bearing must be equal or larger than the y-position of the guiding surface. For concave deformation, the slipper should bend away, thus the y-position of the bearing should be lower or equal to the y-position of the guiding surface. This is written down in equations (6.7)-(6.14).

$$y_{\text{LB}} \ge y_{\text{L}} \quad \Rightarrow \{0 \le x_L \le \pi\} \tag{6.7}$$

$$y_{\text{RB}} \ge y_{\text{R}} \quad \Rightarrow \{0 \le x_R \le \pi\} \tag{6.8}$$

$$y_{\text{LB}} \le y_{\text{L}} \quad \Rightarrow \{\pi \le x_L \le 2\pi\} \tag{6.9}$$

$$y_{\text{RB}} \le y_{\text{R}} \quad \Rightarrow \{\pi \le x_L \le 2\pi\} \tag{6.10}$$

$$A\sin x_1 + vL \ge A\sin x_1 - \frac{L}{2} \quad \Rightarrow \{0 \le x_R \le \pi\} \tag{6.11}$$

$$A\sin x_1 + vL \ge A\sin x_1 + \frac{L}{2} \quad \Rightarrow \{0 \le x_L \le \pi\} \tag{6.12}$$

$$A\sin x_1 - vL \le A\sin x_1 + \frac{L}{2} \quad \Rightarrow \{\pi \le x_R \le 2\pi\} \tag{6.13}$$

$$A\sin x_1 - vL \le A\sin x_1 - \frac{L}{2} \quad \Rightarrow \{\pi \le x_L \le 2\pi\} \tag{6.14}$$

Due to symmetry $y_L = y_R$, this was already seen in equations (6.5) and (6.6). Because of the symmetry, the left side of the slipper equals the right side. For these positions $x_1 = \frac{\pi}{2} \vee \frac{3\pi}{2}$, equation (6.11) is equal to equation (6.12), and equation (6.13) equals equation(6.14). And these can then be further be simplified and using that the relations that $A\sin\frac{1}{2}\pi = -A\sin\frac{3}{2}\pi = A$. And using the definition that $\le$ equals $-\ge$, allows us to write the concave and convex deformation the same, as seen in equations (6.15)-(6.17).

$$A + vL \ge A\sin\left(\frac{\pi}{2} + \frac{L}{2}\right) \quad \Rightarrow \left\{x = \frac{1}{2}\pi\right\} \tag{6.15}$$

$$-A - vL \le A\sin\left(\frac{3\pi}{2} + \frac{L}{2}\right) \quad \Rightarrow \left\{x = \frac{3}{2}\pi\right\} \tag{6.16}$$

$$-A - vL \le -A\sin\left(\frac{\pi}{2} + \frac{L}{2}\right) \tag{6.17}$$

Therefore, it can be concluded that if either the top or bottom is checked, both will pass the deformation criteria and thus the bearing will be parallel for all positions on the guiding surface.

$$x_{\text{RB}} = x_1 + L\cos\phi + vL\sin\phi \quad \Rightarrow \{0 \le x_1 \le \pi\} \tag{6.18}$$

$$x_{\text{RB}} = x_1 + L\cos\phi - vL\sin\phi \quad \Rightarrow \{\pi \le x_1 \le 2\pi\} \tag{6.19}$$

$$y_{\text{RB}} = A\sin x_1 + L\sin\phi - vL\cos\phi \quad \Rightarrow \{0 \le x_1 \le \pi\} \tag{6.20}$$

$$y_{\text{RB}} = A\sin x_1 + L\sin\phi + vL\cos\phi \quad \Rightarrow \{\pi \le x_1 \le 2\pi\} \tag{6.21}$$

For this statement to be true, it has to be checked that deformation is largest on the peaks and valleys. For this it is first required to set up the deformed slipper for non-symmetrical positions. As the bearings are symmetric, the bearing deformation can be simplified by only using the right side of the deforming slipper. As the previous equations already showed the symmetry of the deforming slipper. Equations (6.18) to (6.21) are the coordinates of the right side of the deformed slipper as defined in 6.3, for convex and concave deformations.

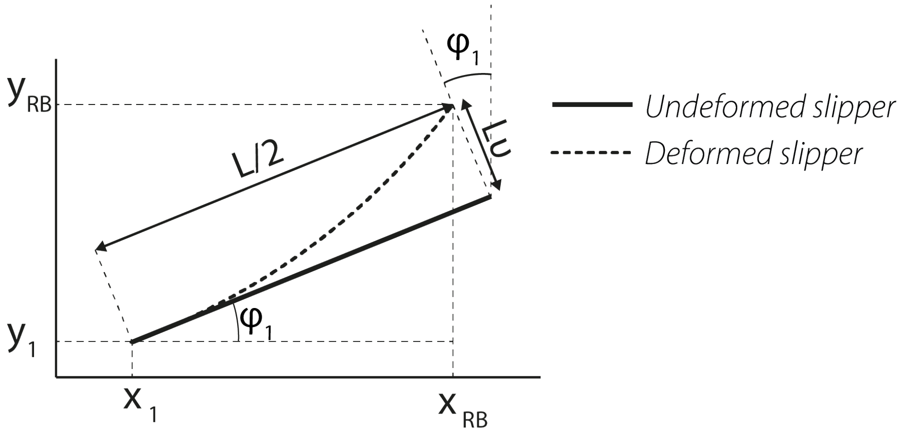

Figure 6.3: Illustration used to define the position of the most right side of the deformed slipper for convex shapes, thus valid from $\pi \leq x \leq 2\pi$

$$y_{\mathrm{R}} = Asin\left(x_1 + L\sin\phi\right) \tag{6.22}$$

$$-vL\cos\phi \quad \Rightarrow \{0 \leq x_1 \leq \pi\} \tag{6.23}$$

$$vL\cos\phi \quad \Rightarrow \{\pi \leq x_1 \leq 2\pi\} \tag{6.24}$$

The gap between the bearing and the guiding surface is diffrent between (6.20) or (6.21), and (6.22). This difference is seen in equations (6.23) and (6.24). It is seen that the deformation will be largest if the angle ϕ is either equal to zero or π. In equation (4.4) ϕ is defined and it showed to be equal to zero on both peaks and valleys. Therefore if the deformation criteria as stated in (6.15) is passed it will mean that the bearing will be parallel for all positions on the guiding surface. In absolute terms, this means the deformation criteria is defined as followed;

$$sA + vsL \geq sA\sin\left(\frac{\pi}{2} + \frac{sL}{2}\right) \tag{6.25}$$

This function has been introduced in section II and is used to create figure 6.5 which shows that smaller slippers and more complaint slippers are better to follow wavy guiding surfaces. Which is illustrated in figure 6.4. This deformation criteria shows the major improvement of the implementation of pivots as compensation for tilt allows for this huge improvement, it also shows that improvements can be made if the deformation factor is increased.

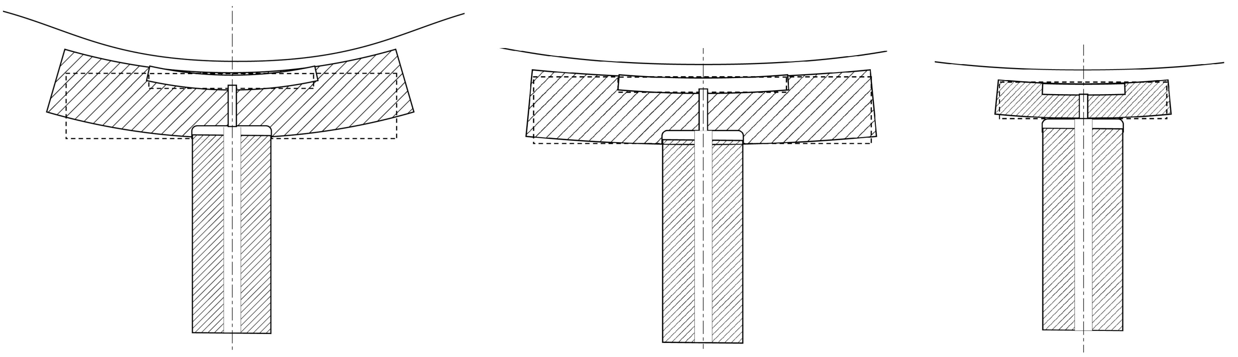

(a) Large deforming hydrostatic bearing

(b) Deforming hydrostatic bearing

(c) Smaller deforming hydrostatic bearing

Figure 6.4: Three hydrostatic bearings slippers, deforming to a curved guiding surface. Limiting on the maximum deformation are elasticity of the elastic bearing support and bearing slipper size.

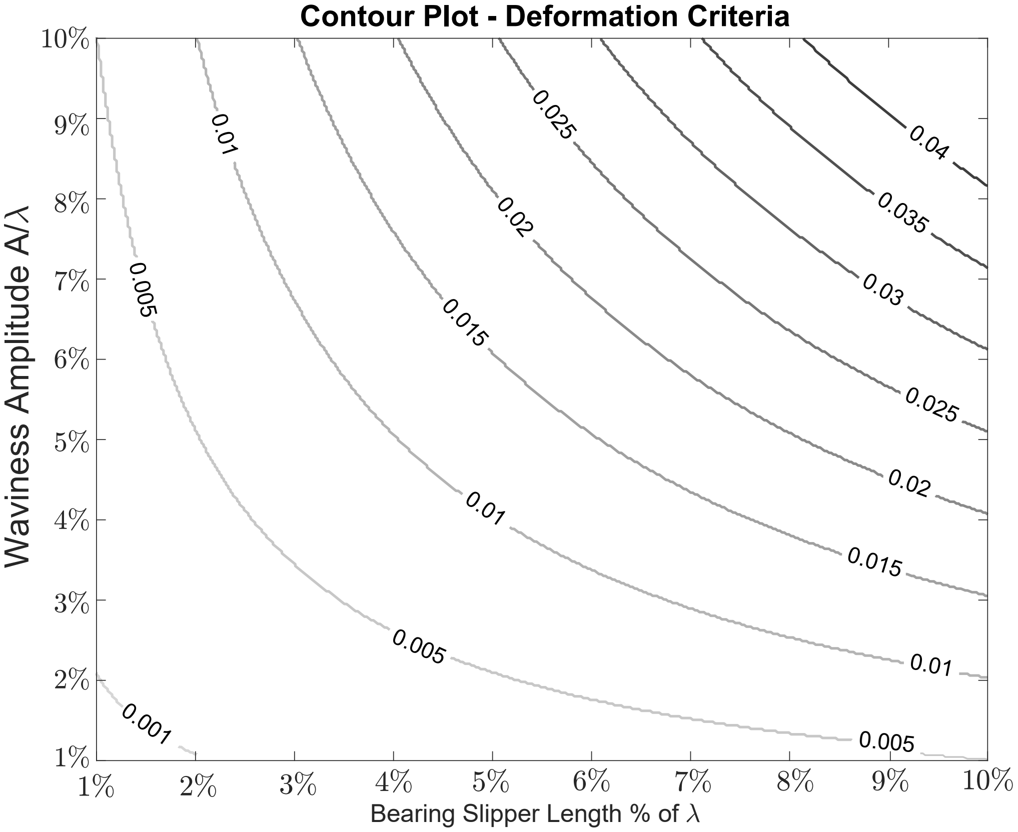

Figure 6.5: Contour plot of maximum running track waviness a slipper can follow for a given slipper length and slipper deformation factor. The waviness and slipper length are expressed relative to the guiding surface wavelength. The contour lines give the axial deformation factor, the fraction of a slipper's length it can deform.

Derivation of Whiffletree Kinematics

This section elaborates the kinematic derivation used to model the whiffletree. The kinematics are presented in chapter III but, a step by step derivation is not provided, therefore, an elaboration is presented here. The coordinates of a single deforming slipper on a guiding surface have been defined in figure 4.3. These coordinates are the input for the whiffletree from which the kinematics model expands.

Figure 6.6 shows a two slipper cell, which can be defined as a whiffletree branch. Using the relative waviness amplitude, A, relative slipper length, L and relative position x, all scaled with the factor s as defined in equation (4.2), the angles of two slippers, ϕ_1 and ϕ_2 are defined in equations (6.26) and (6.27). The amplitude A, will include the scaling factor; s. Thus whenever guiding surface amplitude is mentioned, this is the relative waviness amplitude, as the amplitude is relative to the wavelength. Similar scaling is applied to the position on the guiding surface, length of the slippers and length of whiffletree elements. These will all include scaling by s. The distance between two slippers, L_f, changes depending on positions of the slipper with one another. A linearisation has been introduced, meaning the distance between two slippers are fixed at a distance d from one another.

$$\phi_1 = \arctan(A\cos(x_1)) \tag{6.26}$$

$$\phi_2 = \arctan(A\cos(x_1 + d)) \tag{6.27}$$

The linearisation on slipper positioning is noted as $x_2 = x_1 + L_f$, where L_f for now is fixed a distance d. The effects of this linearisation compared to the actual distance have been investigated, the derivations has been taken up into appendix B. Figure 6.6 shows that the angle of the intermediate body, ϕ_{12}, between the two slippers equals to the angle between the two pivot points. In the previous chapter it was discussed that the coupling elements are half the length of the slipper and that the pivot point is taken halfway on the coupling element perpendicular to the slipper. This lever arm therefore has a length of $\frac{1}{4}L$, other lengths are treated in the appendix B. Using these relations the angles are defined as in (6.28)-(6.33).

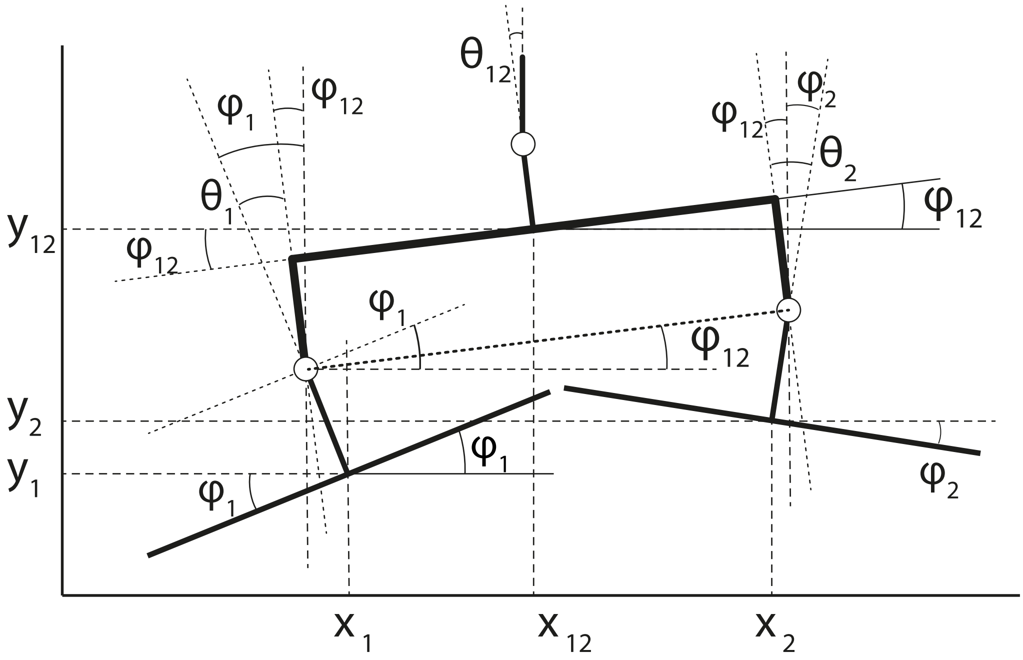

Figure 6.6: Representation on angle definitions of a slipper cell, with pivot points in the middle of the perpendicular rigid beam elements. In this illustration the uppermost pivot is connected to the normal load and therefor vertical.

$$\phi_{12} = \arctan \frac{\Delta x_{12}}{\Delta y_{12}} \tag{6.28}$$

$$\Delta x_{12} = x_2 - \frac{L}{4}\sin(\phi_2) - x_1 + \frac{L}{4}\sin(\phi_1) \tag{6.29}$$

$$\Delta y_{12} = y_2 + \frac{L}{4}\cos(\phi_2) - y_1 - \frac{L}{4}\cos(\phi_1) \tag{6.30}$$

$$\phi_{12} = \arctan\left(\frac{x_2 - \frac{L}{4}\sin(\phi_2) - x_1 + \frac{L}{4}\sin(\phi_1)}{y_2 + \frac{L}{4}\cos(\phi_2) - y_1 - \frac{L}{4}\cos(\phi_1)}\right) \tag{6.31}$$

$$\theta_1 = \phi_1 - \phi_{12} \tag{6.32}$$

$$\theta_2 = \phi_2 - \phi_{12} \tag{6.33}$$

For a system with more than two slippers, an additional level of pivots is required. The geometric relationship of the new level is similar to the two slipper-cell. The angles of intermediate bodies ϕ_{12} and ϕ_{34} can be compared with the angles of ϕ_1 and ϕ_2. These are used to calculate the angle of the coupling body, which in turn is used to calculate the pivot angles. Like the intermediate body that connected two slippers, the angle of the body that connects two cells (four slippers) is equal to the angle between the pivot points. This gives equations (6.41)-(6.43) as definitions for the angles ϕ_{1234}, θ_{12} and θ_{34}.

$$x_{12} = x_1 - \frac{L}{4}\sin(\phi_1) - \frac{L}{4}\sin(\phi_{12}) + \frac{L}{2}\cos(\phi_{12}) \tag{6.34}$$

$$x_{34} = x_3 - \frac{L}{4}\sin(\phi_3) - \frac{L}{4}\sin(\phi_{34}) + \frac{L}{2}\cos(\phi_{34}) \tag{6.35}$$

$$y_{12} = y_1 + \frac{L}{4}\cos(\phi_1) + \frac{L}{4}\cos(\phi_{12}) + \frac{L}{2}\cos(\phi_{12}) \tag{6.36}$$

$$y_{34} = y_3 + \frac{L}{4}\cos(\phi_3) + \frac{L}{4}\cos(\phi_{34}) + \frac{L}{2}\cos(\phi_{34}) \tag{6.37}$$

$$\phi_{1234} = \arctan\left(\frac{\Delta x_{1234}}{\Delta y_{1234}}\right) \tag{6.38}$$

$$\Delta x_{1234} = x_{34} - \frac{L}{2}\sin(\phi_{34}) - x_{12} + \frac{L}{2}\sin(\phi_{12}) \tag{6.39}$$

$$\Delta y_{1234} = y_{34} + \frac{L}{2}\cos(\phi_{34}) - y_{12} - \frac{L}{2}\cos(\phi_{12}) \tag{6.40}$$

$$\phi_{1234} = \arctan\left(\frac{x_{34} - \frac{L}{2}\sin(\phi_{34}) - x_{12} + \frac{L}{2}\sin(\phi_{12})}{y_{34} + \frac{L}{2}\cos(\phi_{34}) - y_{12} - \frac{L}{2}\cos(\phi_{12})}\right) \tag{6.41}$$

$$\theta_{12} = \phi_{12} - \phi_{1234} \tag{6.42}$$

$$\theta_{34} = \phi_{34} - \phi_{1234} \tag{6.43}$$

Note the resemblance with the equations of the lower level, which repeats for higher levels as well. The lengths between slippers has been replaced by lengths between cells and the length of coupling elements is doubled as those now couple twice as large substructures. This is an advantage of the whiffletree, in which the functions are in essence the same only the inputs change. Only the angle of the uppermost level is to be calculated differently, depending on the number of levels. If the bearing would have only two slippers, the angle of the intermediate body connecting the two is the uppermost intermediate body. Therefore $\phi_{12} = \phi_{ax}$ and the pivot connecting this uppermost body to the axial load is the uppermost pivot. Giving us $\theta_{12} = \theta_{ax}$. For the uppermost level, the pivot is connected to the axial load. And as the axial load must always be placed vertically, this angle is defined as in equation (6.44).

$$\theta_{ax} = \pi - \phi_{ax} \tag{6.44}$$

In the previous chapter an eight slipper whiffletree system was introduced and the angles of both the intermediate bodies and the flexure angles have been set up. While these equations can be used to find the angle on any point of the guiding surface it is more interesting to look at the maximum flexure angles as these will likely cause mechanical failure. Figure 6.7 shows the contour plots, in appendix C one can find the matlab code used to make these. The range chosen for slipper length is up to $\frac{1}{8}$ of λ, as our assumptions do not hold for deformable bearing that cover a larger running track than one wavelength or slippers that cover more than a forth of a wavelength. Therefore, relative waviness also goes up to a similar percentage. From a design perspective these plots shows that choosing specific lengths for a given waviness can decrease maximum flexure angles.

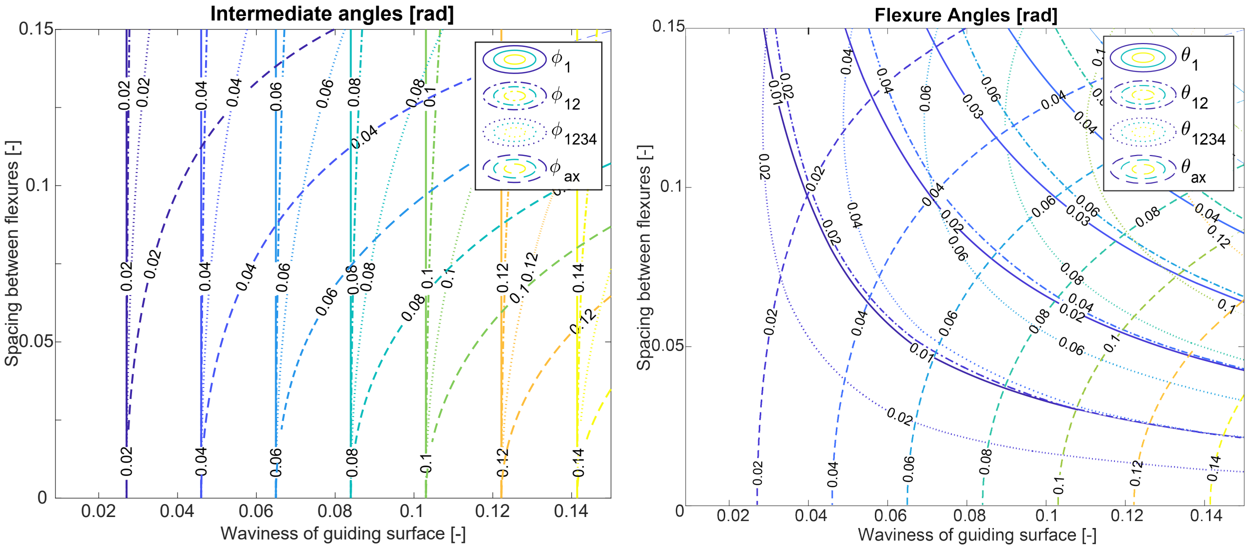

(a) Maximum angles of coupling elements

(b) Maximum angles of pivots elements

Figure 6.7: Contour plots of maximum angles as functions of distance between slippers and the relative waviness of the guiding surface.

Model Interface

The kinematic model has been completed in the previous chapter and the model has been visually represented in 4. This model together with the implementations introduced before, serves as a design tool for a demonstrator to be created as a verification of the model. It combines all the elements presented in this thesis. However, this thesis also presents many design options, thus as a design tool it would require many options therefore a Graphical User Interface was chosen to represent this. But with the increasing complexity due to implementation of cross flexures, hydrostatic bearing model and the many design choices left open within the model. The model could not long be verified and due to time pressure the guided user interface is now a tool to visualize the results of the model.

The matlab code behind this Graphical User Interface (GUI) can be found in appendix C. It will present all of the individual scripts running as the callbacks for this GUI as well as a more elaborate user manual. The main principles of the GUI has been visualized in figure 4. This section elaborates on the modeling used in the GUI from the perspective of the user interface.

Graphical User Interface

The user interface is seen in figure 7.1, it shows the results of a eight slipper whiffletree placed on a 1 metre guiding surface. The compliant slippers, with a deformation factor of $\frac{1}{100}$, have a length of 5 cm and are able to deform to the given waviness, which is 1% of the guiding surface. These slippers would provide 40 N which is a result of their effective area being multiplied by the recess pressure, which followed from equation (7.1). This recess pressure follows from the input supply pressure of 5 bar and film thickness of 100 µm. The kinematic model represented in this chapter leads to the flexure angles and whiffletree angles shown in this interface for this slipper length and waviness, the maximum angles being around 0.5 deg. These maximum angles lead to a maximum flexure stress of 190 MPa according to equation (7.4), introduced in the previous chapter. As this is below the stress endurance limit of 270 MPa for 10^7 cycles, the background colour is presented as green. Turning to orange and an eventual red if the stress criteria is not met.

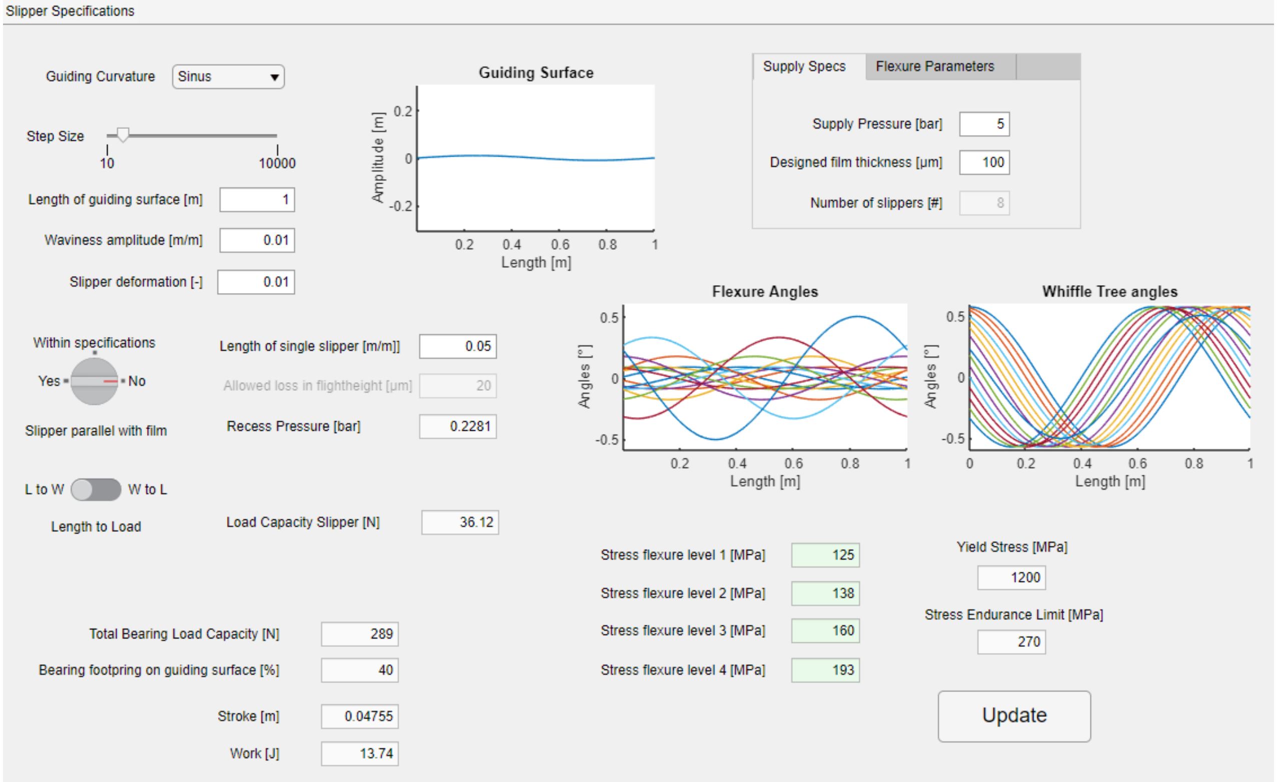

Guiding Curvature: Sinus

Step Size: 10 – 10000

Length of guiding surface [m]: 1

Waviness amplitude [m/m]: 0.01

Slipper deformation [-]: 0.01

Within specifications: Yes ○ No

Slipper parallel with film

L to W ○ W to L

Length to Load

Length of single slipper [m/m]]: 0.05

Allowed loss in flightheight [µm]: 20

Recess Pressure [bar]: 0.2281

Load Capacity Slipper [N]: 36.12

Total Bearing Load Capacity [N]: 289

Bearing footpring on guiding surface [%]: 40

Stroke [m]: 0.04755

Work [J]: 13.74

Supply Pressure [bar]: 5

Designed film thickness [µm]: 100

Number of slippers [#]: 8

Stress flexure level 1 [MPa]: 125

Stress flexure level 2 [MPa]: 138

Stress flexure level 3 [MPa]: 160

Stress flexure level 4 [MPa]: 193

Yield Stress [MPa]: 1200

Stress Endurance Limit [MPa]: 270

Figure 7.1: A screen capture of the guided user interface created with matlab[2].

Figure 7.1 shows an example of a configuration of inputs for which the whiffletree based deformable bearing will remain parallel to the guiding surface and for which stress levels of the flexures are below the maximum allowed tolerance. Increasing any one of these inputs slightly results in a configuration which fails. For a eight slipper configuration with slippers that have a axial deformation factor of $\frac{1}{200}$ requires the slipper size to decrease, in order to maintain parallel with the guiding surface, this in turn results in larger flexure angles. And these flexure will then fail due to extensive stress levels, this will then be made clear to the user by the aforementioned color coding. The deformation criteria also has a build-in check to inform the user if the check is met or not. If, for example, a slipper size of 0.075% of the guiding surface length are used, the model will return a warning as seen in figure 7.2.

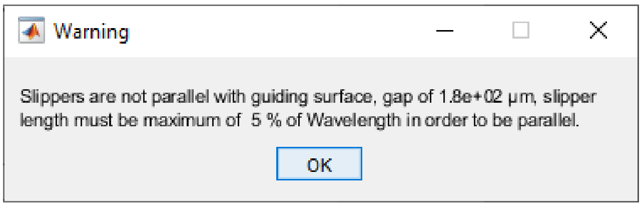

Slippers are not parallel with guiding surface, gap of 1.8e+02 μm, slipper length must be maximum of 5 % of Wavelength in order to be parallel.

Figure 7.2: A screen capture of the warning given by the GUI, if the deformation criteria is not met.

This warning is one of the features of the design tool, the GUI also has an option to find the maximum allowed slipper size for a given wavelength and deformation factor. This is done when the knob *Slipper parallel with film* on the User interface panel has the option *Yes* selected, then the user is unable to edit slipper size, as the maximum size will be entered once the *Update* button is pressed. The accuracy of the result depends on the step size, which can be altered using the slider in the upper left corner, the default settings use a step size of 1000. It is also possible to allow the slipper a loss in film height, this is actually the mismatch between the slipper not being able to deform parallel to the guiding surface and the actual gap size because of this. Thus selecting with the knob *Slipper parallel with film* the option *Within specification* will enable editing this as input variable. And after pressing update, the GUI will output a slipper length that will deform to the given waviness amplitude with a given deformation factor with the specified gap size remaining undeformed. This gap is simplified and added to the designed film height therefore the model also outputs a lower load capacity of the bearing. The load capacity is calculated by the chosen hydrostatic bearing model, one of the many models implemented in the GUI.

Modeling implementations

In this section the implemented models in the GUI are treated, as these are often specific design choices. Let us start by the hydrostatic slipper model which is used to calculate the force for a given film thickness. A model of a orifice multi recess bearing has been used, a multi recess bearing was chosen for the tilt stiffness it would provide[46]. The recess pressure could be calculated through equation (7.1), which holds true for multi recess bearings[55].

$$P_r = \frac{\sqrt{1+4P_s\frac{\rho}{2(C_oA_o)^2}(\frac{\bar{B}h^3}{\eta})^2}}{2\frac{\rho}{2(C_oA_o)^2}\frac{\bar{B}h^3}{\eta}} \tag{7.1}$$

Here supply pressure is defined as P_s η, described the dynamic viscosity of the lubricant. C_o and A_o represent orifice parameters. $\bar{B}$ and $\bar{A}$ are shape factors, a geometry dependent parameters describing the effective flow and effective bearing land area. Using the effective bearing land area, the force on a slipper can be formulated as in equation (7.2). In the top left of the GUI selecting slipper specifications will present a drop down menu that allows one to plot all data from the hydrostatic bearing model for a given slipper length, supply pressure and film height.

$$F_n = \bar{A}AP_r \tag{7.2}$$

The effective area is multiplied by the real bearing land area, A, and recess pressure to give the normal force acting upon one slipper. Using the angle of the slipper, the axial load can be derived from this as seen in equation (7.3). This can in turn be done for each slipper to give the total load acting upon the whiffletree for a certain film thickness. This is where the model of the hydrostatic slipper ends as it gives the forces upon the flexures for a given angle. Therefore, this is coupled to the kinematics and used as input for the flexure model.

$$F_{ax} = F_n \sin\phi_{ax} \tag{7.3}$$

The flexure used was chosen to be a cross flexure, as seen in figure 7.4, as this was amongst the highest ratio of axial stiffness to rotational stiffness[38] and could be studied analytical. The rotational stiffness of a cross flexure depends on many parameters such as designed intersection angle, and it is non linear [27]. For small angles however, it can be assumed that linear elastic bending occurs and assuming that this is due to a pure bending moment gives equations (7.4) and (7.5) to calculate the stress on the outer edge of a cross flexure and the rotational stiffness [63].

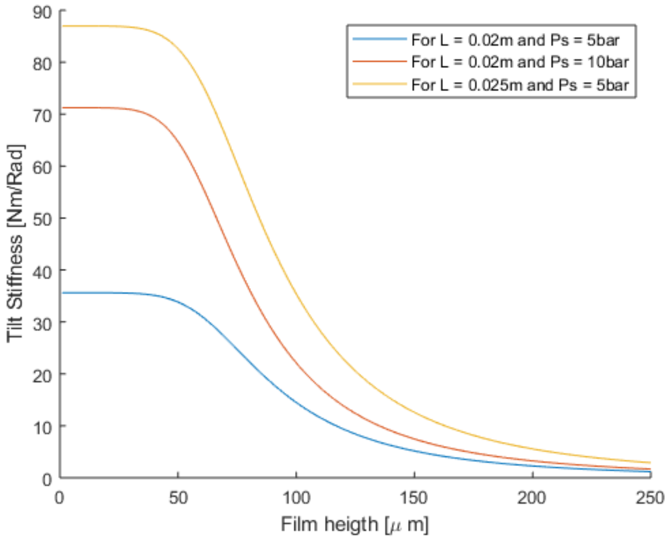

Figure 7.3: Tilt stiffness for a few example hydrostatic slippers as given in the GUI.

$$\sigma = \frac{Et}{2L_s}\theta + \frac{F_x}{tb_s} \tag{7.4}$$

In equation (7.4) the stress is calculated in two parts, the first is the bending stress. It is expressed as function of the Young's Modulus, E, length of a cross flexure spring element, L_s, and the flexure angle, θ. The second part is loading stress as expressed by the normal load, F_x, the thickness of the flexure elements is defined as t and width of the flexure elements, b_s. This could all be seen in figure 7.4. The stress is calculated for each angle θ and for all flexure levels, as the force doubles but so does length, this is seen in the bottom right of the GUI. The stress on each of the flexures would be different, as each is under a different angle and for the higher levels as they will be under a higher load, while simultaneously allowing a bigger slipper to be placed and the slipper itself undergoing different angles. The stress levels would eventually be checked with the endurance limit cycle stress level found online. For spring steel, which is likely to be used in a cross flexure this is 650 MPa[3]. Or regular carbon steel which is likely to be used for a first order demonstrator 270 MPa. The guided user interface also allows manual entry of stress levels criteria, or the entry of a common material type.

$$K_\theta = \frac{EI_{total}}{L_s} \tag{7.5}$$

The rotational stiffness is calculated in equation (7.5). Again using the material property E, the Young's Modulus. The total second moment of inertia is denoted as I_{total}, this is twice the moment of inertia of a single cross spring element, as the chosen pivot was a two strip cross flexure. The second moment of inertia of a spring element is calculated in (7.6). Here, L_s again describes the length of a spring element. This length, for cross flexures with a size equal to the slippers is equal to $\sqrt{2}L$, as the cross flexures under a angle of 45°. The rotational stiffness is calculated to compare with tilt stiffness of the slippers. The tilt stiffness of the bearing slipper, as seen in figure 7.3, can be generated by the GUI by selecting this from the drop down menu of *Slipper Specifications*. The hydrostatic bearing model to calculate this tilt stiffness is treated in more detail in section VI.

$$I = \frac{bh^3}{12} \tag{7.6}$$

Equation (7.6) describes the area moment of inertia of a rectangle. Where, h is the height of the rectangle and b is the width. Using the spring element definitions from figure 7.4 to determine bending stiffness over the Z-axis, this requires the moment of inertia over the z-axis. Rewriting equation (7.6) to (7.7).

$$I_z = \frac{b_s t^3}{12} \tag{7.7}$$

Putting in parameters as found in literature, a length of 20 mm, width of 4 mm and thickness of 0.15 mm with a young's modulus of 70 GPa results in a bending stiffness of 0.0079 N m rad^{-1}, this is equal to the value provided by literature for this cross flexure[38]. Thus for small angles this function is accurate and is therefore used as an implementation of the cross flexure. And it can be used to confirm that rotational stiffness is smaller than the tilt stiffness, this is calculated for a 10 mm and a 100 mm slipper. The results are found below in table 7.1.

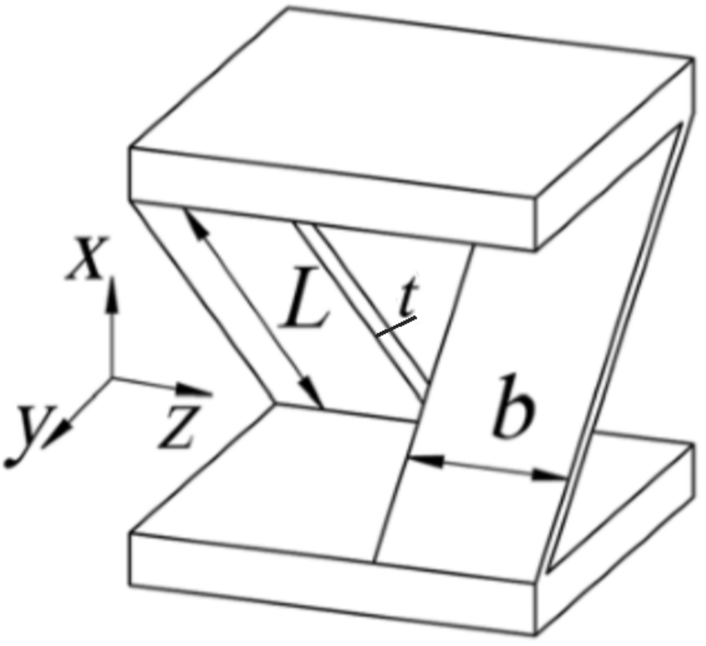

Figure 7.4: The chosen cross flexure design, the cross strip elements are under a 45° to the slipper and connecting element[38]. The elements have a spring length of L_s, a width of b_s and thickness t. With the defined coordinate system the rotation stiffness is defined as K_θ=$K_\theta z$.

Flexure	L	L_s	b_s	t	I_z	E	$K_{\theta z}$
Literature example	-	20 mm	4 mm	0.15 mm	1.125×10^{-15} m^4	70 GPa	0.0079 N m rad^{-1}
Small slipper	10 mm	14.14 mm	5 mm	0.5 mm	5.21×10^{-14} m^4	70 GPa	0.517 N m rad^{-1}
Larger slipper	100 mm	141.42 mm	50 mm	0.5 mm	5.21×10^{-13} m^4	70 GPa	0.517 N m rad^{-1}
Large steel flexure	100 mm	141.42 mm	50 mm	0.5 mm	5.21×10^{-13} m^4	200 GPa	1.467 N m rad^{-1}
Small and thick	10 mm	14.14 mm	5 mm	1 mm	4.16×10^{-13} m^4	70 GPa	4.13 N m rad^{-1}
Larger and thick	100 mm	141.42 mm	50 mm	1 mm	4.16×10^{-12} m^4	70 GPa	4.13 N m rad^{-1}
Largest flexure	-	500 mm	50 mm	2 mm	3.33×10^{-11} m^4	200 GPa	23.59 N m rad^{-1}

Table 7.1: A few cross flexures rotational stiffnesses, to compare with tilt stiffnesses and literature. Parameters as thickness, Young's modulus and slipper size can be altered in the GUI, width and spring length are coupled to slipper length and can therefor not be changed directly.

The results show that the rotational stiffnesses for a variety of different parameters. The thickness of the flexures could be increased if stress levels due to loading are dominant. However, for the rotational stiffness it is best to keep thickness as low as possible. As it scales with the power three. The largest flexure considered here, is again for the eight slipper whiffletree with even with the largest possible slipper size this flexure would not become larger than the tilt stiffness. The tilt stiffness for the higher levels also have a leverage effect such that for the higher levels effective tilt stiffness is larger, and therefor these flexure can be more stiff. The tilt stiffness vs rotational stiffness need to be watched closely for different design parameters as they are only one order of magnitude apart for thicker flexures. It is recommended to use low thickness 0.5 mm and a flexible material with Young's Modulus of 70 GPa or lower if stress levels allow it. The GUI unfortunately is unable make this trade-off as there are many parameters and design variables involved, so this has to be done manually.

Note that cross flexure also has compliance in other directions and even though loading in those direction is not intentional, these must be taken into account as instability may become an issue for the higher level flexures and the risk on buckling will increase for ever larger flexures if the width and thickness do not increase. This along with the transnational stiffness, the axial shift and non-linearity are recommended to be look at in further research. The next chapter will provide multiple topics on which the GUI implementation may be improved upon.

Conclusion, Discussion and Future research

Research objectives evaluation

Inspired by past research in deformable fluid bearings and complaint support structures. It was possible set-up a model from which it is now possible to reflect on the research objectives. To answer this question a number of sub-questions were formulated. This chapter reflect on the research objective by treating the sub question first, then the research goal followed by recommendations for future research and end with a general conclusion.

Can compliant mechanisms be combined with elastic slippers to improve overall compliance?

The compliant pivot is a great addition to deformable slippers. The use of pivots decreases the deformation needed by the slipper, by allowing the slipper to become tangent to the guiding surface. Therefore, overall compliance is increased by these pivot. Complaint mechanisms were investigated but the cross flexure was chosen as a result of a trade-off, a high as possible axial stiffness was required while having as low as possible rotational stiffness. The cross flexure was chosen as it had the highest axial to rotational stiffness ratio[38]. In hindsight the axial stiffness might be of much more importance as long as the tilt stiffness of the slippers proved to be higher than the rotational stiffness of these flexures. And as stress levels of the cross flexure are limiting the system, this requires a more detailed investigation. Figure 8.1 shows a very simplified cross flexure finite element model which could be used to verify modeled stress levels.

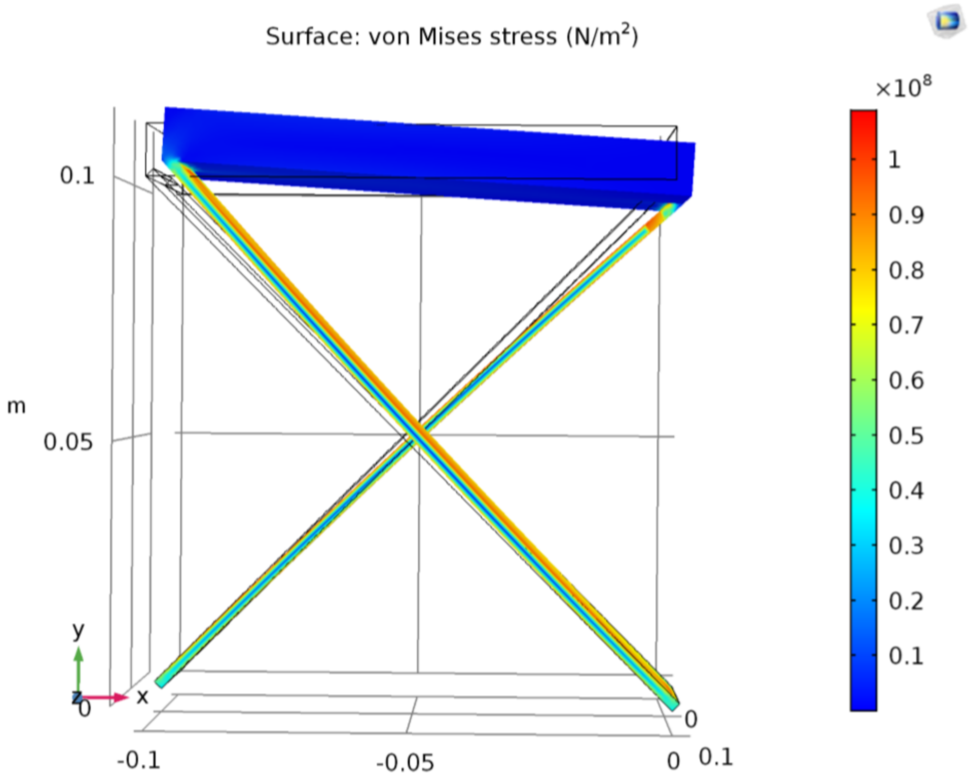

Figure 8.1: Example of comsol verification on stress levels for a simplified cross flexure

How large of a waviness can be followed using elastic hydrostatic slippers?

The principle used to determine the maximum waviness an elastic slipper can follow has been thoroughly explained in 6.1. As pivots were introduced, a large improvement in waviness following capabilities is seen for. However, the model showed that the deformation of elastic slippers is currently limiting on waviness following capabilities. These limitations are based on assumptions inspired by literature, which need to be further verified. As this introduced the axial deformation factor, υ. Which determines the magnitude of compression and lead to compression stress levels which eventually lead to mechanical failure [44].

A finite element model of an elastic support undergoing linear compression can be seen in figure 8.2. It shows two rubber blocks fixed on the top and a fixed displacement on the bottom representing the concave or convex displacement. Using linear elastic solid mechanics the output stress level show that for $\upsilon = \frac{1}{1000}$ the stress levels are not in the levels that cause mechanical failure, considering they are made out of a Reomas BV. Rupulan rubber, able to handle $10\,\mathrm{N/mm^2}$[44]. This means it might be possible to improve υ, therefore, in the next section this is introduced as a future research topic. It also shows that the maximum deformation factor might depend on slipper length. Note that this model also shows that convex and concave stress levels are not the same, thus, the assumption that υ is the same for concave and convex curvature will no longer hold. The deformation criteria of equations (6.12) and (6.14), for positive and negative bending, will have to be used separately. If stress due to convex deformation is dominant, as seems to be when comparing 8.2a with 8.2b, it might become possible to use the convex deformation factor to describe the full range of deformation motion.

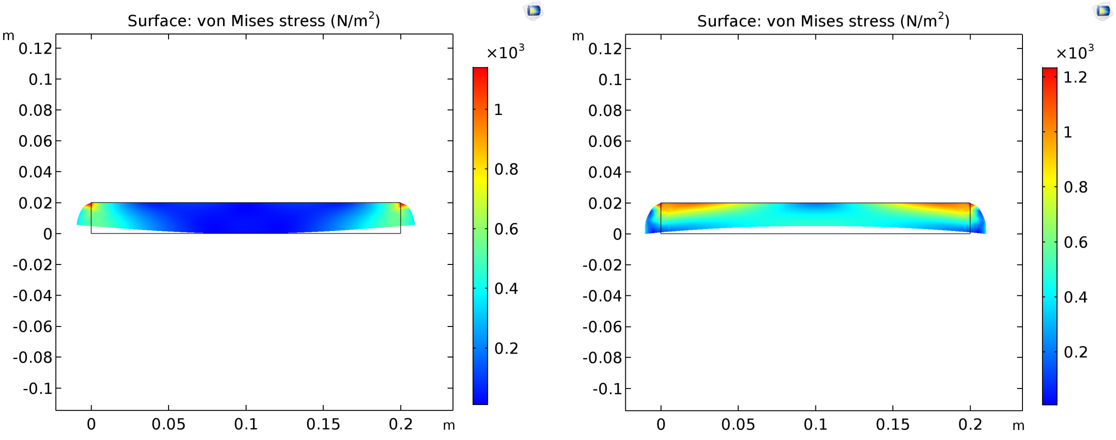

(a) Comsol model of concave compression

(b) Comsol model of convex compression

Figure 8.2: Example of verification using comsol multiphysics[1] to show that axial deformation factor can be improved upon

The deformation criteria showed that waviness following capabilities improve when the slipper size is decreased. In order to keep load capacity the same the number of slipper must increase to compensate for their size. But increasing whiffletree size comes with an increase in complexity in the system. And with the height of the whiffletree the slippers lateral motion increases as the movement of coupling bodies due to tilt also moves the slippers. This means the slippers must be made smaller, resulting in a further decrease in load capacity.

What are the kinematics of a whiffletree-like structure on a wavy guiding surface?

The kinematics of a whiffletree can be set up for a system where the lengths of the connecting elements are known. Therefore, the length of the horizontal coupling elements that connect one slipper to the next is equal to the length of a slipper. The vertical element is equal to this half this length. This and the linearisation that the slippers are positioned exactly one slipper length apart from one another. With these assumptions an exact description has been given of the position of each slipper and all the connecting elements, however it has already been noted that an error up to 7% is introduced by the linearisation. For pivots that are less high, the maximum angle will decrease as there is less of amplification arm. This in turn also decreases lateral motion of the slippers.

Can multiple deformable hydrostatic slippers be combined in a force distribution mechanism to improve waviness following capabilities?

The large deformable hydrostatic bearing has been modeled. The model of the kinematic behaviour granted insight on how a force distribution mechanism could be implemented. Investigating mechanical support structures in literature inspired the design of a whiffletree based bearing. While a comparison between multiple complaint pivots resulted in the choice of a cross flexure. Therefore a whiffletree with cross flexure elements as pivots proved to be a interesting option. And it proved to be capable of following wavy surfaces to some extent.
Therefore, it can be concluded that the research objective;

Design and model a hydrostatic bearing for large deformations and high loading conditions using a mechanical support structure.

has been achieved.

Kinematic modeling showed that the introduction of pivots increased the capabilities of deformable hydrostatic slippers to follow wavy guiding surfaces. And loads can be disturbed over multiple slipper to increase load capacity. The model showed that the combination of these two topics within a whiffletree improved the waviness following capabilities of deforming hydrostatic bearings. The design implemented cross flexures as the compliant pivots and using the kinematics from the model as input, showed that cross flexures are limiting in this design. Other factors are also limiting, therefore further work is required on this topic before it could be implemented in a system.

Recommendations for future research

The recommendations are based upon current limitations of the concept and on assumptions which require more research. Each of the following subsections could be a research project on its own.

Verification of whiffletree based model

The current model is based on the whiffletree concept, however no experimental verification has been done. It was the intention to do so when the project was first introduced, however setting up the kinematic model was first required. And too many unknown factors were to be investigated before implementation could be achieved. Therefore it is highly recommended for future research. For this it would be required to;

- Expand the kinematic model to include stiffnesses of the pivot elements and tilt of the bearings
- Introducing compliance of coupling element in idealized whiffletree model
- Implement pivots and verify internal stress levels using finite element modeling
- Investigate compliance and stress levels of elastic bearing slipper

Once this is done an experimental set-up can be created where the large deformable hydrostatic bearing concept can be proven to be feasible. For the experimental set-up it would be required to measure film thickness between the deforming bearing and a guiding surface with a wavy profile.

Compliant pivots

When implementing compliant pivots their on-axis rotational stiffness was compared to the off-axis stiffness in z-direction. As it was thought that the ratio between load capacity to rotational stiffness would be a good indication on how suitable this concept would be. In reality the axial stiffness must simply be as high as possible, as long as rotational stiffness is low enough such the slipper will not be lift from the guiding surface. From this comparison of ratios the cross flexure came out as a promising candidate. The alternatives were seen as complex therefore the cross flexure was chosen as compliant pivot due to their relative ease to implement. However, as concluded they proved to be limiting in both ability to carry axial loads and due to internal stress build up as a result of rotation.

Two other types of pivots which were investigated but not implemented were;

- Compliant rolling element
- Q-LIFT pivots

A more in depth look into stress and failure mechanism would be recommended in order chose a design. As an alternative a compliant pivot could be designed purely for this application. An optimization in pivot design could lead to a far more suitable type of complaint pivot.

Hydraulic pressurized cell support

A interesting way to provide elastic slipper support would be to use pressurized chambers. These chambers would be complaint on their own but as they are filled they would be able to deform by moving fluids, this would allow the bearing land surface to form to the guiding surface profile, while the internal pressure provides axial stiffness. This hydraulic principle could be a solution to provide very high axial stiffness while being rotational compliant at the same time. And this principle could also be used to compensate for the tilting of the hydrostatic bearings. Thus slippers and pivots might be combined in a single support structure. So these could be implemented as slippers and pivots within a whiffletree.

A lot of research would be required on these type of structures, as stress levels within the pressure cell would be critical. Elaborate finite element modeling is required, while investigating the different type of concepts of pressure cells. As these cells could either be directly connected to recess chamber or have separate cells. Therefore, additional research is recommended in;

- Open cell structures as pivots
- Closed cell structures as pivots

General Conclusion

The kinematic model created achieved the goal of proving knowledge such that we were able to make design choices and set-up a concept of a large deformable hydrostatic bearing. The implementation of deformable hydrostatic slippers with a rubber support and cross flexures as compliant pivots were good additions and allowed for large wavy guiding surfaces to be followed. These however introduced many assumptions which were not thoroughly investigated. Similarly the internal stress levels are non-negligible but interest was directed more at proof of concept rather than into feasibility, therefor this was not done up until the very end. The complete model was put together as a design tool to set-up a demonstrator which was to be created as a verification of the model. Due to difficulties connecting the many models into one and implementing the cross flexures, with many design choices still left open, a verification on the model was no longer possible within this project. The graphical user interface does provide visualization of the results of the model. It directly shows the relation between slipper compliance, waviness and slipper size as given by the deformation criteria. Slipper size, in turn directly relates to the flexure angles, which in combination with the load criteria allowed for a analytic stress analysis. This is the main working principle behind the complete model shown in figure 8.3.

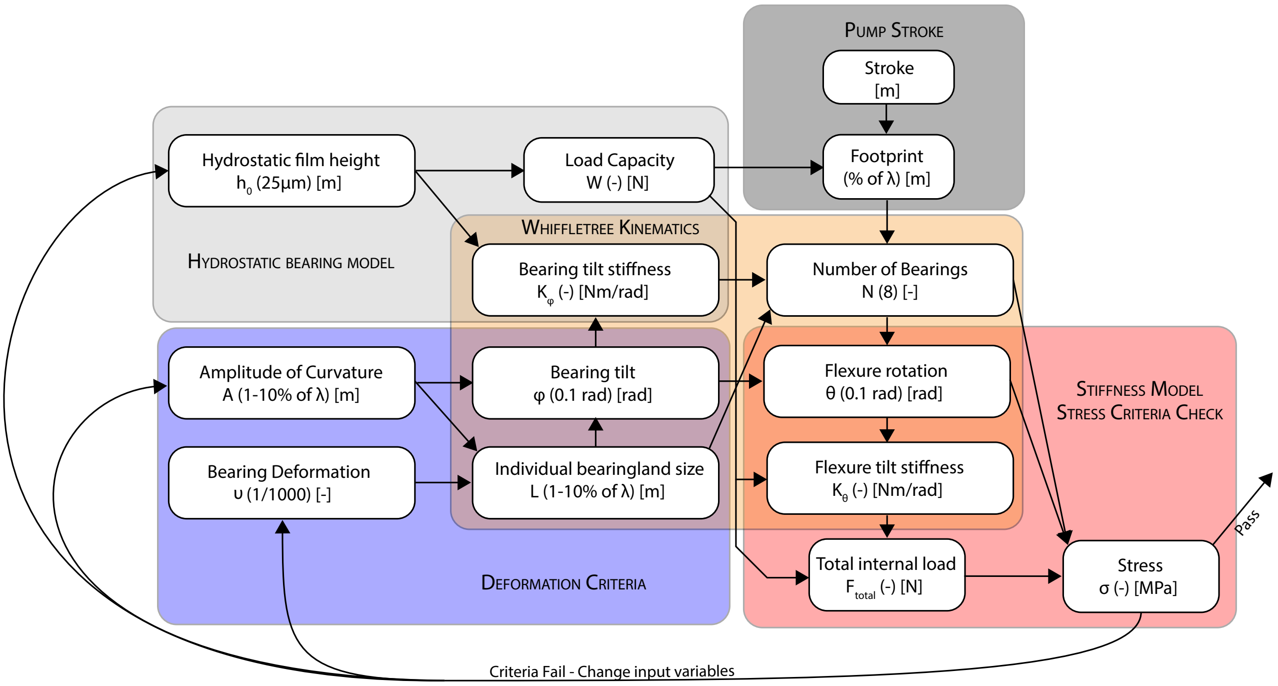

Pump Stroke
Stroke [m]
Footprint (% of λ) [m]
Hydrostatic film height h_0 (25μm) [m]
Load Capacity W (-) [N]
Whiffletree Kinematics
Hydrostatic bearing model
Bearing tilt stiffness K_φ (-) [Nm/rad]
Number of Bearings N (8) [-]
Amplitude of Curvature A (1-10% of λ) [m]
Bearing tilt φ (0.1 rad) [rad]
Flexure rotation θ (0.1 rad) [rad]
Stiffness Model
Stress Criteria Check
Bearing Deformation υ (1/1000) [-]
Individual bearingland size L (1-10% of λ) [m]
Flexure tilt stiffness K_θ (-) [Nm/rad]
Pass
Deformation Criteria
Total internal load F_{total} (-) [N]
Stress σ (-) [MPa]
Criteria Fail - Change input variables

Figure 8.3: Visual representation of the models and relationships used to set up the graphical user interface.

Within this model the tilt stiffness of the hydrostatic slipper is also investigated and checked whether it is much smaller than the rotational stiffness of the cross flexure, as this was assumed. If this was false, then full film lubrication could not be maintained. These and other assumptions are listed in appendix A. Most of these assumptions are still quite logical choices, others do require some more attention if the whiffletree concept is further investigated. Overall the model grants good insight on possibilities and applications. It brought forth new insights, as for the application of pumps, the power pumped normally is transferred through a single point. A whiffletree based deformable bearing would distribute the force over an area. Resulting in a lower stroke, and thus less power transferred, this resulted in the new insight that specifically for the application of pumps a new constraint is likely to be introduced for the design.

In the end a large deforming hydrostatic bearing is not created, however the foundation is laid for future research.

Appendix A

Assumptions

The paper made a large number of assumptions many of which are used to set up the kinematic models and lead to the results presented in this work. Effects of some assumptions are simply unknown for example; The deformation of a single slipper was assumed to be vL and for this it was assumed the bearing would be parallel. However it is only known that the bearing does not make contact. Thus full film lubrication is maintained.

A related assumption has been made for this configuration. This assumption has been made in order to prevent statements on stress levels, as this thesis does not focus on slipper stress and is a topic on its own. Therefore it has not been investigated whether internal stress levels are below the endurance limit for a deformation factor of v.

I. Assumptions not mentioned or investigated in this thesis

- Change of geometric area shape factor and flow shape factor, $\bar{A}, \bar{B}$, due to tilt or deformation. The geometric shapes are recommendations found in literature [55]. For the hydrostatic multi-recess slipper model the optimal values were used for high load capacity and stability.
- Rotational stiffness of the cross flexure does not influence film height as it is much lower than tilt stiffness of the bearing. In reality the rotational stiffness of the flexure always influences the film height, as spring in series.

II. Assumptions introduced through literature

- Small angle assumption for flexure rotation, so linear bending can be applied [63]. This is required for equations (7.4) and (7.5) to be valid.
- High translational (out-of-plane) stiffness of the cross flexures so lateral deformation is low[38]. With no designed out-of-plane forces the effects of out-of-plane stiffness are out-of-the scope of this research.
- Constant position of flexure rotation point, so no
  - Displacement due to axial compression [27]
  - Axis drift due to rotation, related to small angle assumption [63]

III. Summary of modeling assumptions

The following assumptions were introduced in this thesis.

- The guiding surface can be described by sine wave [chap. 1][chap. 4]
- Bearing slipper is small and can therefore be tangent to the guiding surface [sec. 4.1]
- With an axial deformation factor of $\frac{1}{1000}$ full film lubrication is maintained [sec. 4.1][sec. II]
- No elastic deformation of the guiding surface, very stiff compared to the slipper. [sec. II]
- Deformation is small, thus linear beam bending can be applied [sec. 6.1]7.2]
- Axial deformation factor is the same for concave, convex and asymmetric deformation [sec. 6.1][sec. II]
- Deformation is always perpendicular to bearing land, ideal flexures transfer forces perpendicular to guiding surface [sec. 4.1]
- Film thickness is negligible compared to length of deformable slipper or waviness of guiding surface [sec. 6.1]
- Slippers are at a fixed distance from one another [sec. 6.2][sec. III]
- Intermediate coupling bodies are fixed length and do not deform when loaded [sec. 6.2]
- Tilt of a multi recess bearing can be represented by two serpate chambers with an uniform increase in height at one side and loss at the other [sec. VI]
- Resultant force as result of bearing tilt has a moment arm exactly at the recess centroid. [sec. VI]

Appendix B

Kinematic Derivations

In this appendix elaborations are given on kinematics that are derived but not implemented in the final model. Some of these kinematics were investigated in hopes to simplify the problems at hand. So, while some for there was never the intention to implement them, only to check if a assumption was correct. Others were not implement due to them being mathematically incomplete or illogical design choices.

Whiffletree Kinematics, pivot arm length.

In figure 6.6 the pivots were introduced to be on coupling elements which were half the length of the slippers. However, what if the coupling elements would be much larger, smaller or the pivot point would not be in the middle of the coupling elements? This has been investigated and it was concluded that this only has a small influence on the maximum angles of the pivot, the slipper and intermediate bodies.

$$\phi_{12} = \arctan\frac{\Delta x_{12}}{\Delta y_{12}} \tag{1}$$

$$\Delta x_{12} = x_2 - R\sin(\phi_2) - x_1 + R\sin(\phi_1) \tag{2}$$

$$\Delta y_{12} = y_2 + R\cos(\phi_2) - y_1 - R\cos(\phi_1) \tag{3}$$

$$\phi_{12} = \arctan\left(\frac{x_2 - R\sin(\phi_2) - x_1 + R\sin(\phi_1)}{y_2 + R\cos(\phi_2) - y_1 - R\cos(\phi_1)}\right) \tag{4}$$

$$\theta_1 = \phi_1 - \phi_{12} \tag{5}$$

$$\theta_2 = \phi_2 - \phi_{12} \tag{6}$$

Replacing the length of the arm $\frac{L}{4}$ by a variable R in equations 6.28 to 6.33 gives 1 to 6. This is repeated for higher levels up unto a third level, so it has been implemented for an eight slipper system. Figure 4 shows that there is a difference for angle depending on the size of the pivot arm, however it is only a small difference.

In order to investigate that this is not a local behaviour but to show that this pivot arm length has only a small influence on maximum angles this is investigated more thoroughly. The results can be seen in figures 5, these contour plot show the maximum angles for different waviness guiding surfaces and lengths of the slippers. Yet the differences are so small that they can not be observed.

Error due to linearisation

The slippers are set a fixed distance apart, this linearisation introduces an error, here the magnitude of that error is investigated. The maximum error occurs with the first slipper on the point of maximum curvature with the second slipper on the point of zero curvature. These positions are given by $x_1 = \frac{1}{2}\pi + n\pi$ and $x_2 = \pi + n\pi$ with n being any real integer. On these positions the amplitude difference is exactly A, as the maximum amplitude used in the model is $\%10\lambda$. The maximum error can be calculated, the equations (7)-(12) are used to calculate an estimation on error positioning.

$$\Delta x_r = \sqrt{d^2 - A^2} \tag{7}$$

$$e = 1 - \frac{\Delta x_r}{\Delta x_a} \tag{8}$$

$$d = \sqrt{\left(\frac{1}{2}\pi\right)^2 + A^2} \tag{9}$$

$$\frac{\Delta x_r}{\Delta x_a} = \frac{\frac{1}{2}\pi}{d} = \frac{\pi}{2\sqrt{\left(\frac{1}{2}\pi\right)^2 + A^2}} \tag{10}$$

$$d_{max} = \sqrt{\Delta x_{max}^2 + A^2} \overbrace{=}^{A=0.1} \sqrt{(1/4\pi)^2 + (\pi 0.2)^2} \tag{11}$$

$$e_{max} = 1 - \frac{\Delta x_r}{d_{max}} = 1 - 0.928 = 7\% \tag{12}$$

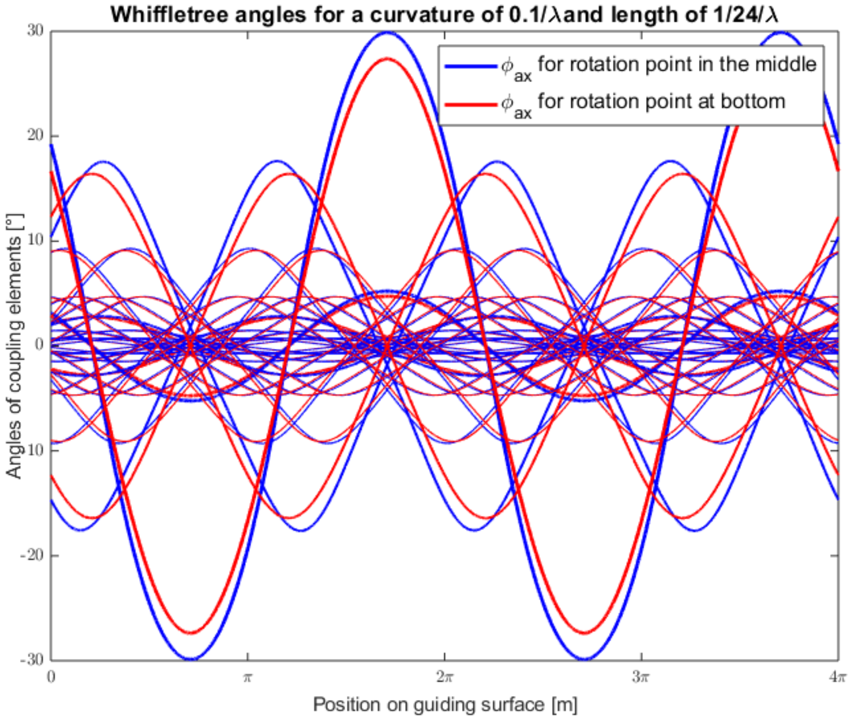

Figure 4: A comparison between angles of the intermediate bodies for two different pivot arm lengths. As the pivot is in the middle, the arm length R equals $\frac{L}{4}$, at the bottom the arm length equals zero.

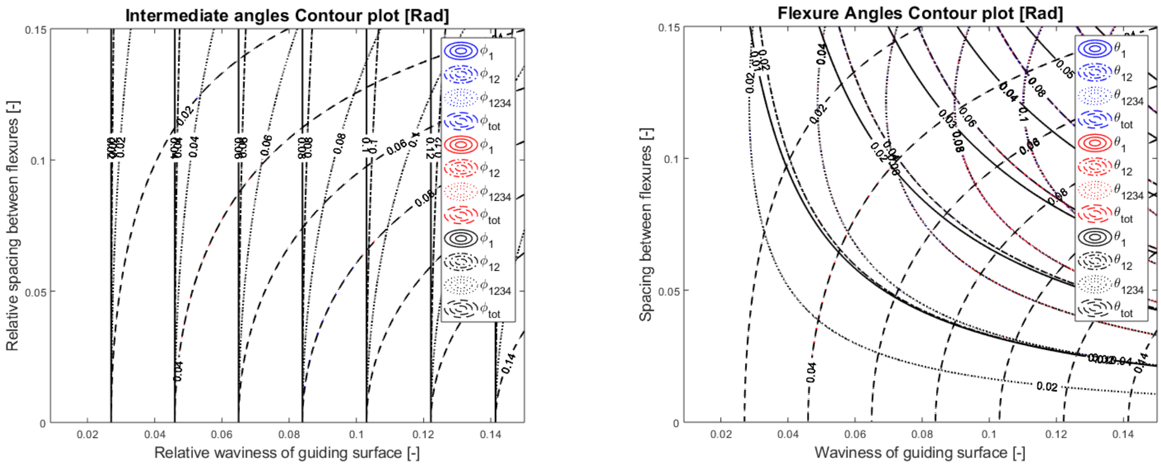

(a) Maximum angles of coupling elements

(b) Maximum angles of pivots elements

Figure 5: Contour plots of maximum angles as functions of distance between slippers and the relative waviness of the guiding surface. With three colors to represent the difference in pivot arm length. Blue represents the maximum angles for no pivot arm, red a pivot arm length of $\frac{L}{4}$ and black a pivot arm length of $\frac{L}{2}$

The error on location due to the linearisation for a 10% relative waviness amplitude is 7%. This is the largest possible derivation, for a two slipper whiffletree, spaced $\frac{1}{2}\pi$ apart. Other assumptions also have an error in their calculation, however those could not be quantified as correctly as this one.

Lateral motion slippers

In reality the slipper are not a fixed distance apart, but due to the rotation of the pivot they will move close or further from another. To prevent contact it will be required to check how much lateral motion the individual slippers experience. The most critical case would be where the first slipper has a lateral motion equal to the exact opposite of the second slipper. Figure 6.6 is used to define this lateral drift of the slippers.

$$x_{d1,2} = R\sin\phi_1 \tag{13}$$

$$x_{d2,2} = R\sin\phi_2 \tag{14}$$

$$x_{gap12,2} = x_{d2} - x_{d1} \tag{15}$$

$$\tag{16}$$

This has been investigated in the same manner as the pivot arm length. In order to find out that the lateral motion is not only a local effect but it's influence depends on pivot arm length, again three different pivot arm lengths have been take to investigate this behaviour. For a whiffletree with multiple cells the lateral motion of the cells has also be taken into account. With equations (6.34) and (6.35) this can be calculated in a similar fashion. Only the contact will likely occur between the second and third slipper, so the motion of these slippers has to be added.

$$x_{d12,4} = 2R\sin\phi_{12} \tag{17}$$

$$x_{d34,4} = 2R\sin\phi_{34} \tag{18}$$

$$x_{d2,4} = x_{d2,2} + x_{d12,4} \tag{19}$$

$$x_{gap23,4} = x_{d3,4} - x_{d2,4} \tag{20}$$

Figure 6 shows the contour plot of the lateral motion, it shows that pivot arm length has little to no influence on the motion, which is unexpected, compared to the effects of waviness and slipper spacing. Which does behave as expected, the slippers lateral drift due to rotation increases as the waviness increases, because the angles required will be bigger. But they also increase with increasing slipper spacing, at first the lateral motion appears small. However this should be taken into perspective that the slippers themselves are also small. The lateral motion also has to encompass the motion of all the three levels combined, as the slipper also moves if the cell is drifting.

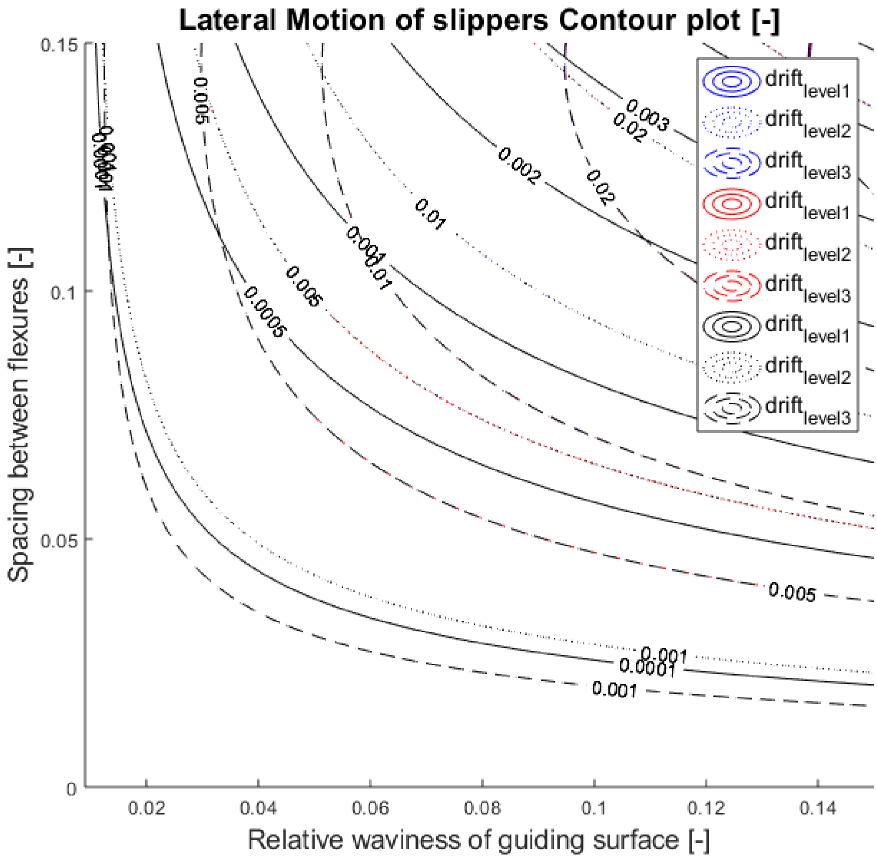

Figure 6: A contour plot showing the lateral motion between slippers as a function of relative waviness and relative slipper spacing. Blue represents lateral motion for no pivot arm, red represents lateral motion for a pivot arm length of $\frac{L}{4}$ and black represents lateral motion for a pivot arm length of $\frac{L}{2}$

Function for maximum angles

As the angles are known for any position on the guiding surface, it was tried to find a relationship between the maximum angles on the guiding surface. Equation 6.31 is used to determine the maximum angles of the intermediate bodies for higher levels of whiffletrees if these higher levels exist. For this purpose, a bearing is placed on a peak thus $x = \frac{1}{2}\pi$ is filled into these equations. This gives a function dependent on slipper spacing, d, and relative waviness amplitude, A. These are simplified using the following trigonometric relations were used to simplify the problem.

$$\cos x = -\cos x \tag{21}$$

$$2\arctan(x) = \arctan\left(\frac{2x}{1+x^2}\right) \tag{22}$$

$$\cos(\arctan(x) = \sqrt{\frac{1}{x^2+1}} \tag{23}$$

$$\sin(\arctan(A\cos x) = \sqrt{\frac{A\cos x}{A^2\cos x^2+1}} \tag{24}$$

$$||\phi_{12,max}|| = \frac{1}{2}\arctan\left(4A\frac{4A\cos\frac{d}{2}}{2-A^2\cos d}\right) \tag{25}$$

$$||\phi_{1234,max}|| = \frac{1}{2}\arctan\left(4A\frac{4A\cos d\cos\frac{d}{2}}{2-A^2\cos d-A^2\cos 2d}\right) \tag{26}$$

Equations (25) and (26) gave the impression that for each level the equation adds an additional term, therefore higher levels were also written out.

$$||\phi_{12345678,max}|| = \frac{1}{2}\arctan\left(\frac{\frac{4A\cos d\cos\frac{1}{2}d}{2-A^2\cos 2d-A^2\cos d}+\frac{4A\cos 3d\cos\frac{1}{2}d}{2-A^2\cos 6d-A^2\cos d}}{1-\frac{4A\cos d\cos\frac{1}{2}d}{2-A^2\cos 2d\cos d}\frac{4A\cos 3d\cos\frac{1}{2}d}{2-A^2\cos 6d-A^2\cos d}}\right) \tag{27}$$

However, this recursive addition to the function however was not found. Since it proved to be ineffective and not further relevant to investigate the angles for higher levels as no clear connection was found. Equations (25)-(27) were tools created to give insight in a relationship between the amount of levels of a whiffletree and the angles that it would make. However it proved less insight-full than expected of the problem at hand. And as the goal of this thesis is not to make mathematical derivations and descriptions of angles of the kinematics this was not further looked into.

Appendix C

Matlab Model Manuals

In this appendix the models are given as their matlab script. And an elaboration is given on the scripts so that they can be ran, altered and used in further research. As supplement to this thesis you are able to find these scripts and the figures, animations or interfaces they produce. The names of the scripts are given as sub titles in the following sections.

Manuals

Deformation Criteria

DeformationCriteria.m

The deformation criteria was expressed by equation (6.25) as defined in section 6.1. The contour plot 6.5 was generated by the following script. The script starts by setting up the number of steps and the largest slipper spacing and maximum relative waviness, which are the values on the x and y axis. Then through for-loops, the deformation criteria is check for every different value of slipper spacing, waviness amplitude and deformation factor. The smallest value of the deformation factor for which the criteria is satisfied for a given length and waviness is stored in a matrix. This matrix is then plotted, which gives us the contour plot seen in figure 6.5.

```
%% 22-11-2018
%% Simplified Deformation Criteria
%% Jan van Willigen
%% This script plots the deformation criteria, with as contours the deformation factor

close all
clear all
an=400;     %Step size
% bn=200;
Amax=0.1;   %Maximum Relative Waviness
Lmax=0.1;   %Maximum Slipper spacing
DFmin=1001; %Minimum deformation factor
DFdiff=991; %Steps of deformation factor
dH=00*(10^-6);  %Allow loss in flight height

l=1; b=1; a=1; ln=400;
Bok=zeros(an,ln,DFdiff);    %Allocating free space
Bplot=zeros(ln,an);         %Allocating free space
for A=linspace(0.01,Amax,an)
    for    L=linspace(0.01,Lmax,ln)
        for B=linspace(1/(DFmin-DFdiff),1/DFmin,DFdiff)
            if (A*sin((0.25+0.5*L)*2*pi))+dH>(A-B*L)
```

```
                Bok(a,l,b)=B;   %If Criteria is met, store current B
            end
            if Bok(a,l,b)~=0 && l==1   %If it is not met, it will never be met
                Bplot(l,a)=Bok(a,l,b);
            elseif Bok(a,l,b)~=0 && Bok(a,l−1,b) == 0 % If at the current length the
                deformation is not reached it will never be reached.
                if Bplot(l,a)==0    %If this was the first entry, thus its value was zero
                    Bplot(l,a)=Bok(a,l,b);     %Make sure the plotted will also be zero.
                end
% This aditional Loop is required to prevent over writng as the script would find Larger L's
    that also met the requirements.
% If the maximum length is reached store the maximum length
            elseif (l~=1 && Bok(a,l,b)~=0 && Bok(a,l,b)==Bok(a,l−1,b))
                Bplot(l,a)=Bok(a,l,b);
            elseif Bok(a,l,b)==1/1000
                Bplot(l,a)=Bok(a,l,b);
            end
            b=b+1;
        end
        b=1;
        l=l+1;
    end
    l=1;
    a=a+1;
end
%% Ploting data
Bplot;

L=linspace(0.01,Lmax,ln);
A=linspace(0.01,Amax,an);
B=linspace(1/(DFmin−DFdiff),1/DFmin,DFdiff);

figure(2)
axis equal
% [Data,Cplot]=contour(L,A,Bplot',[0 0.001 0.005 0.01 0.015 0.02 0.025 0.03 0.035 0.04], '
    showtext','on');
[Data,Cplot]=contourf(L,A,Bplot',[0 0.001 0.002 0.003 0.004 0.005 0.006 0.007 0.008 0.009
    0.01 0.015 0.02 0.025 0.03 0.035 0.04], 'showtext','on');
Cplot.LineWidth=1;
Cplot.LabelSpacing=350;
% Cplot.LineStyle='−';
colormap(flipud(0.6∗(gray+0.4))); %cool %hsv %pink %spring %autumn %hot
clabel(Data,Cplot,'FontSize',16)

set(gca,'FontSize',14, 'TickLabelInterpreter','latex','yTickLabel', {'1\%','2\%','3\%','4\%',
    '5\%','6\%','7\%','8\%','9\%','10\%'});
set(gca, 'XTickLabel', {'1\%','2\%','3\%','4\%','5\%','6\%','7\%','8\%','9\%','10\%'});

title('Contour Plot − Deformation Criteria','FontSize',18)
xlabel('Bearing Slipper Length % of \lambda','FontSize',18)
ylabel('Waviness Amplitude A/\lambda','FontSize',18)
```

DeformationCriteriaLengthContour.m

A variation on this script is that instead of the criteria is being plotted as a contour of the deformation factor, it is given as contour of the slipper length. This script runs similar to the last. Only instead of the for-loops saving the smallest deformation factor for which the criteria is satisfied, the largest slipper length is stored. Therefore, it is possible to create a contour plot with on the x and y axis, the deformation factor and waviness while the contour lines represent different relative slipper lengths. This can be seen in figure 7

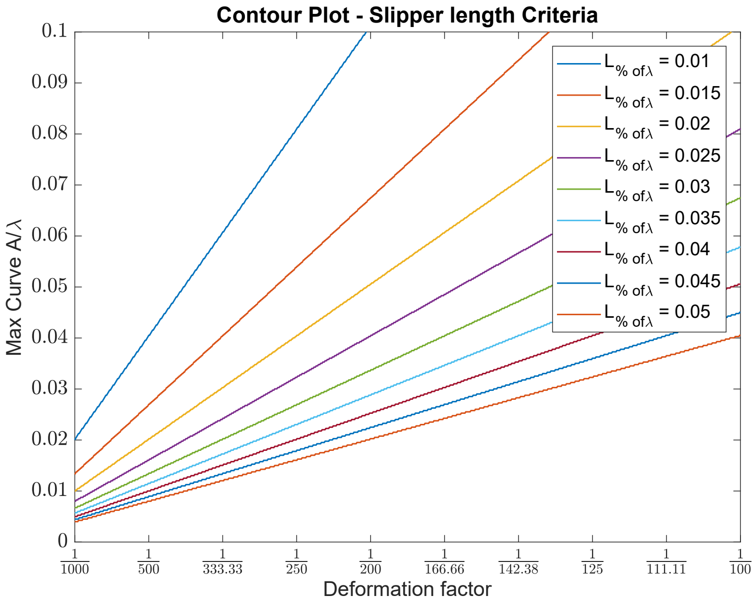

Figure 7: Contour plot of the deformation criteria with as contour lines the maximum slipper size corresponding the waviness and deformation factor.

```
%% 18-12-2018
%% Reversed Deformation Criteria
%% Jan van Willigen
%% This script plots the deformation criteria plot, not as contours of the deformation factor
%% But as contourlines of the maximum slipper size, with on the x-axis the deformation factor.

close all
clear all
an=1000;
% bn=1000;
Amax=0.25;  %Maximum Relative Waviness
DFmin=1000; %Minimum deformation factor
DFdiff=900; %Steps of deformation factor


l=1; b=1; a=1; ln=5;
Aok=zeros(ln,DFdiff,an);    %Allocating free space
Aplot=zeros(ln,DFdiff);     %Allocating free space
for A=linspace(0,Amax,an)   %Taking steps for each wavelength
    for B=linspace(1/DFmin,1/(DFmin-DFdiff),DFdiff) %Taking steps for each Deformation Factor
        for L=[0.01 0.015 0.02 0.025 0.03 0.035 0.04 0.045 0.05];
            if (A*sin((0.25+0.5*L)*2*pi))>(A-B*L)   %If the the deformation facotr is satisfied
                Aok(l,b,a)=A;                       %Store current wave-length A in Aok
            end

            if Aok(l,b,a)~=0 && b==1                     % If the deformation could not reach the curve at the smallest length, thus
                Aplot(l,b)=Aok(l,b,a);                   % at v==1 then it will never be reaced at this Deformation factor thus store Lplot = 0
            elseif Aok(l,b,a)~=0 && Aok(l,b-1,a) == 0    % If at the current length the deformation is no longer reached
                if Aok(l,b,a)>Aplot(l,b)
                    Aplot(l,b)=Aok(l,b,a);   % for which the deformation can be reached at
```

```
                        this deformation factor
                end
            elseif (b~=1 && Aok(l,b,a)~=0 && Aok(l,b,a)==Aok(l,b-1,a))
                Aplot(l,b)=Aok(l,b,a);% This aditional Loop is required to prevent over writng as the script would find Larger L's that also met the requirements.
            elseif Aok(l,b,a)>=Amax-Amax/an            % If the maximum length is reached store the maximum length
                Aplot(l,b)=Aok(l,b-1,a);                 % That means the length should be even larger than this to deform towards the curve.
            end
            l=l+1;
        end
        l=1;
        b=b+1;
    end
    b=1;
    a=a+1;
end
%% Ploting Data
% L=linspace(0.01,Lmax,ln);
L=[0.01 0.015 0.02 0.025 0.03 0.035 0.04 0.045 0.05];
A=linspace(1/100,Amax,an);
% B=linspace(1/1000,1/100,bn);
B=linspace(1/DFmin,1/(DFmin-DFdiff),DFdiff);

figure
L1=plot(B,Aplot(1,:));
hold on;
L2=plot(B,Aplot(2,:));
L3=plot(B,Aplot(3,:));
L4=plot(B,Aplot(4,:));
L5=plot(B,Aplot(5,:));
L6=plot(B,Aplot(6,:));
L7=plot(B,Aplot(7,:));
L8=plot(B,Aplot(8,:));
L9=plot(B,Aplot(9,:));

% legend([L1,L2,L3,L4,L5],['L_{\% of \lambda} = ' num2str(L(1))],['L_{\lambda=1} = ' num2str(L(2))],['L_{\lambda=1} = ' num2str(L(3))],['L_{\lambda=1} = ' num2str(L(4))],['L_{\lambda=1} = ' num2str(L(5))])%,['A_{\lambda=2\pi} = ' num2str(L(6))],['A_{\lambda=2\pi} = ' num2str(L(7))],['A_{\lambda=2\pi} = ' num2str(L(8))],['A_{\lambda=2\pi} = ' num2str(L(9))]);
legend([L1,L2,L3,L4,L5,L6,L7,L8,L9],['L_{% of\lambda} = ' num2str(L(1))],['L_{% of\lambda} = ' num2str(L(2))],['L_{% of\lambda} = ' num2str(L(3))],['L_{% of\lambda} = ' num2str(L(4))],['L_{% of\lambda} = ' num2str(L(5))],['L_{% of\lambda} = ' num2str(L(6))],['L_{% of\lambda} = ' num2str(L(7))],['L_{% of\lambda} = ' num2str(L(8))],['L_{% of\lambda} = ' num2str(L(9))])%,['A_{\lambda=2\pi} = ' num2str(L(6))],['A_{\lambda=2\pi} = ' num2str(L(7))],['A_{\lambda=2\pi} = ' num2str(L(8))],['A_{\lambda=2\pi} = ' num2str(L(9))]);

axis([1/1000 1/100 0 0.1])
set(gca, 'TickLabelInterpreter', 'latex', 'XTickLabel', {'$\frac{1}{1000}$', '$\frac{1}{500}$', '$\frac{1}{333.33}$', '$\frac{1}{250}$', '$\frac{1}{200}$','$\frac{1}{166.66}$', '$\frac{1}{142.38}$', '$\frac{1}{125}$','$\frac{1}{111.11}$', '$\frac{1}{100}$'},'FontSize',12);
title('Contour Plot - Slipper length Criteria','FontSize',15)
xlabel('Deformation factor','FontSize',14)
ylabel('Max Curve A/\lambda','FontSize',14)
```

SingleBearingDeformationMatrix.m

The previous plots showed how the contour plot was generated on the deformation criteria. However in the thesis presentation some visuals were presented that are not treated in this thesis. These can be seen in figure 8. These explain how the deformation criteria is defined as was illustrated by figure 6.2.

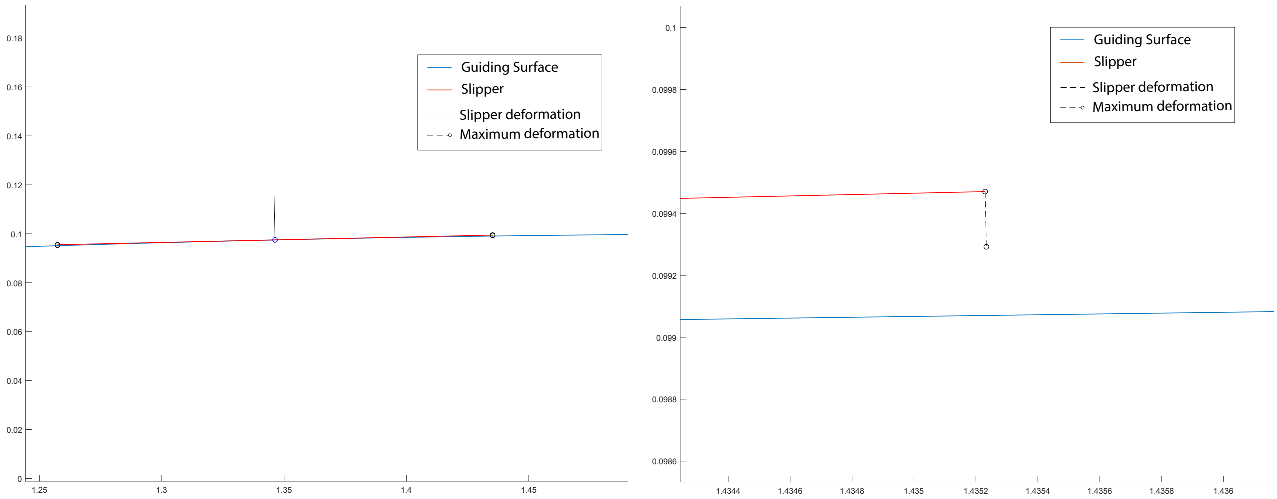

(a) Visualisation of slipper on the guiding surface

(b) Zoom on visualisation of slipper deformation

Figure 8: Simplified representation of slipper deformation, the slipper here does not meet the deformation criteria. As the deformed slipper does not reach the guiding surface.

This script stats by creating the guiding surface, and placing the slipper on top of as a tangent line. The deformation lines are place as tangent lines on the ends of the slipper with a length of $\frac{1}{1000}$th of the slipper length. This script also generates a gif, illustrating how a single slipper moves over the guiding surface. This GIF image is generated by taking a snapshot of the figure of a slipper at one location, then placing it a bit further and taking another snapshot. This process is repeated to let the bearing move over the complete guiding surface.

```
%% Jan van Willigen
%% 27−11−2018
%% This script follows a single bearing as it moves over a sinus curve with amplitude A.
%% Where the length L of the bearing is variable as well as it's deformation capability BF.
%%


%% Initilazation
clear all;
close all;

n=10000;                          %We discretize our sinus in N pieces
Amin=0.02;                       %The maximum amplitude of our sinus
Amax=0.2;                        %The maximum amplitude of our sinus
step=Amax/1000;                  %I wanted big step sizes to increase compuational speed, but
    small to make the curvature appear smooth, this is was a good trade−off

Lmax=pi/8;                       %As the total area we are looking at is pi/2, half this size
    seemed to me to be a good maxium size for length
increment=Lmax/1000;             %For the Length increments I wanted them to be a fragment of
    the maxium Length


Xx=linspace(0,pi,n);    %We are currently looking to an area around the peak of th sinus
y=Amax.*sin(Xx);                  %Let us start with  plotting the maximum amplitude sinus
figure(1)
plot(Xx,y)
hold on;

```

```
xt=1/2.*pi;                      %We are only intrested in the area around the peak for now, for a sinus the peak lies at pi/2

h=0.000005;                     % Designed fluid film thickness


% Prealocation of Storage Memory
Bx=0.001;
Ax=0.1;
Lx=[increment:increment:Lmax];



Lstorage=zeros(length(Bx), length(Lx),length(Xx));
Lplot=zeros(length(Bx),length(Ax),length(Xx));

Lstorage1=zeros(length(Xx), length(Lx));
Lstorage2=zeros(length(Xx), length(Lx));


b=1;s=1;d=1;v=1;                %Variables to check in which iteration we are at, b for Deformation Factor, s for Sinus Amplitude, v for Length and d for position X

hold on;
%%

x=Xx;
B=Bx %
A=Ax;
L=Lx';
x1=x;
y1=A.*sin(x1);                %for x=1/2pi it is known that y1=y2, but for other x this is not known!
% Location xt is the middle point between the two bearings
theta1=atan(A*cos(x1));       % sin(x)=y, cos(x)=dy/dx, tan(theta)=dy/dx
                              % Thus atan(cos(x))=theta, in this case x=xt
                              % We found out how to find the perpendicular vector to point X
dx1p=1/10*L*sin(theta1);      % I decided to give this vectors length depending on L to give them more visibilty
dy1p=1/10*L*cos(theta1);      % See Figure Geomtery1 for more info in WorkDocument, Week 43.

x1p=x1-dx1p;                  %X1p is the x location of the end of the vector perpendicular to x1
y1p=y1+dy1p;                  %Y1p is the x location of the end of the vector perpendicular to y

dx1=L./(2..*sqrt(A.*cos(x1).^2+1));
bx1=x1-dx1;
tx1=x1+dx1;
tx1p=tx1+B.*L.*sin(theta1);
bx1p=bx1+B.*L.*sin(theta1);
dy1=(L.*A.*cos(x1))./(2.*sqrt(A.*cos(x1).^2+1));
by1=y1-dy1;
ty1=y1+dy1;
ty1p=ty1-B.*L.*cos(theta1);
by1p=by1-B.*L.*cos(theta1);

Theta=rad2deg(theta1);

%%
```

```
% How to use data, x is a row, L is a column
% Thus tx1(:,1) is the location of tx1 for position 1 (x=0) and all
% Lengths L

% Plotting postions
% Number of steps plotted N
N=100;
P=int16(linspace(1,length(x),N));

% Plotting for a certain Length Ln and finding at what index of Lx this
% length is found and stored in i.
Ln=0.178;
i=1
while L(i)-Ln<0
    i=i+1
end
%% Plotting Gif
gif=figure;

% axis tight manual % this ensures that getframe() returns a consistent size
% axis([0 max(Xx) Amin Amax]);
axis equal

filename = 'Equal.gif';

plot(x,A*sin(x))
hold on

for n = 1:N
    axis equal

    % Draw plot for every N
    a=plot(x1(P(n)),y1(P(n)),'ob');
    b=plot([x1(P(n)) x1p(i,P(n))],[y1(P(n)) y1p(i,P(n))],'-k');
    c=plot([bx1(i,P(n)) tx1(i,P(n))],[by1(i,P(n)) ty1(i,P(n))],'r');
    d=plot([tx1(i,P(n)) tx1p(i,P(n))],[ty1(i,P(n)) ty1p(i,P(n))],'--ok');
    e=plot([bx1(i,P(n)) bx1p(i,P(n))],[by1(i,P(n)) by1p(i,P(n))],'--ok');
    n
    drawnow
%     pause(0.05)
    % Capture the plot as an image
    frame = getframe(gif);
    im = frame2im(frame);
    [imind,cm] = rgb2ind(im,256);
    % Write to the GIF File
    if n == 1
        imwrite(imind,cm,filename,'gif', 'Loopcount',inf,'DelayTime',0);
    else
        imwrite(imind,cm,filename,'gif','WriteMode','append','DelayTime',0.1);
    end
    delete(a)
    delete(b)
    delete(c)
    delete(d)
    delete(e)
end


%%

```

```matlab
N=8;
P=int16(linspace(1,length(Xx),N));

figure
axis equal
x=linspace(0,2*pi,2*n);
hold on

plot(x,A*sin(x))

for n = 1:N
    % Draw plot for every N
    a=plot(x1(P(n)),y1(P(n)),'ob');
    b=plot([x1(P(n)) x1p(i,P(n))],[y1(P(n)) y1p(i,P(n))],'-k');
    c=plot([bx1(i,P(n)) tx1(i,P(n))],[by1(i,P(n)) ty1(i,P(n))],'r');
    d=plot([tx1(i,P(n)) tx1p(i,P(n))],[ty1(i,P(n)) ty1p(i,P(n))],'--ok');
    e=plot([bx1(i,P(n)) bx1p(i,P(n))],[by1(i,P(n)) by1p(i,P(n))],'--ok');
end


%%
% Plotting for a certain Length Ln and finding at what index of Lx this
% length is found and stored in i.
Ln=0.08;
i=1
while L(i)-Ln<0
    i=i+1;
end
Lf=ty1p.*(ty1p-A*sin(tx1p)<0);
Lr=by1p.*(by1p-A*sin(bx1p)<0);
figure
hold on
PLr=plot(Xx,Lr(i,:),'b');
PLf=plot(Xx,Lf(i,:),'r');

xlabel('x location on sinus')
ylabel('Height')
title('Can it follow the curve')
legend([PLr,PLf],['Front of the bearing for a bearing size of ' num2str(Ln)],['Rear of the bearing for a bearing size of ' num2str(Ln)]);


figure
hold on
FB=plot(Xx,ty1p(i,:)-A*sin(tx1p(i,:)),'b');
RB=plot(Xx,by1p(i,:)-A*sin(bx1p(i,:)),'r');
xlabel('Location on sinus')
ylabel('Deformation distance')
title('Diffrence between tip of bearing and sinus in vertical direction')
legend([FB,RB],['Front of the bearing for a bearing size of ' num2str(Ln)],['Rear of the bearing for a bearing size of ' num2str(Ln)]);
```

TheActualAngles.m

The kinematics have been thoroughly elaborated in chapter 6. Below is the script that give both a plot for the intermediate angles and the flexure angles for different positions on the guiding surface. The slipper size and amplitude of the guiding surface are chosen at the beginning of the script. The calculations follows the kinematic descriptions of section 4.1 once the calculations are done, a plot is created of the guiding surface, after that the intermediate angles are plotted followed by the flexure angles. The later two can be seen in figure 9

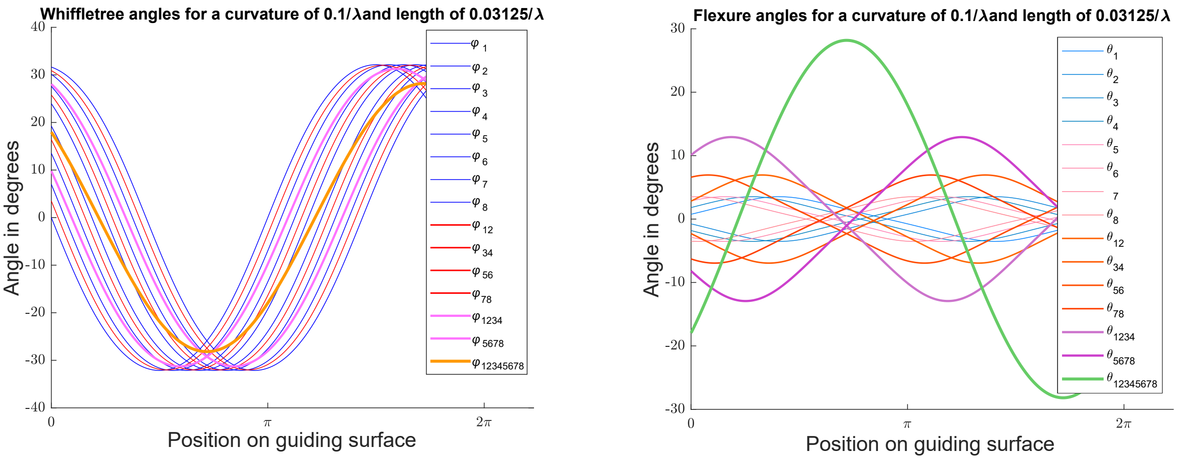

(a) Intermediate body angles

(b) Flexure angles

Figure 9: Whiffletree angles for a given wavelength and slipper size of a eight slipper whiffletree design.

```
%% This script calculates the whiffletree angles
%% Of both the intermediate bodies and the flexure angles
%% Jan van Willigen 29-4-2019

%% Initialisation
clear all
close all

xn=1000;
dn=100;
N=8;
f=2*pi;                     %Scaling factor turns 1 into 2pi.
x=linspace(0,1*f,xn)';    %Guiding surface of 1 metre
d=(1/32)*f;   %Slipper spacing
A=0.1*f;    %Wavelength percentage of wavlength
L=d;        %Length of pivots

% Memory allocation
phi=zeros(N,xn);
xr=zeros(N,xn);
yr=zeros(N,xn);

%% Calculations

%For eigth slippers calculate the angle of the slipper with guiding surface
for i=1:N
    phi(i,:)=atan(A.*cos(x+i*d));
    xr(i,:)=x-sin(phi(i,:)').*L;    %Calculate the rotation point of pivot
    yr(i,:)=A*sin(x)+cos(phi(i,:)').*L;
end

%
phi_12=atan((yr(2,:)-yr(1,:))./(xr(2,:)-xr(1,:)));
```

```
phi_34=atan((yr(4,:)-yr(3,:))./(xr(4,:)-xr(3,:)));
phi_56=atan((yr(6,:)-yr(5,:))./(xr(6,:)-xr(5,:)));
phi_78=atan((yr(8,:)-yr(7,:))./(xr(8,:)-xr(7,:)));

theta(1,:)=(phi(1,:)-phi_12);
theta(2,:)=(phi(2,:)-phi_12);
theta(3,:)=(phi(3,:)-phi_34);
theta(4,:)=(phi(4,:)-phi_34);
theta(5,:)=(phi(5,:)-phi_56);
theta(6,:)=(phi(6,:)-phi_56);
theta(7,:)=(phi(7,:)-phi_78);
theta(8,:)=(phi(8,:)-phi_78);

x12=(xr(1,:)+xr(2,:))/2;
x34=(xr(3,:)+xr(4,:))/2;
x56=(xr(5,:)+xr(6,:))/2;
x78=(xr(7,:)+xr(8,:))/2;

y12=(yr(1,:)+yr(2,:))/2;
y34=(yr(3,:)+yr(4,:))/2;
y56=(yr(5,:)+yr(6,:))/2;
y78=(yr(7,:)+yr(8,:))/2;

phi_1234=atan((y34-y12)./(x34-x12));
phi_5678=atan((y78-y56)./(x78-x56));

theta_12=phi_12-phi_1234;
theta_34=phi_34-phi_1234;
theta_56=phi_56-phi_5678;
theta_78=phi_78-phi_5678;

x1234=mean(xr([1,2,3,4],:));
x5678=mean(xr([5,6,7,8],:));
y1234=mean(yr([1,2,3,4],:));
y5678=mean(yr([5,6,7,8],:));

phi_12345678=atan((y5678-y1234)./(x5678-x1234));

theta_1234=phi_1234-phi_12345678;
theta_5678=phi_5678-phi_12345678;

theta_12345678=phi_12345678-0;


figure(1)   % Check wether amplitude and waviness are correct
plot(x,A*sin(x));
title('Scaled guiding surface, x=1m, A=0.1%');
xlabel('x-position on guiding surface');
ylabel('y-position Waviness')


figure
plot(x,phi,'b');
hold on
plot(x,phi_12,'r');
plot(x,phi_34,'r');
plot(x,phi_56,'r');
plot(x,phi_78,'r');
hold on
plot(x,phi_1234,'LineWidth',1.5,'color',[1 0.45 1]);
plot(x,phi_5678,'LineWidth',1.5,'color',[1 0.45 1]);
plot(x,phi_12345678,'LineWidth',2,'color',[1 0.6 0.0]);

% legend([q1,q2,q3,q4,q5,q6,q7,q8,w12,w34,w56,w78,z1234,z5678,y12345678],['\theta_1'],['\theta_2'],['\theta_{3}'],['\theta_{4}'],['\theta_5'],['\theta_6'],['\theta_{7}'],['\theta_{8}'],['\theta_{12}'],['\theta_{34}'],['\theta_{56}'],['\theta_{78}'],['\theta_{1234}'],['\theta_{5678}'],['\theta_{12345678}']);
set(gca, 'XTick', [0 1 2 3 4 5 6]*pi,'TickLabelInterpreter', 'latex', 'XTickLabel', {'0','$\pi$', '$2\pi$','$3\pi$', '$4\pi$','$5\pi$', '$6\pi$'});
title(['Whiffletree angles for a curvature of ' num2str(A) '/\lambda' 'and length of ' num2str(d/(2*pi)) '/\lambda']);
xlabel('position on guiding surface');
ylabel('angle in degrees')

% %%
figure
hold on
%
%
q1=plot(x,360/(2*pi)*theta(1,:),'color',[0 0.5 1]);     %Blue
q2=plot(x,360/(2*pi)*theta(2,:),'color',[0 0.5 0.85]);
q3=plot(x,360/(2*pi)*theta(3,:),'color',[0 0.5 0.8]);
q4=plot(x,360/(2*pi)*theta(4,:),'color',[0 0.5 0.75]);
q5=plot(x,360/(2*pi)*theta(5,:),'color',[1 0.5 0.7]);
q6=plot(x,360/(2*pi)*theta(6,:),'color',[1 0.5 0.65]);
q7=plot(x,360/(2*pi)*theta(7,:),'color',[1 0.5 0.6]);
q8=plot(x,360/(2*pi)*theta(8,:),'color',[1 0.5 0.55]);
%
w12=plot(x,360/(2*pi)*theta_12,'LineWidth',1,'color',[1 0.4 0]);     %Red
w34=plot(x,360/(2*pi)*theta_34,'LineWidth',1,'color',[1 0.35 0]);
w56=plot(x,360/(2*pi)*theta_56,'LineWidth',1,'color',[1 0.3 0]);
w78=plot(x,360/(2*pi)*theta_78,'LineWidth',1,'color',[1 0.25 0]);
%
z1234=plot(x,360/(2*pi)*theta_1234,'LineWidth',1.5,'color',[0.8 0.45 0.8]);  %Purple
z5678=plot(x,360/(2*pi)*theta_5678,'LineWidth',1.5,'color',[0.8 0.25 0.8]);

y12345678=plot(x,360/(2*pi)*theta_12345678,'LineWidth',2,'color',[0.4 0.8 0.4]); %Green
% legend([q1,q2,q3,q4,q5,q6,q7,q8],['\theta_1'],['\theta_2'],['\theta_{3}'],['\theta_{4}'],['\theta_5'],['\theta_6'],['\theta_{7}'],['\theta_{8}']);
%
legend([q1,q2,q3,q4,q5,q6,q7,q8,w12,w34,w56,w78,z1234,z5678,y12345678],['\theta_1'],['\theta_2'],['\theta_{3}'],['\theta_{4}'],['\theta_5'],['\theta_6'],['\theta_{7}'],['\theta_{8}'],['\theta_{12}'],['\theta_{34}'],['\theta_{56}'],['\theta_{78}'],['\theta_{1234}'],['\theta_{5678}'],['\theta_{12345678}']);
title(['Flexure angles for a curvature of ' num2str(A/(2*pi)) '/\lambda' 'and length of ' num2str(d/(2*pi)) '/\lambda']);
xlabel('position on guiding surface');
ylabel('angle in degrees')
set(gca, 'XTick', [0 1 2 3 4 5 6]*pi,'TickLabelInterpreter', 'latex', 'XTickLabel', {'0','$\pi$', '$2\pi$','$3\pi$', '$4\pi$','$5\pi$', '$6\pi$'});
```

CompleteAnglesChaos.m

The calculation of the maximum angle requires alot of effort. And as explained in section B a single function for the maximum angles is not found. Therefore it is required to calculate every angle while varying both slipper length and the guiding surface waviness. Thus to find the maximum angles requires a lot of computational power. However, one can use it to calculate both the angles of the intermediate bodies and the flexures at the same time. As well as calculating the lateral motion of the slippers. This is all combined in this script and is thus used to create figures 5a, 5b and 5.

This script was written to run per section. In the initialisation one can choose a value for the pivot arm length.

After the calculation section is done, it is recommended to store this data, so it can later be loaded as the calculation takes a lot of time. In the section `Compare to others` the script loads three .mat files, which are the results of the calculation for a specific arm length of either 0, 0.25L or 0.5L.

```
%% Jan van Willigen
%% March 2019
%% Script for determining maximum angles
%% As a function of Relative Waviness amplitude
%% and distance between slippers (slipper size)

clear all
close all

%Defining the step sizes
xn=1000;
ND=500;
NA=502;

% Alocating free space
phimax=zeros(15,ND,NA);
thetamax=zeros(16,ND,NA);
driftmax=zeros(7,ND,NA);
id=0;
ia=0;

% Chose the maximia a further than actual maxima so it's easier to plot
dmax=0.15;     %Max slipper size is 1/8 of 2*pi
Amax=0.15;     %Max Waviness amplitude is 10% of 2*pi

%% Calculation of the Angles and Drift
for d=linspace(0,dmax,ND)
    ia=0;
    id=id+1;
    for A=linspace(0.0009,Amax,NA)
        ia=ia+1;
        dn=100;
        N=8;

        x=linspace(0,2,xn)';
        % d=(1/(8*3));
        % A=0.1;
        L=d;

        f=2*pi;
        %Refresh for each new loop (new length of new waviness)
        phi=zeros(N,xn);
        xr=zeros(N,xn);
        yr=zeros(N,xn);
        %Arm length of connecting elements, this varies from R1=0, 0.25L and 0.5L
        %The results of the diffrent arm lengths are explained in the appendix.
        R1=0.5*L;
        R2=2*R1;
        R3=2*R2;

        % For each bearing (i) calaculate; tangent angle phi, x-pos and y-position
        for i=1:N
            phi(i,:)=atan(A.*cos(f*(x+(i-1)*d)));
            xr(i,:)=f*(x+d*(i-1))-sin(phi(i,:)').*R1;
            yr(i,:)=A*sin(f*(x+d*(i-1)))+cos(phi(i,:)').*R1;
        end

        %Angles of intermediate bodies connecting two slippers in one cell.
        phi_12=atan((yr(2,:)-yr(1,:))./(xr(2,:)-xr(1,:)));
        phi_34=atan((yr(4,:)-yr(3,:))./(xr(4,:)-xr(3,:)));
        phi_56=atan((yr(6,:)-yr(5,:))./(xr(6,:)-xr(5,:)));
        phi_78=atan((yr(8,:)-yr(7,:))./(xr(8,:)-xr(7,:)));

        %Angles of first level flexures connected to slipper coupling element
        theta(1,:)=(phi(1,:)-phi_12);
        theta(2,:)=(phi(2,:)-phi_12);
        theta(3,:)=(phi(3,:)-phi_34);
        theta(4,:)=(phi(4,:)-phi_34);
        theta(5,:)=(phi(5,:)-phi_56);
        theta(6,:)=(phi(6,:)-phi_56);
        theta(7,:)=(phi(7,:)-phi_78);
        theta(8,:)=(phi(8,:)-phi_78);

        dx=1/4*sin(theta)*L;
        %For checking how linearistion holds up
        l1d12=dx(1,:)-dx(2,:);
        l1d34=dx(3,:)-dx(4,:);
        l1d56=dx(5,:)-dx(6,:);
        l1d78=dx(7,:)-dx(8,:);

        %Calculating positions of the middle of coupling elements.
        x12=(xr(1,:)+xr(2,:))/2;
        x34=(xr(3,:)+xr(4,:))/2;
        x56=(xr(5,:)+xr(6,:))/2;
        x78=(xr(7,:)+xr(8,:))/2;
        %Only relative motion is importance not absolute
        y12=(yr(1,:)+yr(2,:))/2;
        y34=(yr(3,:)+yr(4,:))/2;
        y56=(yr(5,:)+yr(6,:))/2;
        y78=(yr(7,:)+yr(8,:))/2;

        %Calculating rotationalpoints of second flexure pivot
        x12r=x12-R2*sin(phi_12);
        x34r=x34-R2*sin(phi_34);
        x56r=x56-R2*sin(phi_56);
        x78r=x78-R2*sin(phi_78);

        y12r=y12+R2*cos(phi_12);
        y34r=y34+R2*cos(phi_34);
        y56r=y56+R2*cos(phi_56);
        y78r=y78+R2*cos(phi_78);

        %Angles of second level coupling elements, conneting 4 slippers.
        phi_1234=atan((y34r-y12r)./(x34r-x12r));
        phi_5678=atan((y78r-y56r)./(x78r-x56r));
        %Angles of second level pivots, connecting a two slipper cell
        theta_12=phi_12-phi_1234;
        theta_34=phi_34-phi_1234;
        theta_56=phi_56-phi_5678;
        theta_78=phi_78-phi_5678;

        l2d1234=L*sin(theta_12)-L*sin(theta_34);
        l2d5678=L*sin(theta_56)-L*sin(theta_78);
        %Calculating positions of the middle of coupling elements.
        x1234=mean(xr([1,2,3,4],:));
        x5678=mean(xr([5,6,7,8],:));
        y1234=mean(yr([1,2,3,4],:));
        y5678=mean(yr([5,6,7,8],:));
        %Calculating positions of the rotation point of third level flexure
        x1234r=x1234-L*sin(phi_1234);
        x5678r=x5678-L*sin(phi_5678);
        y1234r=y1234+L*cos(phi_1234);
        y5678r=y5678+L*cos(phi_5678);
        %Fourth and final level angle of coupling element
        phi_12345678=atan((y5678r-y1234r)./(x5678r-x1234r));
        %Third level flexure angles
        theta_1234=phi_1234-phi_12345678;
        theta_5678=phi_5678-phi_12345678;
        %Third level - drift between 1234 and 5678
        l3d12345678=L*sin(theta_1234)-L*sin(theta_5678);
        %Final flexure connecting the vericle
        theta_12345678=phi_12345678-0;
        theta_12345678_2=pi-phi_12345678;

        % Capturing data, we are only intrested in the maximum angles
        phimax([1:8],id,ia)=max(phi');

        phimax(9,id,ia)=max(phi_12');
        phimax(10,id,ia)=max(phi_34');
        phimax(11,id,ia)=max(phi_56');
        phimax(12,id,ia)=max(phi_78');

        phimax(13,id,ia)=max(phi_1234');
        phimax(14,id,ia)=max(phi_5678');

        phimax(15,id,ia)=max(phi_12345678);


        thetamax([1:8],id,ia)=max(theta');

        thetamax(9,id,ia)=max(theta_12');
        thetamax(10,id,ia)=max(theta_34');
        thetamax(11,id,ia)=max(theta_56');
        thetamax(12,id,ia)=max(theta_78');

        thetamax(13,id,ia)=max(theta_1234');
        thetamax(14,id,ia)=max(theta_5678');

        thetamax(15,id,ia)=max(theta_12345678);
        thetamax(16,id,ia)=max(theta_12345678_2);

        %Check how much lateral motion there is between the bearings
        driftmax(1,id,ia)=max(l1d12);
        driftmax(2,id,ia)=max(l1d34);
        driftmax(3,id,ia)=max(l1d56);
        driftmax(4,id,ia)=max(l1d78);
        driftmax(5,id,ia)=max(l2d1234);
        driftmax(6,id,ia)=max(l2d5678);
        driftmax(7,id,ia)=max(l3d12345678);
    end

end
%% Contour plot of maximum values of the angles
close all
d=linspace(0,dmax,ND);
A=linspace(0.009,Amax,NA);
```

```
figure(4)
[Data,Cplot]=contour(A,d,squeeze(phimax(1,:,:)), 'showtext','on','LineStyle','-');
hold on;
[Data1,Cplot1]=contour(A,d,squeeze(phimax(9,:,:)), 'showtext','on','LineStyle','-.');
[Data2,Cplot2]=contour(A,d,squeeze(phimax(13,:,:)), 'showtext','on','LineStyle',':');
[Data3,Cplot3]=contour(A,d,squeeze(phimax(15,:,:)), 'showtext','on','LineStyle','--');

legend([Cplot,Cplot1,Cplot2,Cplot3],['\phi_1'],['\phi_{12}'],['\phi_{1234}'],['\phi_{tot}']);


title('Intermediate angles Contour plot [Rad]','FontSize',16);
xlabel('Relative waviness of guiding surface [-]','FontSize',14);
ylabel('Relative spacing between flexures [-]','FontSize',14)

figure(5)
[Bata,Dplot]=contour(A,d,squeeze(thetamax(1,:,:)), 'showtext','on','LineStyle','-');
hold on
[Bata1,Dplot1]=contour(A,d,squeeze(thetamax(9,:,:)), 'showtext','on','LineStyle','-.');
[Bata2,Dplot2]=contour(A,d,squeeze(thetamax(13,:,:)), 'showtext','on','LineStyle',':');
[Bata3,Dplot3]=contour(A,d,squeeze(thetamax(15,:,:)), 'showtext','on','LineStyle','--');
title('Flexure Angles Contour plot [Rad]','FontSize',16);
xlabel('Waviness of guiding surface [-]','FontSize',14);
ylabel('Spacing between flexures [-]','FontSize',14)
legend([Dplot,Dplot1,Dplot2,Dplot3],['\theta_1'],['\theta_{12}'],['\theta_{1234}'],['\theta_{
    tot}']);

figure(6)
hold on
[Gata1,Hplot1]=contour(A,d,squeeze(driftmax(1,:,:)),[0.0001 0.0005 0.001 0.002 0.003 0.004
    0.005], 'showtext','on','Labelspacing',5,'LineStyle','-');
[Gata2,Hplot2]=contour(A,d,squeeze(driftmax(5,:,:)),[0.001 0.005 0.01 0.02 0.03 0.04 0.05], '
    showtext','on','Labelspacing',50,'LineStyle',':');
[Gata3,Hplot3]=contour(A,d,squeeze(driftmax(7,:,:)),[0.001 0.005 0.01 0.02 0.03 0.04 0.05], '
    showtext','on','Labelspacing',500,'LineStyle','--');
legend([Hplot1,Hplot2,Hplot3],['drift_{level1}'],['drift_{level2}'],['drift_{level3}']);

title('Lateral Motion of slippers Contour plot [-]','FontSize',16);
xlabel('Relative waviness of guiding surface [-]','FontSize',14);
ylabel('Spacing between flexures [-]','FontSize',14)

%% To Compare Add The Other Calculations of the angles with diffrent R values

load('ZomerChaosR0.mat','driftmax','thetamax','phimax')
figure(8)
1
[R0Data,R0Cplot]=contour(A,d,squeeze(phimax(1,:,:)), 'showtext','on','Labelspacing',450,'
    LineStyle','-','color','b');
R0Cplot.LineWidth=1;
hold on;
[R0Data1,R0Cplot1]=contour(A,d,squeeze(phimax(9,:,:)), 'showtext','on','Labelspacing',450,'
    LineStyle','-.','color','b');
[R0Data2,R0Cplot2]=contour(A,d,squeeze(phimax(13,:,:)), 'showtext','on','Labelspacing',450,'
    LineStyle',':','color','b');
[R0Data3,R0Cplot3]=contour(A,d,squeeze(phimax(15,:,:)), 'showtext','on','Labelspacing',450,'
    LineStyle','--','color','b');

load('ZomerChaosR0.25.mat','driftmax','thetamax','phimax')
[R025Data,R025Cplot]=contour(A,d,squeeze(phimax(1,:,:)), 'showtext','on','Labelspacing',450,'
    LineStyle','-','color','r');
hold on;
```

```
[R025Data1,R025Cplot1]=contour(A,d,squeeze(phimax(9,:,:)), 'showtext','on','Labelspacing'
    ,450,'LineStyle','-.','color','r');
[R025Data2,R025Cplot2]=contour(A,d,squeeze(phimax(13,:,:)), 'showtext','on','Labelspacing'
    ,450,'LineStyle',':','color','r');
[R025Data3,R025Cplot3]=contour(A,d,squeeze(phimax(15,:,:)), 'showtext','on','Labelspacing'
    ,450,'LineStyle','--','color','r');


load('ZomerChaosR0.5.mat','driftmax','thetamax','phimax')
[R05Data,R05Cplot]=contour(A,d,squeeze(phimax(1,:,:)), 'showtext','on','Labelspacing',450,'
    LineStyle','-','color','k');
hold on;
[R05Data1,R05Cplot1]=contour(A,d,squeeze(phimax(9,:,:)), 'showtext','on','Labelspacing',450,'
    LineStyle','-.','color','k');
[R05Data2,R05Cplot2]=contour(A,d,squeeze(phimax(13,:,:)), 'showtext','on','Labelspacing',450,
    'LineStyle',':','color','k');
[R05Data3,R05Cplot3]=contour(A,d,squeeze(phimax(15,:,:)), 'showtext','on','Labelspacing',450,
    'LineStyle','--','color','k');

legend([R0Cplot,R0Cplot1,R0Cplot2,R0Cplot3,R025Cplot,R025Cplot1,R025Cplot2,R025Cplot3,
    R05Cplot,R05Cplot1,R05Cplot2,R05Cplot3],['\phi_1'],['\phi_{12}'],['\phi_{1234}'],['\phi_{
    tot}'],['\phi_1'],['\phi_{12}'],['\phi_{1234}'],['\phi_{tot}'],['\phi_1'],['\phi_{12}'],[
    '\phi_{1234}'],['\phi_{tot}']);

title('Intermediate angles Contour plot [Rad]','FontSize',16);
xlabel('Relative waviness of guiding surface [-]','FontSize',14);
ylabel('Relative spacing between flexures [-]','FontSize',14)

load('ZomerChaosR0.mat','driftmax','thetamax','phimax')
figure(9)
[R0Bata,R0Dplot]=contour(A,d,squeeze(thetamax(1,:,:)), 'showtext','on','Labelspacing',450,'
    LineStyle','-','color','b');

hold on;
[R0Bata1,R0Dplot1]=contour(A,d,squeeze(thetamax(9,:,:)), 'showtext','on','Labelspacing',450,'
    LineStyle','-.','color','b');
[R0Bata2,R0Dplot2]=contour(A,d,squeeze(thetamax(13,:,:)), 'showtext','on','Labelspacing',450,
    'LineStyle',':','color','b');
[R0Bata3,R0Dplot3]=contour(A,d,squeeze(thetamax(15,:,:)), 'showtext','on','Labelspacing',450,
    'LineStyle','--','color','b');
load('ZomerChaosR0.25.mat','driftmax','thetamax','phimax'); 6
R0Dplot.LineWidth=1;
R0Dplot1.LineWidth=1;
R0Dplot2.LineWidth=1;
R0Dplot3.LineWidth=1;

[R025Bata,R025Dplot]=contour(A,d,squeeze(thetamax(1,:,:)), 'showtext','on','Labelspacing'
    ,450,'LineStyle','-','color','r');
[R025Bata1,R025Dplot1]=contour(A,d,squeeze(thetamax(9,:,:)), 'showtext','on','Labelspacing'
    ,450,'LineStyle','-.','color','r');
[R025Bata2,R025Dplot2]=contour(A,d,squeeze(thetamax(13,:,:)), 'showtext','on','Labelspacing'
    ,450,'LineStyle',':','color','r');
[R025Bata3,R025Dplot3]=contour(A,d,squeeze(thetamax(15,:,:)), 'showtext','on','Labelspacing'
    ,450,'LineStyle','--','color','r');
load('ZomerChaosR0.5.mat','driftmax','thetamax','phimax'); 7

[R05Bata,R05Dplot]=contour(A,d,squeeze(thetamax(1,:,:)), 'showtext','on','Labelspacing',450,'
    LineStyle','-','color','k');
[R05Bata1,R05Dplot1]=contour(A,d,squeeze(thetamax(9,:,:)), 'showtext','on','Labelspacing'
    ,450,'LineStyle','-.','color','k');
```

```
[R05Bata2,R05Dplot2]=contour(A,d,squeeze(thetamax(13,:,:)), 'showtext','on','Labelspacing',450,'LineStyle',':','color','k');
[R05Bata3,R05Dplot3]=contour(A,d,squeeze(thetamax(15,:,:)), 'showtext','on','Labelspacing',450,'LineStyle','--','color','k');

legend([R0Dplot,R0Dplot1,R0Dplot2,R0Dplot3,R025Dplot,R025Dplot1,R025Dplot2,R025Dplot3,R05Dplot,R05Dplot1,R05Dplot2,R05Dplot3],['\theta_1'],['\theta_{12}'],['\theta_{1234}'],['\theta_{tot}'],['\theta_1'],['\theta_{12}'],['\theta_{1234}'],['\theta_{tot}'],['\theta_1'],['\theta_{12}'],['\theta_{1234}'],['\theta_{tot}']);

title('Flexure Angles Contour plot [Rad]','FontSize',16);
xlabel('Waviness of guiding surface [-]','FontSize',14);
ylabel('Spacing between flexures [-]','FontSize',14)

load('ZomerChaosR0.mat','driftmax','thetamax','phimax');8
figure(10)
hold on
[R0Gata1,R0Hplot1]=contour(A,d,squeeze(driftmax(1,:,:)),[0.0001 0.0005 0.001 0.002 0.003 0.004 0.005], 'showtext','on','Labelspacing',450,'LineStyle','-','color','b');
[R0Gata2,R0Hplot2]=contour(A,d,squeeze(driftmax(5,:,:)),[0.001 0.005 0.01 0.02 0.03 0.04 0.05], 'showtext','on','Labelspacing',450,'LineStyle',':','color','b');
[R0Gata3,R0Hplot3]=contour(A,d,squeeze(driftmax(7,:,:)),[0.001 0.005 0.01 0.02 0.03 0.04 0.05], 'showtext','on','Labelspacing',450,'LineStyle','--','color','b');
load('ZomerChaosR0.25.mat','driftmax','thetamax','phimax');9

[R025Gata1,R025Hplot1]=contour(A,d,squeeze(driftmax(1,:,:)),[0.0001 0.0005 0.001 0.002 0.003 0.004 0.005], 'showtext','on','Labelspacing',450,'LineStyle','-','color','r');
[R025Gata2,R025Hplot2]=contour(A,d,squeeze(driftmax(5,:,:)),[0.001 0.005 0.01 0.02 0.03 0.04 0.05], 'showtext','on','Labelspacing',450,'LineStyle',':','color','r');
[R025Gata3,R025Hplot3]=contour(A,d,squeeze(driftmax(7,:,:)),[0.001 0.005 0.01 0.02 0.03 0.04 0.05], 'showtext','on','Labelspacing',450,'LineStyle','--','color','r');
load('ZomerChaosR0.5.mat','driftmax','thetamax','phimax');10
[R05Gata1,R05Hplot1]=contour(A,d,squeeze(driftmax(1,:,:)),[0.0001 0.0005 0.001 0.002 0.003 0.004 0.005], 'showtext','on','Labelspacing',450,'LineStyle','-','color','k');
[R05Gata2,R05Hplot2]=contour(A,d,squeeze(driftmax(5,:,:)),[0.001 0.005 0.01 0.02 0.03 0.04 0.05], 'showtext','on','Labelspacing',450,'LineStyle',':','color','k');
[R05Gata3,R05Hplot3]=contour(A,d,squeeze(driftmax(7,:,:)),[0.001 0.005 0.01 0.02 0.03 0.04 0.05], 'showtext','on','Labelspacing',450,'LineStyle','--','color','k');

legend([R0Hplot1,R0Hplot2,R0Hplot3,R025Hplot1,R025Hplot2,R025Hplot3,R05Hplot1,R05Hplot2,R05Hplot3],['drift_{level1}'],['drift_{level2}'],['drift_{level3}'],['drift_{level1}'],['drift_{level2}'],['drift_{level3}'],['drift_{level1}'],['drift_{level2}'],['drift_{level3}']);

title('Lateral Motion of slippers Contour plot [-]','FontSize',16);
xlabel('Relative waviness of guiding surface [-]','FontSize',14);
ylabel('Spacing between flexures [-]','FontSize',14)
```

RUN.m

Besides the Graphical User Interface another tool has been created to visualize the possibilities of a whiffletree based hydrostatic bearing. This script creates a GIF with four subs-screens as seen in figure 10. The first subplot in the top left shows the eight slippers moving side by side over the guiding surface. To the right of this one can see the total stroke the bearing mechanism would make. On the bottom left one can see the whiffletree angles of the intermediate body angles. Only a single slipper or intermediate body is shown at the time, otherwise this figure would become to cluttered. In the last figure one is able to see a close-up of a single slipper moving over the guiding surface, which is checked for the deformation criteria, if it passes the criteria the bearing turns green, otherwise it is red.

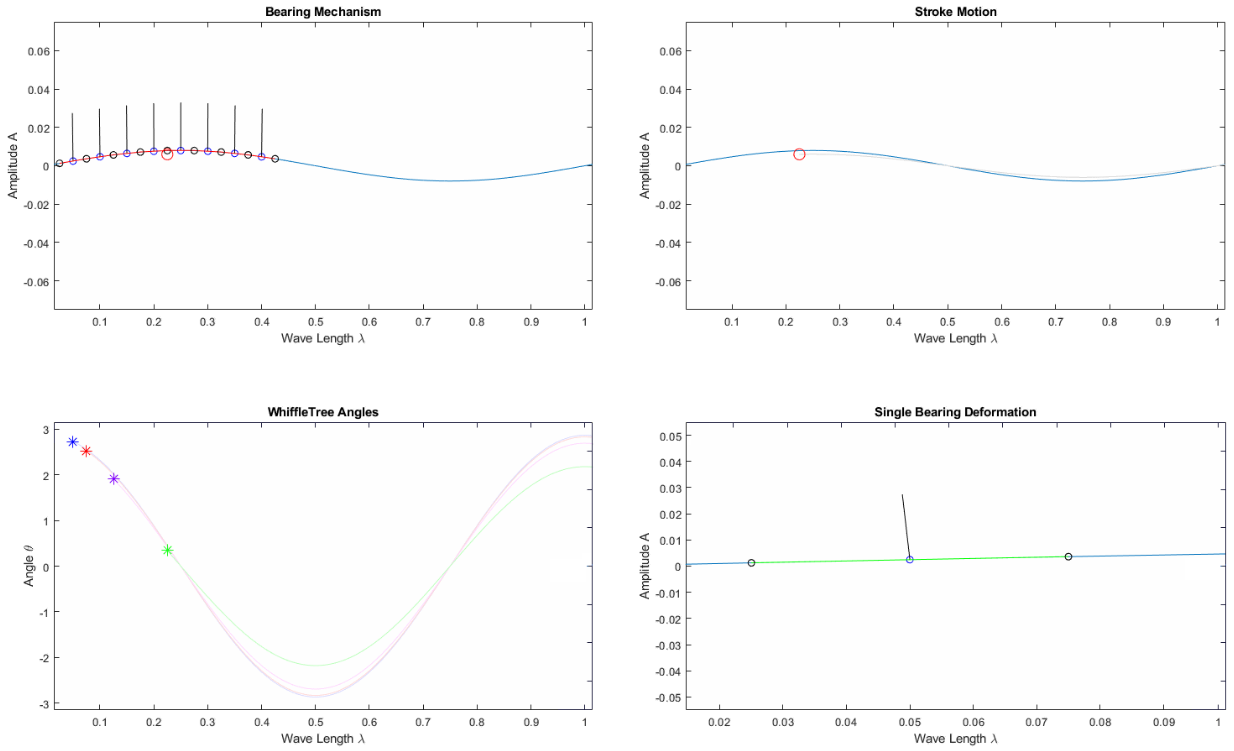

Figure 10: A single frame of the GIF which is the result of running the script RUN.m

One can alter the length of the bearing sizes and waviness amplitude in the Initialization. With the parameters known for the bearing size and guiding surface, the kinematics are run by an external matlab function *Bearing_Curve_Following.m*, this function requires the bearing position, waviness amplitude, length of the bearing, bearing deformation factor and scaling factor to run. It then outputs the all the kinematic parameters of a single slipper and the angle it is making with the guiding surface. Using this data the plot is created, first the guiding surface is plotted in all four subplots, as well as the trajectory for the whiffletree angles. Then the bearings are plotted upon this surface, the stroke on this current position, the angles for the current position and deformation criteria for a single slipper is checked. This image is stored as the first frame as the GIF, then the current positions are cleared and the bearing is moved, the new positions, stroke, angles etc. are plotted. This is repeated until the end of the wave is reached, as denoted by x in the initialisation. The step size for which the bearing is moved each step is denoted by Q. If the end is reached the GIF is stored in the current file directory under the name; **Green_*Lb*.gif**, where the *Lb* is the variable of the slipper length, thus the name is related to the slipper length. If the name already exists _1 is added to the name.

```
%%%%%%%%%%%%%%%%%%%%%%%%%%%%%%%%%%%%%%%%%%%%%%%%%
%% Jan van Willigen
%% 12-12-2018
%% This script will be the main visualiation of this research.
%% We split it up in four pieces:
%% Initialization, what variables and ranges of motion are we using.
%% Bearing Model Calculation, all calculation on bearing geometry
%% Post processing, making calculation into usefull information
%% Plotting, showing the results.
%%%%%%%%%%%%%%%%%%%%%%%%%%%%%%%%%%%%%%%%%%%%%%%%%

```

```matlab
%% Initialization
clear all;
close all;

Amin=0.02;                      % The miniumum amplitude of our sinus
Amax=0.05;                       % The maximum amplitude of our sinus
step=Amax/1000;                 % I wanted big step sizes to increase compuational speed, but small to make the curvature appear smooth, this is was a good trade-off

Lmax=pi/16;                      % As the total area we are looking at is pi/2, half this size seemed to me to be a good maxium size for length
increment=Lmax/10000;            % For the Length increments I wanted them to be a fragment of the maxium Length

nf=10000;                       % We discretize our sinus in nf pieces
xmax=3;                         % xmax is 1 so our sinus will be 1.
f=2*pi;                         % Scaling factor such that x=1 is a period
Xx=linspace(0,1.5,nf);          % The x-axis length in n steps from 0 to ..
y=Amax.*sin(f*Xx); % Here we multiply by f to scale to a sinus of length 1.
figure(1)
plot(Xx,y)         % Plot a sinus for the length Xx with amplitude of Amax.
hold on;


% Prealocation of Storage Memory
Bmax=0.001;                       % Deformation factor
Ax=0.1;                         % Amplitude of curve
Lx=increment:increment:Lmax;  % Length of bearing

% As it is faster to replace zeros by values to lengthen vectors
% afterwards. It also gives insight that we make sure we are collecting all
% data we need and want.

xn=zeros(13,length(Xx));        % storage assigned for bearings.

% b=1;s=1;d=1;v=1;                % Variables to check in which iteration we are at, b for Deformation Factor, s for Sinus Amplitude, v for Length and d for position X
x=linspace(0,3,nf);
B=Bmax;
A=Amax;
L=Lx';
%%
N=8;           % with this number of bearings we can fit in bearings of
% Lb=0.01;  % size Lb onto a guiding surface of length 1/2 xmax.
Lb=0.05;
i=1;
while L(i)-Lb<0 % What index matches this bearing length
    i=i+1;
end
Lb=L(i);         % This is the length that matches the requirement
clear L

%% Curve follower
% Deterimine the postition of each of the bearings
% With each of them a distance Lb removed from the previous bearing

for n=1:N
    [xb,yb,xp,yp,rxb,fxb,ryb,fyb,fxp,fyp,rxp,ryp,Theta] = Bearing_Curve_following(x+Lb*n,A,Lb,B,f);
    xn(:,:,n)=[xb;yb;xp;yp;rxb;fxb;ryb;fyb;fxp;fyp;rxp;ryp;Theta];
    n
end
%     xn(1,:,:,n)=xb;
%     xn(2,:,:,n)=yb;
%     xn(3,:,:,n)=xp;
%     xn(4,:,:,n)=yp;
%     xn(5,:,:,n)=rxb;
%     xn(6,:,:,n)=fxb;
%     xn(7,:,:,n)=ryb;
%     xn(8,:,:,n)=fyb;
%     xn(9,:,:,n)=fxp;
%     xn(10,:,:,n)=fyp;
%     xn(11,:,:,n)=rxp;
%     xn(12,:,:,n)=ryp;
%     xn(13,:,:,n)=Theta;
%     n
% end
% for n=1:n
%     [xb,yb,xp,yp,rxb,fxb,ryb,fyb,fxp,fyp,rxp,ryp,Theta] = Curve_follower(x+Lb*n,A,L,B);
%     xn(:,:,n)=[xb;yb;xp;yp;rxb;fxb;ryb;fyb;fxp;fyp;rxp;ryp;Theta];
% end

%% Using the Data
% How to use data, x is a row, L is a column
% Thus tx1(:,1) is the location of tx1 for position 1 (x=0) and all
% Lengths L, and tx1(1,:) for all postions x with with smallest length L.
% xn(1,:,10)==xb

% Plotting postions P
% Number of steps plotted q
Q=200;                             % Pick some number of points on which we
P=int16(linspace(1,length(x),Q));  % will plot the movement of the bearing.

%% Plotting Gif
close all
gif=figure(2);

%axis tight manual % this ensures that getframe() returns a consistent size
%axis([0 max(Xx) Amin Amax]);
axis equal
set(gcf, 'Position', get(0, 'Screensize'));

filename = sprintf('Green_%1.3f.gif', Lb);

while exist(filename, 'file') == 2
    filename=char(string(filename([1:length(filename)-4]))+'_1.gif');
end

%Plot all initial lines, plot the guiding surface.
subplot(2,2,1);
plot(x,A*sin(f*x))
title('Bearing Mechanism');
hold on
xlabel('Wave Length \lambda')
ylabel('Amplitude A')

subplot(2,2,2);
plot(x,A*sin(f*x))
title('Stroke Motion');
hold on
```

```
stroke=plot(mean(xn(1,:,:),3),mean(xn(2,:,:),3),'color',[0.85 0.85 0.85]);
xlabel('Wave Length \lambda')
ylabel('Amplitude A')

subplot(2,2,3);
title('WhiffleTree Angles');
hold on
theta_level_1=plot(xn(1,:,1),xn(13,:,1),'color',[0.85 0.85 1]);
theta_level_2=plot((xn(1,:,1)+xn(1,:,2))/2,(xn(13,:,1)+xn(13,:,2))/2,'color',[1 0.85 0.85]);
theta_level_3=plot((xn(1,:,1)+xn(1,:,2)+(xn(1,:,3)+xn(1,:,4)))/4,(xn(13,:,1)+xn(13,:,2)+xn(13,:,3)+xn(13,:,4))/4,'color',[1 0.85 1]);
theta_level_4=plot(mean(xn(1,:,:),3),mean(xn(13,:,:),3),'color',[0.75 1 .75]);

xlabel('Wave Length \lambda')
ylabel('Angle \theta')

subplot(2,2,4);
title('Single Bearing Deformation');
hold on
plot(x,A*sin(f*x))
xlabel('Wave Length \lambda')
ylabel('Amplitude A')

a=zeros(N);
b=zeros(N);
c=zeros(N);
d=zeros(N);
e=zeros(N);

f2=round(length(x)/Q);


for q = 1:(Q-(n*Lb/max(x))*Q)
%         gif=figure(2);

%     axis equal
    axis([0+x(q*f2-q) 1+x(q*f2-q) -1.5*Amax 1.5*Amax])
    for n=1:N
        subplot(2,2,1);
        % Draw plot for every Q
        % xn(:,:,n)=[xb;yb;xp;yp;rxb;fxb;ryb;fyb;fxp;fyp;rxp;ryp;Theta];
        % xn(1,P(q),n) gives xb values for certain positions P(q) for bearing n
        a(n)=plot(xn(1,P(q),n),xn(2,P(q),n),'ob');
        %Plots xb to yb on postions P(q) for bearing n

        b(n)=plot([xn(1,P(q),n) xn(3,P(q),n)],[xn(2,P(q),n) xn(4,P(q),n)],'-k');
        %Plots [xb xp],[yb,yp]

        c(n)=plot([xn(5,P(q),n) xn(6,P(q),n)],[xn(7,P(q),n) xn(8,P(q),n)],'r');
        %plots [rxb ftx],[ryb fyb]

        d(n)=plot([xn(5,P(q),n) xn(11,P(q),n)],[xn(7,P(q),n) xn(12,P(q),n)],'--ok');
        %plots [rxb rxp],[ryb ryp]

        e(n)=plot([xn(6,P(q),n) xn(9,P(q),n)],[xn(8,P(q),n) xn(10,P(q),n)],'--ok');
        %plots [fxb fxp],[fyb fyp]
%         n
        axis([0+x(q*f2-q) 1+x(q*f2-q) -1.5*Amax 1.5*Amax])
    end

    abc=plot(mean(xn(1,P(q),:)),mean(xn(2,P(q),:)),'ro','MarkerSize',10);

    subplot(2,2,2);
    stroke=plot(mean(xn(1,P(q),:)),mean(xn(2,P(q),:)),'ro','MarkerSize',10);
    axis([0+x(q*f2-q) 1+x(q*f2-q) -1.5*Amax 1.5*Amax])

    theta_12345678=mean(xn(13,P(q),:));
    theta_1234=(xn(13,P(q),1)+xn(13,P(q),2)+xn(13,P(q),3)+xn(13,P(q),4))/4-theta_12345678;
    theta_12=(xn(13,P(q),1)+xn(13,P(q),2))/2-theta_1234;
    theta_1=xn(13,P(q),1)-theta_12;

    % sub plot of the angles
    subplot(2,2,3);
    theta_level_1=plot(xn(1,P(q),1),xn(13,P(q),1),'*b','MarkerSize',10);
    theta_level_2=plot((xn(1,P(q),1)+xn(1,P(q),2))/2,(xn(13,P(q),1)+xn(13,P(q),2))/2,'*r','MarkerSize',10);
    theta_level_3=plot((xn(1,P(q),1)+xn(1,P(q),2)+xn(1,P(q),3)+xn(1,P(q),4))/4,(xn(13,P(q),1)+xn(13,P(q),2)+xn(13,P(q),3)+xn(13,P(q),4))/4,'*','color',[0.5 0 1],'MarkerSize',10);
    theta_level_4=plot(mean(xn(1,P(q),:)),mean(xn(13,P(q),:)),'*','color',[0.1 1 0.1],'MarkerSize',10);
    axis([0+x(q*f2-q) 1+x(q*f2-q) -1.1*max(xn(13,:,N)) 1.1*max(xn(13,:,N))])

    subplot(2,2,4);
    % single bearing deformation
    a1=plot(xn(1,P(q),1),xn(2,P(q),1),'ob');
    b1=plot([xn(1,P(q),1) xn(3,P(q),1)],[xn(2,P(q),1) xn(4,P(q),1)],'-k');
    c1=plot([xn(5,P(q),1) xn(6,P(q),1)],[xn(7,P(q),1) xn(8,P(q),1)],'r');
    d1=plot([xn(5,P(q),1) xn(11,P(q),1)],[xn(7,P(q),1) xn(12,P(q),1)],'--ok');
    e1=plot([xn(6,P(q),1) xn(9,P(q),1)],[xn(8,P(q),1) xn(10,P(q),1)],'--ok');
    axis([0+x(q*f2-round(1/N*q)) 0.085+x(q*f2-round(1/N*q)) -1.1*Amax 1.1*Amax])

    % %% Deformation Criteria !!

    % Color the bearing green if the dofrmation criteria is met
    %         if
    %            (fyp < A*sin(f*fxp) & fyp>0 OR fyp > A*sin(f*fxp) & fyp<0)
    %            AND
    %            (ryp < A*sin(f*rxp) & ryp>0 OR fyp > A*sin(f*rxp) & ryp<0)
    %   Where in BearingCurveFollower the deformation curvature can be both
    %   positive and negative, convex or concave
    if (((xn(10,P(q),1))<(A*sin(f*xn(9,P(q),1)))&&(xn(10,P(q),1)>0))||(((xn(10,P(q),1))>(A*sin(f*xn(9,P(q),1))))&&(xn(10,P(q),1)<0)))&&...
            (((xn(12,P(q),1))<(A*sin(f*xn(11,P(q),1)))&&(xn(12,P(q),1)>0))||(((xn(12,P(q),1))>(A*sin(f*xn(11,P(q),1))))&&(xn(12,P(q),1)<0)))
        c1.Color=[0 1 0];
    end




%     q
    drawnow

    % Capture the plot as an image
    frame = getframe(gif);
    im = frame2im(frame);
    [imind,cm] = rgb2ind(im,256);
    % Write to the GIF File
    if q == 1
        imwrite(imind,cm,filename,'gif', 'Loopcount',inf,'DelayTime',0);
    elseif q>0.5*Q
        imwrite(imind,cm,filename,'gif','WriteMode','append','DelayTime',0.1);
    else
        imwrite(imind,cm,filename,'gif','WriteMode','append','DelayTime',0.05);
    end

    delete(a)
    delete(b)
    delete(c)
    delete(d)
    delete(e)
    delete(abc)

    delete(theta_level_1)
    delete(theta_level_2)
    delete(theta_level_3)
    delete(theta_level_4)

    delete(a1)
    delete(b1)
    delete(c1)
    delete(d1)
    delete(e1)

end


%%

Q2=8;
P=int16(linspace(1,length(Xx),Q2));

figure(3)
axis equal

hold on

Xx=linspace(0,f,nf);
plot(Xx,A*sin(f*Xx))

for q = 1:Q2
    for n=1:8
        % Draw plot for every Q2
        a=plot(xn(1,P(q),n),xn(2,P(q),n),'ob');
        b=plot([xn(1,P(q),n) xn(3,P(q),n)],[xn(2,P(q),n) xn(4,P(q),n)],'-k');
        c=plot([xn(5,P(q),n) xn(6,P(q),n)],[xn(7,P(q),n) xn(8,P(q),n)],'r');
        d=plot([xn(5,P(q),n) xn(11,P(q),n)],[xn(7,P(q),n) xn(12,P(q),n)],'--ok');
        e=plot([xn(6,P(q),n) xn(9,P(q),n)],[xn(8,P(q),n) xn(10,P(q),n)],'--ok');
        %          fyp < A*sin(fxp);
        %          if
        %              (fyp < A*sin(f*fxp) & fyp>0 OR fyp > A*sin(f*fxp) & fyp<0)
        %              AND
        %              (ryp < A*sin(f*rxp) & ryp>0 OR fyp > A*sin(f*rxp) & ryp<0)
        %
        if (((xn(10,P(q),n))<(A*sin(f*xn(9,P(q),n)))&&(xn(10,P(q),n)>0))||(((xn(10,P(q),n))>(A*sin(f*xn(9,P(q),n))))&&(xn(10,P(q),n)<0)))&&...
                (((xn(12,P(q),n))<(A*sin(f*xn(11,P(q),n)))&&(xn(12,P(q),n)>0))||(((xn(12,P(q),n))>(A*sin(f*xn(11,P(q),n))))&&(xn(12,P(q),n)<0)))
            c.Color=[0 1 0];
        end

    end
end

%%
figure
plot(A*sin(f*xn(1,:,1)));
hold on
plot((((xn(10,:,1))<(A*sin(f*xn(9,:,1)))&(xn(10,:,1)>0)))|(((xn(10,:,1))>(A*sin(f*xn(9,:,1))))&(xn(10,:,1)<0)))&...
(((xn(12,:,1))<(A*sin(f*xn(11,:,1)))&(xn(12,:,1)>0))|(((xn(12,:,1))>(A*sin(f*xn(11,:,1))))&(xn(12,:,1)<0))))

% (((xn(10,:,1))<(A*sin(f*xn(9,:,1)) && xn(10,:,1)>0)) ||  ((xn(10,:,1))>(A*sin(f*xn(9,:,1)) &&...
%    xn(10,:,1)<0)))&&(((xn(12,:,1))<(A*sin(f*xn(11,:,1)) && xn(12,:,1)>0)) || ((xn(12,:,1))>(A*sin(f*xn(11,:,1)) && xn(11,:,1)<0)))
```

Bearing_Curve _Following.m

```
function [xb,yb,xp,yp,rxb,fxb,ryb,fyb,fxp,fyp,rxp,ryp,Theta] = Curve_follower(x,A,L,B,f)

xb=x;                    % x-location of n-th bearing.
                        % Scaling factor such that xb=1 is 1 period
yb=A.*sin(f*xb);      % bearing y-location of n-th bearing.

theta=atan(A*f*cos(f*x));   % sin(x)=y, cos(x)=dy/dx, tan(theta)=dy/dx
                        % Thus atan(cos(x))=theta, in this case x=xt
                        % Create the perpendicular vector to point X
dxp=1/2*L.*sin(theta);  % Vector length depending on L for more visibilty
dyp=1/2*L.*cos(theta);  % For more info in WorkDocument, Week 43.

% psign=(xb<(max(x)/2)|xb>max(x))-(xb>(max(x)/2)&xb<(max(x)));
% psign=(yb>0)-(yb<0);

psign=1;
xp=xb-psign.*dxp;          %xp is the x location of the vector perpendicular to xb
yp=yb+psign.*dyp;          %Yp is the y location of the vector perpendicular to yb

% dx=L./(2..*sqrt(A.^2.*cos(f*x).^2+1)); % dx of tangent line on x /w length L/2
dx=(L./2).*cos(theta);               % is the same as the line above in%
rxb=xb-dx;                          % x-location rear of the bearing
fxb=xb+dx;                          % x-location front of the bearing


% dy=(A.*L.*cos(f*x))./(2.*sqrt(A.^2.*cos(f*x).^2+1)); % dy of tangent line
dy=(L./2).*sin(theta);    % is the same as the line above in%
ryb=yb-dy;                      % y-location rear of the bearing
fyb=yb+dy;                      % y-location front of the bearing

% fsign=(fxb<(max(x)/2)|fxb>max(x))-(fxb>(max(x)/2)&fxb<(max(x)));
% rsign=(rxb<(max(x)/2)|rxb>max(x))-(rxb>(max(x)/2)&rxb<(max(x)));
% Sign is related to convex or concave deformation
fsign=(fyb>0)-(fyb<0);
rsign=(ryb>0)-(ryb<0);

fxp=fxb+fsign.*B.*L.*sin(theta);  % x-location of bearing front 'deformation'
rxp=rxb+rsign.*B.*L.*sin(theta);  % vector perpendicular to rear of bearing
ryp=ryb-rsign.*B.*L.*cos(theta);  % y location of rear bearing 'deformation'
```

```
fyp=fyb-fsign.*B.*L.*cos(theta);  % vector perpendicular to front of bearing

Theta=rad2deg(theta);
```

DeApp$_zomer_backup.mlapp$

The Graphical User Interface uses three external functions to run, these are *Angles.m*, *Orifice.m* and *Tilt.m*. These are used to calculate the angles, the load capacity of an orifice bearing and the tilt stiffness of a multi-recess bearing. These scripts use the inputs given on default screen of the interface, as guiding surface length, waviness, slipper deformation, slipper length, designed film height and supply pressure. The angles and orifice scripts are run when the update button is pressed. As the interface needs the parameters from the angles and orifice to show the kinematics and loading capacity of the bearing. These are also required to calculate stress levels and are needed for the stress criteria.

The GUI is created using matlab 2018b, with the app designer toolbox. The scripts is run through callbacks and interactions with the interface. Clicking the Update button, turning a knob or clicking a option from a drop down menu will run a series of functions resulting in a visual change on the interface.

```
classdef DeApp_zomer_backup < matlab.apps.AppBase

    % Properties that correspond to app components
    properties (Access = public)
        UserInterfaceBearingDesignerUIFigure  matlab.ui.Figure
        SlipperSpecificationsMenu       matlab.ui.container.Menu
        FilmFluidStiffnessMenu          matlab.ui.container.Menu
        RecessPressureMenu              matlab.ui.container.Menu
        LoadCapacityMenu                matlab.ui.container.Menu
        TiltStiffnessMenu               matlab.ui.container.Menu
        StepSizeSliderLabel             matlab.ui.control.Label
        StepSizeSlider                  matlab.ui.control.Slider
        UIAxes                          matlab.ui.control.UIAxes
        LengthofguidingsurfacemLabel    matlab.ui.control.Label
        EF_x                            matlab.ui.control.NumericEditField
        WavinessamplitudemmLabel        matlab.ui.control.Label
        EF_A                            matlab.ui.control.NumericEditField
        GuidingCurvatureDropDownLabel   matlab.ui.control.Label
        DD_funtion                      matlab.ui.control.DropDown
        LengthofsingleslippermmLabel    matlab.ui.control.Label
        EF_L                            matlab.ui.control.NumericEditField
        SlipperdeformationLabel         matlab.ui.control.Label
        EF_DF                           matlab.ui.control.NumericEditField
        SlipperparallelwithfilmLabel    matlab.ui.control.Label
        Knob_h                          matlab.ui.control.DiscreteKnob
        AllowedlossinflightheightmLabel  matlab.ui.control.Label
        EF_dH                           matlab.ui.control.NumericEditField
        UpdateButton                    matlab.ui.control.Button
        LengthtoLoadSwitchLabel         matlab.ui.control.Label
        Switch_LW                       matlab.ui.control.Switch
        UIAxes_Theta                    matlab.ui.control.UIAxes
        UIAxes_Phi                      matlab.ui.control.UIAxes
        LoadCapacitySlipperNLabel       matlab.ui.control.Label
        EF_W                            matlab.ui.control.NumericEditField
        TotalBearingLoadCapacityNLabel  matlab.ui.control.Label
        EF_F                            matlab.ui.control.NumericEditField
        BearingfootpringonguidingsurfaceLabel  matlab.ui.control.Label
        EF_foot                         matlab.ui.control.NumericEditField
        Stressflexurelevel1MPaLabel     matlab.ui.control.Label
        EF_s1                           matlab.ui.control.NumericEditField
        Stressflexurelevel2MPaLabel     matlab.ui.control.Label
        EF_s2                           matlab.ui.control.NumericEditField
        Stressflexurelevel3MPaLabel     matlab.ui.control.Label
        EF_s3                           matlab.ui.control.NumericEditField
        Stressflexurelevel4MPaLabel     matlab.ui.control.Label
        EF_s4                           matlab.ui.control.NumericEditField
        TabGroup                        matlab.ui.container.TabGroup
        SupplySpecsTab                  matlab.ui.container.Tab
        SupplyPressurebarLabel          matlab.ui.control.Label
        EF_Ps                           matlab.ui.control.NumericEditField
        DesignedfilmthicknessmLabel     matlab.ui.control.Label
        EF_h0                           matlab.ui.control.NumericEditField
        NumberofslippersLabel           matlab.ui.control.Label
        EF_Nu                           matlab.ui.control.NumericEditField
        FlexureParametersTab            matlab.ui.container.Tab
        YoungsModulusGPaDropDownLabel   matlab.ui.control.Label
        DD_E                            matlab.ui.control.DropDown
        ThicknessmmDropDownLabel        matlab.ui.control.Label
        DD_t                            matlab.ui.control.DropDown
        WidthmmDropDownLabel            matlab.ui.control.Label
        DD_b                            matlab.ui.control.DropDown
        RecessPressurebarLabel          matlab.ui.control.Label
        EF_Pr                           matlab.ui.control.NumericEditField
        YieldStressMPaLabel             matlab.ui.control.Label
        EF_sy                           matlab.ui.control.NumericEditField
        StressEnduranceLimitMPaLabel    matlab.ui.control.Label
        EF_se                           matlab.ui.control.NumericEditField
        StrokemLabel                    matlab.ui.control.Label
        EF_Stroke                       matlab.ui.control.NumericEditField
        WorkJLabel                      matlab.ui.control.Label
        EF_Work                         matlab.ui.control.NumericEditField
    end

    % Callbacks that handle component events
    methods (Access = private)

        % Button pushed function: UpdateButton
        function UpdateButtonPushed(app, event)
            %% Update Start
            w=1;                        % Slipper width (1 means equals Length of slipper)
            A=app.EF_A.Value;           % Amplitude of Curvature (waviness)
            B=app.EF_DF.Value;          % Deformation Factor (typical 1/1000)
            if app.EF_L.Value==0        % Make sure the calculations are not done with 0 length bearing, this causes issues
                L=0.0000000001;
            else
                L=app.EF_L.Value;
            end
            N=app.StepSizeSlider.Value;     % Number of steps in calculations (1000 is accurate for most things)
            Nu=app.EF_Nu.Value;             % Number of bearings, will likely not change and stay at 8.
            x=linspace(0,app.EF_x.Value,app.StepSizeSlider.Value);  %The bearing guiding surface
            f=2*pi/app.EF_x.Value;          % Scaling of the guiding surface such that we can see it a single wavelength
            plot(app.UIAxes,x,A*sin(f*x));  % Plotting the guididng surface in the correct window
            axis(app.UIAxes, 'equal');      % Equal axis to see the scale of the waviness more accurate


            %% Update Length of Single Slipper
            if convertCharsToStrings(app.Switch_LW.Value)=='L to W'

                if convertCharsToStrings(app.Knob_h.Value)=='Yes'
                    %% Calculate the Length
                    app.EF_L.Value=StaticSlipperDeformation(app.EF_A.Value,app.EF_DF.Value,app.StepSizeSlider.Value);
                    %% Calculate the Load of single slipper using the found length
                    [W,Pr]=Orifice(app.EF_Ps.Value,app.EF_L.Value,app.EF_h0.Value);
                    if isnan(Pr)
                        W=0;
                        Pr=0;
                    end
                    app.EF_W.Value=W;
                    app.EF_Pr.Value=Pr;
                elseif convertCharsToStrings(app.Knob_h.Value)=='Within specifications'
                    %% Calculate the Length
                    app.EF_L.Value=StaticSlipperDeformation(app.EF_A.Value,app.EF_DF.Value,app.StepSizeSlider.Value,app.EF_dH.Value);
                    %% Calculate the Load of single slipper using the found length and the change in flight height
                    [W,Pr]=Orifice(app.EF_Ps.Value,app.EF_L.Value,app.EF_h0.Value,app.EF_dH.Value);
                    if isnan(Pr)
                        W=0;
                        Pr=0;
                    end
                    app.EF_W.Value=W;
                    app.EF_Pr.Value=Pr;
                else

                    %% Check if length is feasible

                    dy=(A*sin((0.25+0.5*L)*2*pi))-(A-B*L);  %The Deformation Criteria, Putting a slipper on a peak, comparing its deformation with the guiding surface

                    if dy<0     % IF deformation Criteria is NOT met, tell us about how ''bad it really is''
                        msgbox( sprintf('Slippers are not parallel with guiding surface, gap of %2.2g  m , slipper length must be maximum of %2.2g %% of Wavelength in order to be parallel.',-dy*1000000,StaticSlipperDeformation(A,B,N)*100),'Warning');
                    else        % IF deformation Criteria is met, do nothing
                        msgbox('Slipper is parallel', 'Check')
                    end

                    %% Calculate the Load of single slipper using the given length
                    [W,Pr]=Orifice(app.EF_Ps.Value,app.EF_L.Value,app.EF_h0.Value);
                    %% If some sizes are chosen very low, the recess pressure might result in NaN. In this case set the pressure to zero.
                    if isnan(Pr)
                        W=0;
                        Pr=0;
                    end
                    app.EF_W.Value=W;
                    app.EF_Pr.Value=Pr;

                end

            elseif convertCharsToStrings(app.Switch_LW.Value)=='W to L'
```

```
                msgbox('Load to Length is under construction 25-03-2019');
            end

            L=app.EF_L.Value;

            %% Update total load and footprint
            app.EF_F.Value=W*Nu;
            app.EF_foot.Value=L*Nu*100;
            stroke=2*A/(Nu*L)*sin((Nu*L*f)/2);

            if L*Nu*100>100 %% If footprint is larger than 100% of the bearing wavelength change the color, such that the user will notice.
                app.EF_foot.BackgroundColor=[1,0.2,0];
                app.EF_Stroke.BackgroundColor=[1,0.2,0];
            else
                app.EF_foot.BackgroundColor=[1,1,1];
                app.EF_Stroke.BackgroundColor=[1,1,1];
            end

            if isnan(stroke)
                app.EF_Stroke.Value=0;
                app.EF_Work.Value=0;
            else

                app.EF_Stroke.Value=stroke;
                app.EF_Work.Value=W*Nu*stroke;
            end

            %% Update Angles
            [phi,theta]=Angles(x,A,L,N,Nu);
            phideg=rad2deg(phi);
            thetadeg=rad2deg(theta);
            plot(app.UIAxes_Phi,x,phideg);
            plot(app.UIAxes_Theta,x,thetadeg);

            %% First collect parameters on Flexure
            app.EF_sy.Editable='off';
            app.EF_se.Editable='off';
            if convertCharsToStrings(app.DD_E.Value)=='200 (Spring Steel)'
                E=200;
            elseif convertCharsToStrings(app.DD_E.Value)=='69 (Aluminium 6061-T6)'
                E=69;
            elseif convertCharsToStrings(app.DD_E.Value)=='3.5 (PLA)'
                E=3.5;
            elseif convertCharsToStrings(app.DD_E.Value)=='2 (ABS)'
                E=2;
            else
                E=double((convertCharsToStrings(app.DD_E.Value)));
                if isnan(E)
                    msgbox('Error, please enter a numerical value for Youngs Modulus','Error Error');
                    E=0;
                    app.DD_E.Value=0;
                else
                    app.EF_sy.Editable='on';
                    app.EF_se.Editable='on';
                    msgbox('You can now alter the values for Yield Stress and Endurance Limit');
                end
            end

            if convertCharsToStrings(app.DD_t.Value)=='0.7 (Printing Nozzle)'
                t=0.7;
            else
                t=double(app.DD_t.Value);
            end

            if convertCharsToStrings(app.DD_b.Value)=='Slipper Width'
                b=L*w;
            elseif convertCharsToStrings(app.DD_b.Value)=='Half Slipper Width'
                b=L*w*0.5;
            else
                b=double(app.DD_b.Value);
            end

            %% Stress Calculations!
            Lf=sqrt(2)*L;       %Flexure length is Length of Slipper under angle of 45deg.

            if isequal(theta(1,:),zeros(1,N))
                app.EF_s1.BackgroundColor=[1,0,0];
                app.EF_s2.BackgroundColor=[1,0,0];
                app.EF_s3.BackgroundColor=[1,0,0];
                app.EF_s4.BackgroundColor=[1,0,0];
                sigma_1=Inf;
                sigma_2=Inf;
                sigma_3=Inf;
                sigma_4=Inf;
            else
                sigma_1=E*t/(2*Lf)*theta(1,:)+W/(t*b);
                sigma_2=E*t/(2*2*Lf)*theta(9,:)+2*W/(t*b);
                sigma_3=E*t/(2*4*Lf)*theta(13,:)+4*W/(t*b);
                sigma_4=E*t/(2*8*Lf)*theta(15,:)+8*W/(t*b);


            end

            app.EF_s1.Value=max(sigma_1);
            app.EF_s2.Value=max(sigma_2);
            app.EF_s3.Value=max(sigma_3);
            app.EF_s4.Value=max(sigma_4);

            %% Stress Comparison
            if app.EF_s1.Value>=app.EF_sy.Value
                app.EF_s1.BackgroundColor=[.85,0,0];
            elseif app.EF_s1.Value>=app.EF_se.Value
                app.EF_s1.BackgroundColor=[1,0.5,0.2];
            else
                app.EF_s1.BackgroundColor=[0.9,1,0.9];
            end
            if app.EF_s2.Value>=app.EF_sy.Value
                app.EF_s2.BackgroundColor=[.85,0,0];
            elseif app.EF_s2.Value>=app.EF_se.Value
                app.EF_s2.BackgroundColor=[1,0.5,0.2];
            else
                app.EF_s2.BackgroundColor=[0.9,1,0.9];
            end
            if app.EF_s3.Value>=app.EF_sy.Value
                app.EF_s3.BackgroundColor=[.85,0,0];
            elseif app.EF_s3.Value>=app.EF_se.Value
                app.EF_s3.BackgroundColor=[1,0.5,0.2];
            else
                app.EF_s3.BackgroundColor=[0.9,1,0.9];
            end
            if app.EF_s4.Value>=app.EF_sy.Value
                app.EF_s4.BackgroundColor=[.85,0,0];
            elseif app.EF_s4.Value>=app.EF_se.Value
                app.EF_s4.BackgroundColor=[1,0.5,0.2];
            else
                app.EF_s4.BackgroundColor=[0.9,1,0.9];
            end

        end

        % Value changed function: Knob_h
        function Yes_No(app, event)
            value = convertCharsToStrings(app.Knob_h.Value);
            if value == 'Yes'
                app.EF_dH.Enable = 'off';
                app.EF_L.Enable = 'off';
                app.AllowedlossinflightheightmLabel.Enable='off';
            elseif value == 'No'
                app.EF_dH.Enable = 'off';
                app.EF_L.Enable = 'on';
                app.EF_L.Editable = 'on';
                app.AllowedlossinflightheightmLabel.Enable='off';
            else
                app.EF_dH.Enable = 'on';
                app.EF_L.Enable = 'off';
                app.AllowedlossinflightheightmLabel.Enable='on';
            end
        end

        % Menu selected function: RecessPressureMenu
        function PlotRecessPressure(app, event)
            if app.EF_L.Value==0
                L=0.0000000001;
            else
                L=app.EF_L.Value;
            end
            [~,Pr]=Orifice(app.EF_Ps.Value,L,linspace(1,250,app.StepSizeSlider.Value));
            figure(1)
            hold on
            plot(linspace(1,250,app.StepSizeSlider.Value),Pr)
            xlabel('Film heigth [\mu m]')
            ylabel('Recess Pressure [Bar]')

            if isempty(findobj(figure(1), 'Type', 'Legend'))
                legend(['For Ps=' num2str(app.EF_Ps.Value) 'bar'])
            else
                old_legend=findobj(figure(1), 'Type', 'Legend');
                old_legend.String{end}=['For Ps=' num2str(app.EF_Ps.Value) 'bar'];
            end
        end

        % Menu selected function: LoadCapacityMenu
        function PlotLoadCapacity(app, event)
            if app.EF_L.Value==0
                L=0.0000000001;
            else
                L=app.EF_L.Value;
            end

            [W,~]=Orifice(app.EF_Ps.Value,app.EF_L.Value,linspace(1,250,app.StepSizeSlider.Value));
            figure(2)
            hold on
            plot(linspace(1,250,app.StepSizeSlider.Value),W)
            xlabel('Film heigth [\mu m]')
            ylabel('Load Capacity [N]')

            if isempty(findobj(figure(2), 'Type', 'Legend'))
                legend(Load,['For L = ' num2str(L) 'm and Ps = ' num2str(app.EF_Ps.Value) 'bar'])
            else
                old_legend=findobj(figure(2), 'Type', 'Legend');
                old_legend.String{end}=['For L = ' num2str(app.EF_L.Value) 'm and Ps = ' num2str(app.EF_Ps.Value) 'bar'];
            end
        end

        % Menu selected function: TiltStiffnessMenu
        function PlotTiltStiffness(app, event)

            if app.EF_L.Value==0
                L=0.0000000001;
            else
                L=app.EF_L.Value;
            end
            %% Tilt Inputs (Ps,L,h,{optional} Types)
            [M]=Tilt(app.EF_Ps.Value,app.EF_L.Value,linspace(1,250,app.StepSizeSlider.Value));
            figure(3)
            hold on

            plot(linspace(1,250,app.StepSizeSlider.Value),M)
            xlabel('Film heigth [\mu m]')
            ylabel('Tilt Stiffness [Nm/Rad]')

            if isempty(findobj(figure(3), 'Type', 'Legend'))
                legend(['For L = ' num2str(app.EF_L.Value) 'm and Ps = ' num2str(app.EF_Ps.Value) 'bar'])
            else
                old_legend=findobj(figure(3), 'Type', 'Legend');
                old_legend.String{end}=['For L = ' num2str(app.EF_L.Value) 'm and Ps = ' num2str(app.EF_Ps.Value) 'bar'];
            end
        end

        % Callback function
        function UnderConstruction(app, event)
            msgbox('under construction 13-03-2019')
        end

        % Value changed function: DD_E
        function Stress(app, event)
            %% Change of Material Stress level
            app.EF_sy.Editable='off';
            app.EF_se.Editable='off';
            if convertCharsToStrings(app.DD_E.Value)=='200 (Spring Steel)'
                app.EF_sy.Value=1200;
                app.EF_se.Value=270;
            elseif convertCharsToStrings(app.DD_E.Value)=='69 (Aluminium 6061-T6)'
                app.EF_sy.Value=270;            %
                app.EF_se.Value=160;            % Based on 10e6 cycles
            elseif convertCharsToStrings(app.DD_E.Value)=='3.5 (PLA)'
                app.EF_sy.Value=30;
                app.EF_se.Value=7;            % Based on 2e6 cycles
            elseif convertCharsToStrings(app.DD_E.Value)=='2 (ABS)'
                app.EF_sy.Value=20;
                app.EF_se.Value=2.4;            % Based on 2e6 cycles
            else
                app.EF_sy.Editable='on';
                app.EF_se.Editable='on';
            end
        end
    end

    % Component initialization
    methods (Access = private)

        % Create UIFigure and components
        function createComponents(app)

            % Create UserInterfaceBearingDesignerUIFigure and hide until all components are
                created
            app.UserInterfaceBearingDesignerUIFigure = uifigure('Visible', 'off');
            app.UserInterfaceBearingDesignerUIFigure.Position = [100 100 1145 718];
            app.UserInterfaceBearingDesignerUIFigure.Name = 'User Interface - Bearing
                Designer';

            % Create SlipperSpecificationsMenu
            app.SlipperSpecificationsMenu = uimenu(app.UserInterfaceBearingDesignerUIFigure);
            app.SlipperSpecificationsMenu.Text = 'Slipper Specifications';

            % Create FilmFluidStiffnessMenu
            app.FilmFluidStiffnessMenu = uimenu(app.SlipperSpecificationsMenu);
            app.FilmFluidStiffnessMenu.Text = 'Film Fluid Stiffness';

            % Create RecessPressureMenu
            app.RecessPressureMenu = uimenu(app.FilmFluidStiffnessMenu);
            app.RecessPressureMenu.MenuSelectedFcn = createCallbackFcn(app, @
                PlotRecessPressure, true);
            app.RecessPressureMenu.Text = 'Recess Pressure';

            % Create LoadCapacityMenu
            app.LoadCapacityMenu = uimenu(app.FilmFluidStiffnessMenu);
            app.LoadCapacityMenu.MenuSelectedFcn = createCallbackFcn(app, @PlotLoadCapacity,
                true);
            app.LoadCapacityMenu.Text = 'Load Capacity';

            % Create TiltStiffnessMenu
            app.TiltStiffnessMenu = uimenu(app.SlipperSpecificationsMenu);
            app.TiltStiffnessMenu.MenuSelectedFcn = createCallbackFcn(app, @PlotTiltStiffness
                , true);
            app.TiltStiffnessMenu.Text = 'Tilt Stiffness';

            % Create StepSizeSliderLabel
            app.StepSizeSliderLabel = uilabel(app.UserInterfaceBearingDesignerUIFigure);
            app.StepSizeSliderLabel.HorizontalAlignment = 'right';
            app.StepSizeSliderLabel.VerticalAlignment = 'top';
            app.StepSizeSliderLabel.Position = [21 613 57 15];
            app.StepSizeSliderLabel.Text = 'Step Size';

            % Create StepSizeSlider
            app.StepSizeSlider = uislider(app.UserInterfaceBearingDesignerUIFigure);
            app.StepSizeSlider.Limits = [10 10000];
            app.StepSizeSlider.MajorTicks = [10 10000];
            app.StepSizeSlider.MajorTickLabels = {'10', '10000'};
            app.StepSizeSlider.MinorTicks = [];
            app.StepSizeSlider.Position = [98 619 151 3];
            app.StepSizeSlider.Value = 1000;

            % Create UIAxes
            app.UIAxes = uiaxes(app.UserInterfaceBearingDesignerUIFigure);
            title(app.UIAxes, 'Guiding Surface')
            xlabel(app.UIAxes, 'Length [m]')
            ylabel(app.UIAxes, 'Amplitude [m]')
            app.UIAxes.Position = [311 501 300 185];

            % Create LengthofguidingsurfacemLabel
            app.LengthofguidingsurfacemLabel = uilabel(app.
                UserInterfaceBearingDesignerUIFigure);
            app.LengthofguidingsurfacemLabel.HorizontalAlignment = 'right';
            app.LengthofguidingsurfacemLabel.VerticalAlignment = 'top';
            app.LengthofguidingsurfacemLabel.Position = [21 557 162 15];
            app.LengthofguidingsurfacemLabel.Text = 'Length of guiding surface [m]';

            % Create EF_x
            app.EF_x = uieditfield(app.UserInterfaceBearingDesignerUIFigure, 'numeric');
            app.EF_x.ValueDisplayFormat = '%2.4g';
            app.EF_x.Position = [198 553 67 22];
            app.EF_x.Value = 1;

            % Create WavinessamplitudemmLabel
            app.WavinessamplitudemmLabel = uilabel(app.UserInterfaceBearingDesignerUIFigure);
            app.WavinessamplitudemmLabel.HorizontalAlignment = 'right';
            app.WavinessamplitudemmLabel.VerticalAlignment = 'top';
            app.WavinessamplitudemmLabel.Position = [36 521 147 15];
            app.WavinessamplitudemmLabel.Text = 'Waviness amplitude [m/m]';

            % Create EF_A
            app.EF_A = uieditfield(app.UserInterfaceBearingDesignerUIFigure, 'numeric');
            app.EF_A.ValueDisplayFormat = '%2.4g';
            app.EF_A.Position = [198 517 67 22];
            app.EF_A.Value = 0.05;

            % Create GuidingCurvatureDropDownLabel
            app.GuidingCurvatureDropDownLabel = uilabel(app.
                UserInterfaceBearingDesignerUIFigure);
            app.GuidingCurvatureDropDownLabel.HorizontalAlignment = 'right';
            app.GuidingCurvatureDropDownLabel.VerticalAlignment = 'top';
            app.GuidingCurvatureDropDownLabel.Position = [36 666 105 15];
            app.GuidingCurvatureDropDownLabel.Text = 'Guiding Curvature';

            % Create DD_funtion
            app.DD_funtion = uidropdown(app.UserInterfaceBearingDesignerUIFigure);
            app.DD_funtion.Items = {'Sinus'};
            app.DD_funtion.Position = [156 662 100 22];
            app.DD_funtion.Value = 'Sinus';

            % Create LengthofsingleslippermmLabel
            app.LengthofsingleslippermmLabel = uilabel(app.
                UserInterfaceBearingDesignerUIFigure);
            app.LengthofsingleslippermmLabel.HorizontalAlignment = 'right';
            app.LengthofsingleslippermmLabel.VerticalAlignment = 'top';
            app.LengthofsingleslippermmLabel.Position = [191 427 167 15];
            app.LengthofsingleslippermmLabel.Text = 'Length of single slipper [m/m]]';

            % Create EF_L
            app.EF_L = uieditfield(app.UserInterfaceBearingDesignerUIFigure, 'numeric');
            app.EF_L.ValueDisplayFormat = '%2.4g';
            app.EF_L.Editable = 'off';
            app.EF_L.Position = [375 423 69 22];

            % Create SlipperdeformationLabel
            app.SlipperdeformationLabel = uilabel(app.UserInterfaceBearingDesignerUIFigure);
            app.SlipperdeformationLabel.HorizontalAlignment = 'right';
            app.SlipperdeformationLabel.VerticalAlignment = 'top';
            app.SlipperdeformationLabel.Position = [58 484 125 15];
            app.SlipperdeformationLabel.Text = 'Slipper deformation [-]';

            % Create EF_DF
            app.EF_DF = uieditfield(app.UserInterfaceBearingDesignerUIFigure, 'numeric');
            app.EF_DF.ValueDisplayFormat = '%2.4g';
            app.EF_DF.Position = [196 480 69 22];
            app.EF_DF.Value = 0.001;

            % Create SlipperparallelwithfilmLabel
            app.SlipperparallelwithfilmLabel = uilabel(app.
                UserInterfaceBearingDesignerUIFigure);
            app.SlipperparallelwithfilmLabel.HorizontalAlignment = 'center';
            app.SlipperparallelwithfilmLabel.VerticalAlignment = 'top';
            app.SlipperparallelwithfilmLabel.Position = [21 352 135 15];
            app.SlipperparallelwithfilmLabel.Text = 'Slipper parallel with film';

            % Create Knob_h
            app.Knob_h = uiknob(app.UserInterfaceBearingDesignerUIFigure, 'discrete');
            app.Knob_h.Items = {'Yes', 'Within specifications', 'No'};
            app.Knob_h.ValueChangedFcn = createCallbackFcn(app, @Yes_No, true);
            app.Knob_h.Position = [66 382 42 42];
            app.Knob_h.Value = 'Yes';

            % Create AllowedlossinflightheightmLabel
            app.AllowedlossinflightheightmLabel = uilabel(app.
                UserInterfaceBearingDesignerUIFigure);
            app.AllowedlossinflightheightmLabel.HorizontalAlignment = 'right';
            app.AllowedlossinflightheightmLabel.VerticalAlignment = 'top';
            app.AllowedlossinflightheightmLabel.Position = [193 392 176 15];
            app.AllowedlossinflightheightmLabel.Text = 'Allowed loss in flightheight [ m ]';

            % Create EF_dH
            app.EF_dH = uieditfield(app.UserInterfaceBearingDesignerUIFigure, 'numeric');
            app.EF_dH.Enable = 'off';
            app.EF_dH.Position = [375 388 69 22];
            app.EF_dH.Value = 20;

            % Create UpdateButton
            app.UpdateButton = uibutton(app.UserInterfaceBearingDesignerUIFigure, 'push');
            app.UpdateButton.ButtonPushedFcn = createCallbackFcn(app, @UpdateButtonPushed,
                true);
            app.UpdateButton.FontSize = 18;
            app.UpdateButton.Position = [835 83 136 46];
            app.UpdateButton.Text = 'Update';

            % Create LengthtoLoadSwitchLabel
            app.LengthtoLoadSwitchLabel = uilabel(app.UserInterfaceBearingDesignerUIFigure);
            app.LengthtoLoadSwitchLabel.HorizontalAlignment = 'center';
            app.LengthtoLoadSwitchLabel.VerticalAlignment = 'top';
            app.LengthtoLoadSwitchLabel.Position = [45 267 87 15];
            app.LengthtoLoadSwitchLabel.Text = 'Length to Load';

            % Create Switch_LW
            app.Switch_LW = uiswitch(app.UserInterfaceBearingDesignerUIFigure, 'slider');
            app.Switch_LW.Items = {'L to W', 'W to L'};
            app.Switch_LW.Position = [66 297 45 20];
            app.Switch_LW.Value = 'L to W';

            % Create UIAxes_Theta
            app.UIAxes_Theta = uiaxes(app.UserInterfaceBearingDesignerUIFigure);
            title(app.UIAxes_Theta, 'Flexure Angles')
            xlabel(app.UIAxes_Theta, 'Length [m]')
            ylabel(app.UIAxes_Theta, 'Angles [  ]')
            app.UIAxes_Theta.Position = [513 307 300 185];

            % Create UIAxes_Phi
            app.UIAxes_Phi = uiaxes(app.UserInterfaceBearingDesignerUIFigure);
            title(app.UIAxes_Phi, 'Whiffle Tree angles')
            xlabel(app.UIAxes_Phi, 'Length [m]')
            ylabel(app.UIAxes_Phi, 'Angles [  ]')
            app.UIAxes_Phi.Position = [820 307 300 185];

            % Create LoadCapacitySlipperNLabel
            app.LoadCapacitySlipperNLabel = uilabel(app.UserInterfaceBearingDesignerUIFigure)
                ;
            app.LoadCapacitySlipperNLabel.HorizontalAlignment = 'right';
            app.LoadCapacitySlipperNLabel.VerticalAlignment = 'top';
            app.LoadCapacitySlipperNLabel.Position = [196 271 144 15];
            app.LoadCapacitySlipperNLabel.Text = 'Load Capacity Slipper [N]';

            % Create EF_W
            app.EF_W = uieditfield(app.UserInterfaceBearingDesignerUIFigure, 'numeric');
            app.EF_W.ValueDisplayFormat = '%2.4g';
            app.EF_W.Editable = 'off';
            app.EF_W.Position = [377 267 69 22];

            % Create TotalBearingLoadCapacityNLabel
            app.TotalBearingLoadCapacityNLabel = uilabel(app.
                UserInterfaceBearingDesignerUIFigure);
            app.TotalBearingLoadCapacityNLabel.HorizontalAlignment = 'right';
            app.TotalBearingLoadCapacityNLabel.VerticalAlignment = 'top';
            app.TotalBearingLoadCapacityNLabel.Position = [74 172 177 15];
            app.TotalBearingLoadCapacityNLabel.Text = 'Total Bearing Load Capacity [N]';

            % Create EF_F
            app.EF_F = uieditfield(app.UserInterfaceBearingDesignerUIFigure, 'numeric');
            app.EF_F.ValueDisplayFormat = '%2.4g';
            app.EF_F.Editable = 'off';
            app.EF_F.Position = [288 168 69 22];

            % Create BearingfootpringonguidingsurfaceLabel
```

```
        app.BearingfootpringonguidingsurfaceLabel = uilabel(app.
            UserInterfaceBearingDesignerUIFigure);
        app.BearingfootpringonguidingsurfaceLabel.HorizontalAlignment = 'right';
        app.BearingfootpringonguidingsurfaceLabel.VerticalAlignment = 'top';
        app.BearingfootpringonguidingsurfaceLabel.Position = [26 140 225 15];
        app.BearingfootpringonguidingsurfaceLabel.Text = 'Bearing footpring on guiding
            surface [%]';

        % Create EF_foot
        app.EF_foot = uieditfield(app.UserInterfaceBearingDesignerUIFigure, 'numeric');
        app.EF_foot.ValueDisplayFormat = '%2.4g';
        app.EF_foot.Editable = 'off';
        app.EF_foot.Position = [288 136 69 22];

        % Create Stressflexurelevel1MPaLabel
        app.Stressflexurelevel1MPaLabel = uilabel(app.
            UserInterfaceBearingDesignerUIFigure);
        app.Stressflexurelevel1MPaLabel.HorizontalAlignment = 'right';
        app.Stressflexurelevel1MPaLabel.VerticalAlignment = 'top';
        app.Stressflexurelevel1MPaLabel.Position = [530 242 152 15];
        app.Stressflexurelevel1MPaLabel.Text = 'Stress flexure level 1 [MPa]';

        % Create EF_s1
        app.EF_s1 = uieditfield(app.UserInterfaceBearingDesignerUIFigure, 'numeric');
        app.EF_s1.ValueDisplayFormat = '%2.3g';
        app.EF_s1.Editable = 'off';
        app.EF_s1.Position = [705 238 61 22];

        % Create Stressflexurelevel2MPaLabel
        app.Stressflexurelevel2MPaLabel = uilabel(app.
            UserInterfaceBearingDesignerUIFigure);
        app.Stressflexurelevel2MPaLabel.HorizontalAlignment = 'right';
        app.Stressflexurelevel2MPaLabel.VerticalAlignment = 'top';
        app.Stressflexurelevel2MPaLabel.Position = [530 208 152 15];
        app.Stressflexurelevel2MPaLabel.Text = 'Stress flexure level 2 [MPa]';

        % Create EF_s2
        app.EF_s2 = uieditfield(app.UserInterfaceBearingDesignerUIFigure, 'numeric');
        app.EF_s2.ValueDisplayFormat = '%2.3g';
        app.EF_s2.Editable = 'off';
        app.EF_s2.Position = [705 204 61 22];

        % Create Stressflexurelevel3MPaLabel
        app.Stressflexurelevel3MPaLabel = uilabel(app.
            UserInterfaceBearingDesignerUIFigure);
        app.Stressflexurelevel3MPaLabel.HorizontalAlignment = 'right';
        app.Stressflexurelevel3MPaLabel.VerticalAlignment = 'top';
        app.Stressflexurelevel3MPaLabel.Position = [530 175 152 15];
        app.Stressflexurelevel3MPaLabel.Text = 'Stress flexure level 3 [MPa]';

        % Create EF_s3
        app.EF_s3 = uieditfield(app.UserInterfaceBearingDesignerUIFigure, 'numeric');
        app.EF_s3.ValueDisplayFormat = '%2.3g';
        app.EF_s3.Editable = 'off';
        app.EF_s3.Position = [705 171 61 22];

        % Create Stressflexurelevel4MPaLabel
        app.Stressflexurelevel4MPaLabel = uilabel(app.
            UserInterfaceBearingDesignerUIFigure);
        app.Stressflexurelevel4MPaLabel.HorizontalAlignment = 'right';
```

```
            app.Stressflexurelevel4MPaLabel.VerticalAlignment = 'top';
            app.Stressflexurelevel4MPaLabel.Position = [530 140 152 15];
            app.Stressflexurelevel4MPaLabel.Text = 'Stress flexure level 4 [MPa]';

            % Create EF_s4
            app.EF_s4 = uieditfield(app.UserInterfaceBearingDesignerUIFigure, 'numeric');
            app.EF_s4.ValueDisplayFormat = '%2.3g';
            app.EF_s4.Editable = 'off';
            app.EF_s4.Position = [705 136 61 22];

            % Create TabGroup
            app.TabGroup = uitabgroup(app.UserInterfaceBearingDesignerUIFigure);
            app.TabGroup.Position = [670 538 292 156];

            % Create SupplySpecsTab
            app.SupplySpecsTab = uitab(app.TabGroup);
            app.SupplySpecsTab.Title = 'Supply Specs';

            % Create SupplyPressurebarLabel
            app.SupplyPressurebarLabel = uilabel(app.SupplySpecsTab);
            app.SupplyPressurebarLabel.HorizontalAlignment = 'right';
            app.SupplyPressurebarLabel.VerticalAlignment = 'top';
            app.SupplyPressurebarLabel.Position = [47 86 122 15];
            app.SupplyPressurebarLabel.Text = 'Supply Pressure [bar]';

            % Create EF_Ps
            app.EF_Ps = uieditfield(app.SupplySpecsTab, 'numeric');
            app.EF_Ps.Position = [184 82 45 22];
            app.EF_Ps.Value = 5;

            % Create DesignedfilmthicknessmLabel
            app.DesignedfilmthicknessmLabel = uilabel(app.SupplySpecsTab);
            app.DesignedfilmthicknessmLabel.HorizontalAlignment = 'right';
            app.DesignedfilmthicknessmLabel.VerticalAlignment = 'top';
            app.DesignedfilmthicknessmLabel.Position = [9 52 160 15];
            app.DesignedfilmthicknessmLabel.Text = 'Designed film thickness [ m ]';

            % Create EF_h0
            app.EF_h0 = uieditfield(app.SupplySpecsTab, 'numeric');
            app.EF_h0.ValueDisplayFormat = '%.0f';
            app.EF_h0.Position = [184 48 45 22];
            app.EF_h0.Value = 50;

            % Create NumberofslippersLabel
            app.NumberofslippersLabel = uilabel(app.SupplySpecsTab);
            app.NumberofslippersLabel.HorizontalAlignment = 'right';
            app.NumberofslippersLabel.VerticalAlignment = 'top';
            app.NumberofslippersLabel.Position = [45 16 124 15];
            app.NumberofslippersLabel.Text = 'Number of slippers [#]';

            % Create EF_Nu
            app.EF_Nu = uieditfield(app.SupplySpecsTab, 'numeric');
            app.EF_Nu.ValueDisplayFormat = '%.0f';
            app.EF_Nu.Enable = 'off';
            app.EF_Nu.Position = [184 12 45 22];
            app.EF_Nu.Value = 8;

            % Create FlexureParametersTab
            app.FlexureParametersTab = uitab(app.TabGroup);
            app.FlexureParametersTab.Title = 'Flexure Parameters';

            % Create YoungsModulusGPaDropDownLabel
            app.YoungsModulusGPaDropDownLabel = uilabel(app.FlexureParametersTab);
            app.YoungsModulusGPaDropDownLabel.HorizontalAlignment = 'right';
            app.YoungsModulusGPaDropDownLabel.VerticalAlignment = 'top';
            app.YoungsModulusGPaDropDownLabel.Position = [3 86 131 15];
            app.YoungsModulusGPaDropDownLabel.Text = 'Young''s Modulus [GPa]';

            % Create DD_E
            app.DD_E = uidropdown(app.FlexureParametersTab);
            app.DD_E.Items = {'200 (Spring Steel)', '69 (Aluminium 6061-T6)', '3.5 (PLA)', '2 (ABS)', ''};
            app.DD_E.Editable = 'on';
            app.DD_E.ValueChangedFcn = createCallbackFcn(app, @Stress, true);
            app.DD_E.BackgroundColor = [1 1 1];
            app.DD_E.Position = [144 82 100 22];
            app.DD_E.Value = '200 (Spring Steel)';

            % Create ThicknessmmDropDownLabel
            app.ThicknessmmDropDownLabel = uilabel(app.FlexureParametersTab);
            app.ThicknessmmDropDownLabel.HorizontalAlignment = 'right';
            app.ThicknessmmDropDownLabel.VerticalAlignment = 'top';
            app.ThicknessmmDropDownLabel.Position = [40 55 89 15];
            app.ThicknessmmDropDownLabel.Text = 'Thickness [mm]';

            % Create DD_t
            app.DD_t = uidropdown(app.FlexureParametersTab);
            app.DD_t.Items = {'2', '1', '0.7 (Printing Nozzle)', ''};
            app.DD_t.Editable = 'on';
            app.DD_t.BackgroundColor = [1 1 1];
            app.DD_t.Position = [144 51 100 22];
            app.DD_t.Value = '2';

            % Create WidthmmDropDownLabel
            app.WidthmmDropDownLabel = uilabel(app.FlexureParametersTab);
            app.WidthmmDropDownLabel.HorizontalAlignment = 'right';
            app.WidthmmDropDownLabel.VerticalAlignment = 'top';
            app.WidthmmDropDownLabel.Position = [61 22 68 15];
            app.WidthmmDropDownLabel.Text = 'Width [m/m]';

            % Create DD_b
            app.DD_b = uidropdown(app.FlexureParametersTab);
            app.DD_b.Items = {'Slipper Width', 'Half Slipper Width', ''};
            app.DD_b.Editable = 'on';
            app.DD_b.BackgroundColor = [1 1 1];
            app.DD_b.Position = [144 18 100 22];
            app.DD_b.Value = 'Slipper Width';

            % Create RecessPressurebarLabel
            app.RecessPressurebarLabel = uilabel(app.UserInterfaceBearingDesignerUIFigure);
            app.RecessPressurebarLabel.HorizontalAlignment = 'right';
            app.RecessPressurebarLabel.VerticalAlignment = 'top';
            app.RecessPressurebarLabel.Position = [198 356 125 15];
            app.RecessPressurebarLabel.Text = 'Recess Pressure [bar]';

            % Create EF_Pr
            app.EF_Pr = uieditfield(app.UserInterfaceBearingDesignerUIFigure, 'numeric');
            app.EF_Pr.Editable = 'off';
            app.EF_Pr.Position = [375 352 69 22];

            % Create YieldStressMPaLabel
            app.YieldStressMPaLabel = uilabel(app.UserInterfaceBearingDesignerUIFigure);
            app.YieldStressMPaLabel.HorizontalAlignment = 'center';
            app.YieldStressMPaLabel.Position = [849 249 104 15];
            app.YieldStressMPaLabel.Text = 'Yield Stress [MPa]';

            % Create EF_sy
            app.EF_sy = uieditfield(app.UserInterfaceBearingDesignerUIFigure, 'numeric');
            app.EF_sy.ValueDisplayFormat = '%2.4g';
            app.EF_sy.Editable = 'off';
            app.EF_sy.Position = [870 218 61 22];
            app.EF_sy.Value = 1200;

            % Create StressEnduranceLimitMPaLabel
            app.StressEnduranceLimitMPaLabel = uilabel(app.
                UserInterfaceBearingDesignerUIFigure);
            app.StressEnduranceLimitMPaLabel.HorizontalAlignment = 'center';
            app.StressEnduranceLimitMPaLabel.VerticalAlignment = 'top';
            app.StressEnduranceLimitMPaLabel.Position = [820 189 165 15];
            app.StressEnduranceLimitMPaLabel.Text = 'Stress Endurance Limit [MPa]';

            % Create EF_se
            app.EF_se = uieditfield(app.UserInterfaceBearingDesignerUIFigure, 'numeric');
            app.EF_se.ValueDisplayFormat = '%2.3g';
            app.EF_se.Editable = 'off';
            app.EF_se.Position = [870 161 61 22];
            app.EF_se.Value = 270;

            % Create StrokemLabel
            app.StrokemLabel = uilabel(app.UserInterfaceBearingDesignerUIFigure);
            app.StrokemLabel.HorizontalAlignment = 'right';
            app.StrokemLabel.VerticalAlignment = 'top';
            app.StrokemLabel.Position = [192 99 59 15];
            app.StrokemLabel.Text = 'Stroke [m]';

            % Create EF_Stroke
            app.EF_Stroke = uieditfield(app.UserInterfaceBearingDesignerUIFigure, 'numeric');
            app.EF_Stroke.ValueDisplayFormat = '%2.4g';
            app.EF_Stroke.Editable = 'off';
            app.EF_Stroke.Position = [288 95 69 22];

            % Create WorkJLabel
            app.WorkJLabel = uilabel(app.UserInterfaceBearingDesignerUIFigure);
            app.WorkJLabel.HorizontalAlignment = 'right';
            app.WorkJLabel.VerticalAlignment = 'top';
            app.WorkJLabel.Position = [203 66 48 15];
            app.WorkJLabel.Text = 'Work [J]';

            % Create EF_Work
            app.EF_Work = uieditfield(app.UserInterfaceBearingDesignerUIFigure, 'numeric');
            app.EF_Work.ValueDisplayFormat = '%2.4g';
            app.EF_Work.Editable = 'off';
            app.EF_Work.Position = [288 62 69 22];

            % Show the figure after all components are created
            app.UserInterfaceBearingDesignerUIFigure.Visible = 'on';
        end
    end

    % App creation and deletion
    methods (Access = public)

        % Construct app
        function app = DeApp_zomer_backup

            % Create UIFigure and components
            createComponents(app)

            % Register the app with App Designer
            registerApp(app, app.UserInterfaceBearingDesignerUIFigure)

            if nargout == 0
                clear app
            end
        end

        % Code that executes before app deletion
        function delete(app)

            % Delete UIFigure when app is deleted
            delete(app.UserInterfaceBearingDesignerUIFigure)
        end
    end
end
```

Angles.m

```
function [phi,theta]=Angles(x,A,L,N,Nu)

x=x';
d=L;
f=2*pi/max(x);
phi=zeros(Nu,N);
xr=zeros(Nu,N);
yr=zeros(Nu,N);
% For each bearing (i) calaculate; tangent angle phi, x-pos and y-position
for i=1:Nu
    phi(i,:)=atan(A.*cos(f*(x+(i-1)*d)));
    xr(i,:)=f*(x+d*(i-1))-sin(phi(i,:)').*0.5*L;
    yr(i,:)=A*sin(f*(x+d*(i-1)))+cos(phi(i,:)').*0.5*L;
end
%Angles of intermediate bodies connecting two slippers in one cell.
phi_12=atan((yr(2,:)-yr(1,:))./(xr(2,:)-xr(1,:)));
phi_34=atan((yr(4,:)-yr(3,:))./(xr(4,:)-xr(3,:)));
phi_56=atan((yr(6,:)-yr(5,:))./(xr(6,:)-xr(5,:)));
phi_78=atan((yr(8,:)-yr(7,:))./(xr(8,:)-xr(7,:)));
%For very small length or step sizes errors might occur, but for these
%cases the intermediate angles approach slipper angles.
if isnan(phi_12(1))
    phi_12=phi(1,:);
    phi_34=phi_12;
    phi_56=phi_12;
    phi_78=phi_12;
end
%Angles of first level flexures connected to slipper coupling element
theta(1,:)=(phi(1,:)-phi_12);
theta(2,:)=(phi(2,:)-phi_12);
theta(3,:)=(phi(3,:)-phi_34);
theta(4,:)=(phi(4,:)-phi_34);
theta(5,:)=(phi(5,:)-phi_56);
theta(6,:)=(phi(6,:)-phi_56);
theta(7,:)=(phi(7,:)-phi_78);
theta(8,:)=(phi(8,:)-phi_78);
%Calculating positions of the middle of coupling elements.
x12=(xr(1,:)+xr(2,:))/2;
x34=(xr(3,:)+xr(4,:))/2;
x56=(xr(5,:)+xr(6,:))/2;
x78=(xr(7,:)+xr(8,:))/2;
%Only relative motion is importance not absolute
y12=(yr(1,:)+yr(2,:))/2;
y34=(yr(3,:)+yr(4,:))/2;
y56=(yr(5,:)+yr(6,:))/2;
y78=(yr(7,:)+yr(8,:))/2;
%Calculating rotationalpoints of second flexure pivot
x12r=x12-L*sin(phi_12);
x34r=x34-L*sin(phi_34);
x56r=x56-L*sin(phi_56);
x78r=x78-L*sin(phi_78);

y12r=y12+L*cos(phi_12);
y34r=y34+L*cos(phi_34);
y56r=y56+L*cos(phi_56);
y78r=y78+L*cos(phi_78);
%Angles of second level coupling elements, conneting 4 slippers.
phi_1234=atan((y34r-y12r)./(x34r-x12r));
phi_5678=atan((y78r-y56r)./(x78r-x56r));
if isnan(phi_1234(1))
    phi_1234=phi(1,:);
    phi_5678=phi(1,:);
end
%Angles of second level pivots, connecting a two slipper cell
theta_12=phi_12-phi_1234;
theta_34=phi_34-phi_1234;
theta_56=phi_56-phi_5678;
theta_78=phi_78-phi_5678;
%Calculating positions of the middle of coupling elements.
x1234=mean(xr([1,2,3,4],:));
x5678=mean(xr([5,6,7,8],:));
y1234=mean(yr([1,2,3,4],:));
y5678=mean(yr([5,6,7,8],:));
%Calculating positions of the rotation point of third level flexure
x1234r=x1234-L*sin(phi_1234);
x5678r=x5678-L*sin(phi_5678);
y1234r=y1234+L*cos(phi_1234);
y5678r=y5678+L*cos(phi_5678);
%Fourth and final level angle of coupling element
phi_12345678=atan((y5678r-y1234r)./(x5678r-x1234r));

if isnan(phi_12345678(1))
    phi_12345678=phi(1,:);
end
%Third level flexure angles
theta_1234=phi_1234-phi_12345678;
theta_5678=phi_5678-phi_12345678;
%Final flexure connecting the vericle
theta_12345678=phi_12345678-0;

phi=[phi;phi_12;phi_34;phi_56;phi_78;phi_1234;phi_5678;phi_12345678];
theta=[theta;theta_12;theta_34;theta_56;theta_78;theta_1234;theta_5678;theta_12345678];
```

Orifice.m

```
function [W,Pr] = Orifice(varargin)

Ps=varargin{1}*100000;   % [Pa] Supply Pressure 1bar to Pa
L=varargin{2};           % [m] Diameter of Slipper
h0=varargin{3}/1000000;  % [m] Designed flightheigth

if length(varargin)==4;  % [m] Loss or gain in flight heigth
    dh=varargin{4}/1000000;
else
    dh=0;
end

R1=L/2;                 % [m] Outer radius bearing
R2=R1*0.8;              % [m] 40 mm
rho=998.2;              % [kg/m3] density of water
Cd=0.55;                % [-] Orifice discharge coefficient
Ao=0.001*0.001*pi;      % [m2] - Area of Orifice 1mm orifice
eta=0.0010016;          % [Pa s] - Dynamic Viscosity https://www.engineeringtoolbox.com/water-dynamic-kinematic-viscosity-d_596.html
h=h0+dh;                % [m] nominal designed flightheight

Ko=rho/(2*(Cd*Ao)^2);   % [-] Page 38 Rowe

%B_bar=0.75;
B_bar=pi/(6*log(R1/R2));        %Circular flow shape factor
%A_bar=0.54;
A_bar=(1-(R2^2/R1^2))/(2*log(R1/R2)); %Circular shape factor

Pr=((sqrt(1+4.*Ps.*Ko.*(((B_bar.*h.^3)./eta).^2))-1)./(2.*Ko.*(((B_bar.*h.^3)./eta).^2)); %Recess pressure from balance with orfice restrictor page 38
Pr_bar=Pr./100000;
A=pi.*R1.^2;
W=A.*A_bar.*Pr;
Pr=Pr_bar;
```

Tilt.m

```
function [M] = Tilt(varargin)

Ps=varargin{1}*100000;   % [Pa] Supply Pressure 1bar to Pa
L=varargin{2};           % [m] Diameter of Slipper
h=varargin{3}/1000000;  % [m] Fluid film thickness

if length(varargin)==4;  % Optential diffrent type of bearing used
    type=varargin{4};
else
        type=0;
end

if type == 0                % Type 0, circular recess bearing.
    R1=L/2;                 % [m] Outer radius bearing
    R2=R1*0.08;             % [m] 40 mm
end

% Test Parameters
% h=linspace(1,250,1000)/1000000;
% R1=0.05;
% R2=0.04;

rho=998.2;              % [kg/m3] density of water
Cd=0.55;                % [-] Orifice discharge coefficient
Ao=0.001*0.001*pi;      % [m2] - Area of Orifice 1mm orifice
A=pi*R1^2;              % [m2] - Total area of single slipper
eta=0.0010016;          % [Pa s] - Dynamic Viscosity https://www.engineeringtoolbox.com/water-dynamic-kinematic-viscosity-d_596.html

Ko=rho/(2*(Cd*Ao)^2);   % [-] Page 38 Rowe

B_bar=pi/(6*log(R1/R2));        %Circular flow shape factor
A_bar=(1-(R2^2/R1^2))/(2*log(R1/R2)); %Circular shape factor
%
% B_bar=2.2;        %Multi Recss bearings with a/R = 0.2
% A_bar=0.78;       %Page 38 ROWE

ht=0.0000001;%left will be tilted 0.1 micro lower
             %right will be tilted 0.1 micro up

theta=asin(ht/(4/3*R2/pi))      %Angle of tilt with dH lower/higher

%Page 38 ROWE
CF_L=((B_bar.*(h-ht).^3)./eta).^2;         %A tenth of a micrometre lower
Pr_L=(sqrt(1+4.*Ps.*Ko.*CF_L)-1)./(2.*Ko.*CF_L);
F_L=A_bar.*A./2.*Pr_L;

CF_R=((B_bar.*(h+ht).^3)./eta).^2;
Pr_R=(sqrt(1+4.*Ps.*Ko.*CF_R)-1)./(2.*Ko.*CF_R);
F_R=A_bar.*A./2.*Pr_R;


M=F_L.*4./3.*R2./pi+F_R.*4/3.*R2/pi;

y_s=(M/theta);

%Pr*A*A_bar = W = Load capacity
M=y_s;

end
```

Appendix D

Literature Overview

Table 1: Literature review

	Keywords	Result	Research Topics
Hydrostatic bearings	Surface Curvature	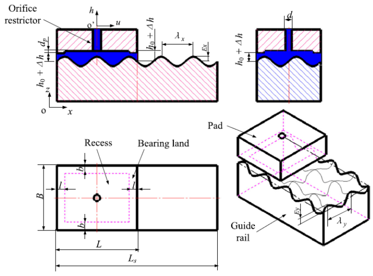 Orifice restrictor Recess Bearing land Pad Guide rail B L L_s h u x o	Linear Guidance Surface Roughness [51]
	Hydraulic Pumps	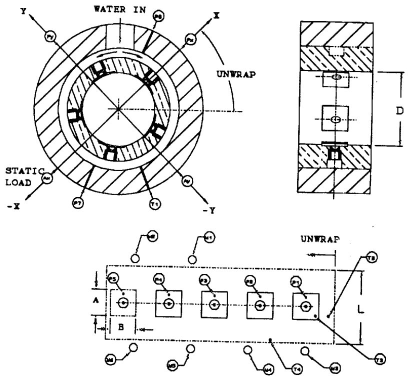 WATER IN UNWRAP STATIC LOAD X Y -X -Y D A B L	Turbo-pumps Rotor dynamics Multi-recess [16]
	Elastic bearing deformation	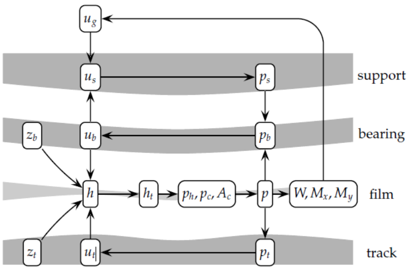 u_g u_s p_s support z_b u_b p_b bearing h h_t p_h, p_c, A_c p W, M_x, M_y film z_t u_t p_t track	Elastic support model Deformation effects Surface roughness [46]
	Multi-recess	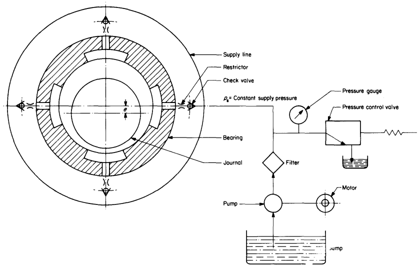 Supply line Restrictor Check valve Constant supply pressure Pressure gauge Pressure control valve Bearing Journal Filter Motor Pump Sump	Journal bearing Number of recess Shape variations Tilt compensation [22]

	Keywords	Result	Research Topics
Hydrostatic bearings	Geometric Imperfections	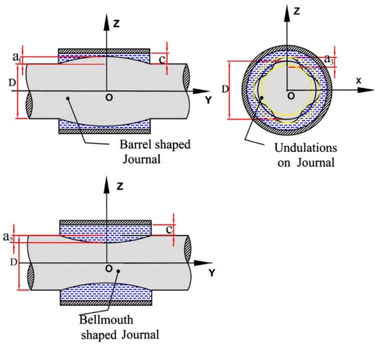 z a₁ c D O Y Barrel shaped Journal z D a₃ x O Undulations on Journal z a₂ c D O Y Bellmouth shaped Journal	Hybrid journal bearings Performance comparison [58]
	Cryogenic Turbo-pump	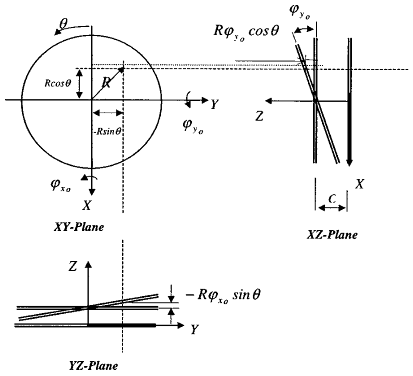 θ Rcosθ R Y -Rsinθ φ_{y_o} φ_{x_o} X XY-Plane $R\varphi_{y_o}\cos\theta$ φ_{y_o} Z X C XZ-Plane Z $-R\varphi_{x_o}\sin\theta$ Y YZ-Plane	Hybrid thrust bearing Effects of Misalignment [56]
	Hydraulic pumps	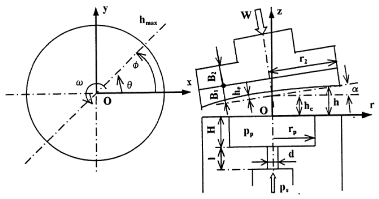 y h_{max} φ θ ω O x W z r_2 B_2 B_1 h_0 O h_c h α r H p_p r_p d p_s	Disk thrust bearing Concentric support Compressible bearing [67]
	Multi-recess	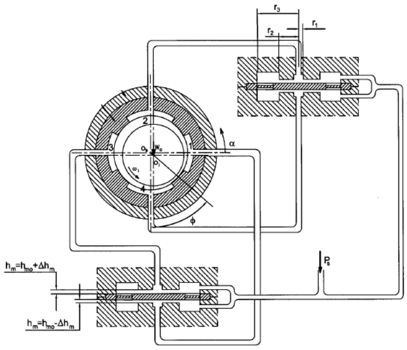 r_3 r_2 r_1 α φ p_s $h_m=h_{mo}+\Delta h_m$ $h_m=h_{mo}-\Delta h_m$	Journal bearing Membrane compensated Shape variations Hybrid journal bearing [59]

	Keywords	Result	Research Topics
Compliant	Foil support	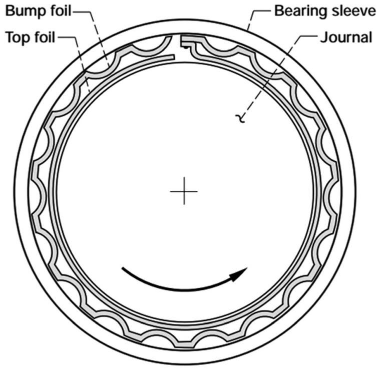	Gas foil overview Journal bump-type bearing [14]
	Hybrid bearing	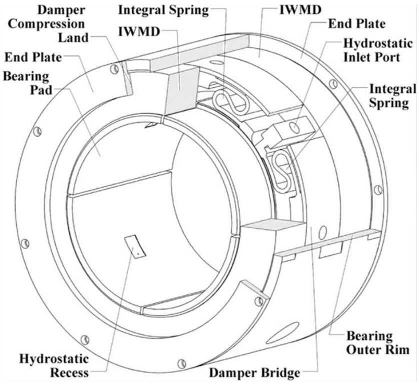 Damper Compression Land Integral Spring IWMD IWMD End Plate Hydrostatic Inlet Port End Plate Bearing Pad Integral Spring Hydrostatic Recess Damper Bridge Bearing Outer Rim	Hybrid bearing Journal bearing Partitioned bearing-pads Multi-recess [20]
	Thrust bearing	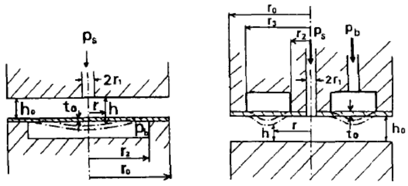 ps 2r1 h0 t0 r h pb r2 r0 r0 r2 r2 ps pb 2r1 h r t0 h0	Comparison Gas lubrication Compliant Surfaces [28]
	Thrust bearing	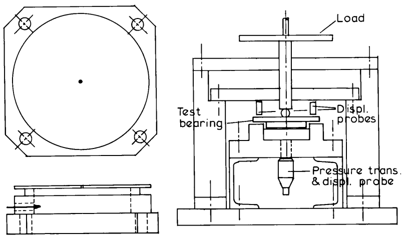 Load Test bearing Displ. probes Pressure trans. & displ. probe	Aerostatic bearing Compliant Surfaces Concave flexible diaphragm [13]

	Keywords	Result	Research Topics
Compliant	Foil support	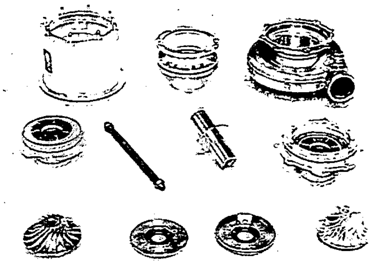	Gas foil overview [9]
	Hybrid bearing	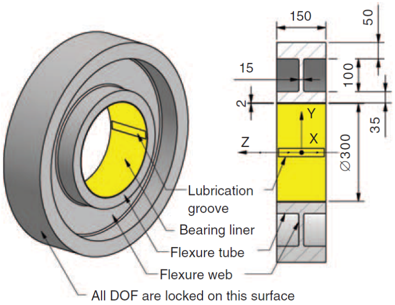 150 50 15 100 2 Y Z X 35 ∅300 Lubrication groove Bearing liner Flexure tube Flexure web All DOF are locked on this surface	Journal Bearings Flexture Misalignment Multi-recess [64]
	Thrust bearing	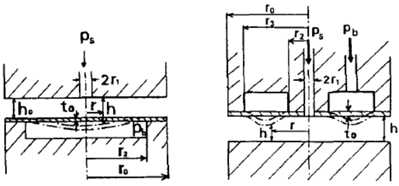 p_s $2r_1$ h_0 t_0 r h p_b r_2 r_0	Comparison Gas lubrication Compliant Surfaces [28]
	Thrust bearing	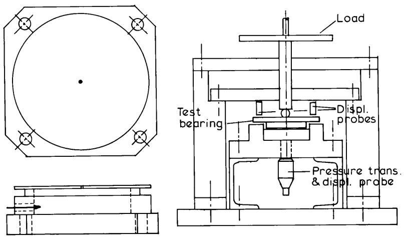 Load Test bearing Displ. probes Pressure trans. & displ. probe	Aerostatic bearing Compliant Surfaces Concave flexible diaphragm [13]

	Keywords	Result	Research Topics
Tilting pad	Flexure	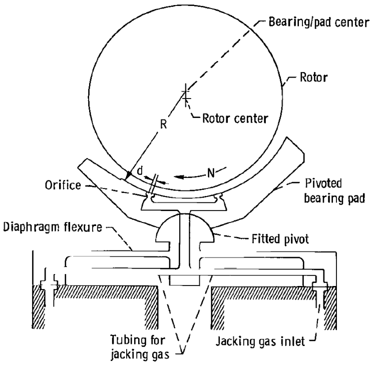 Bearing/pad center Rotor Rotor center R d N Orifice Pivoted bearing pad Diaphragm flexure Fitted pivot Tubing for jacking gas Jacking gas inlet	Pivoted pad Journal bearing diaphragm flexure [42]
	Self-compensation	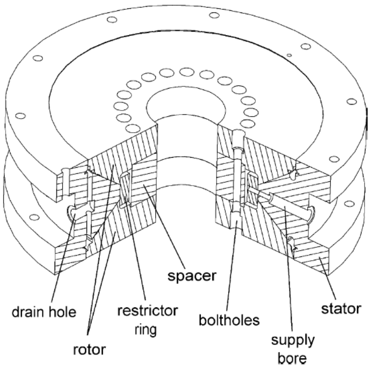 spacer drain hole restrictor ring boltholes stator rotor supply bore	Rotary bearing Complex fluid restrictor [34]
	Spring supported	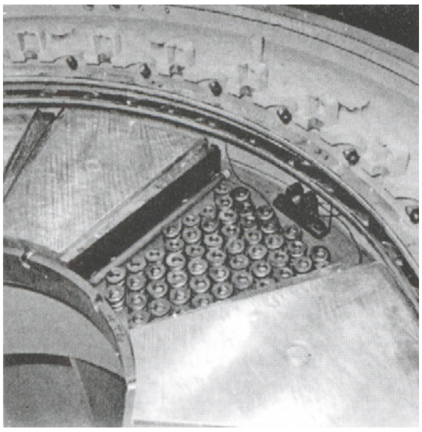	Thrust bearing Large pad [24]
	Pivot	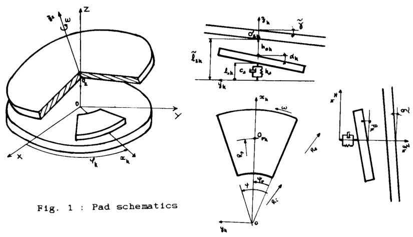 Fig. 1 : Pad schematics	Dynamic analysis Thrust pad bearing [43]

Keywords		Result	Research Topics
Multi-recess	Effect of number and size	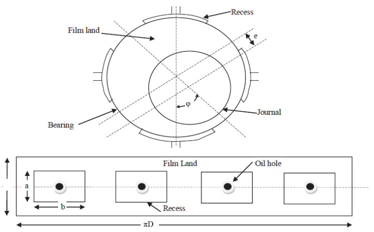 Recess Film land e φ Bearing Journal Film Land Oil hole a b Recess πD	Hybrid journal bearing Eccentricity Geometric comparison [19]
	Hole-entry Configurations	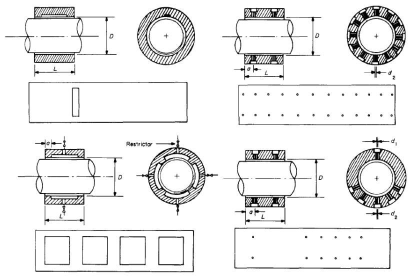	Hybrid bearing Journal bearing Computational analysis [53]
	Load-capacity	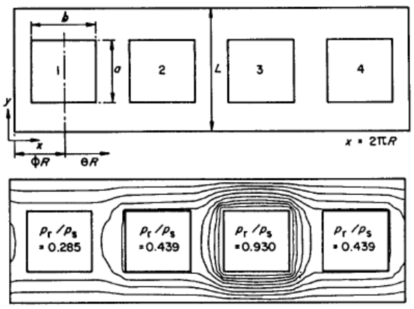 b a 1 2 L 3 4 y x ΦR θR x = 2πR Pr /Ps = 0.285 Pr /Ps =0.439 Pr /Ps =0.930 Pr /Ps = 0.439	Eccentricity Journal bearings [39]
	Geometric shape	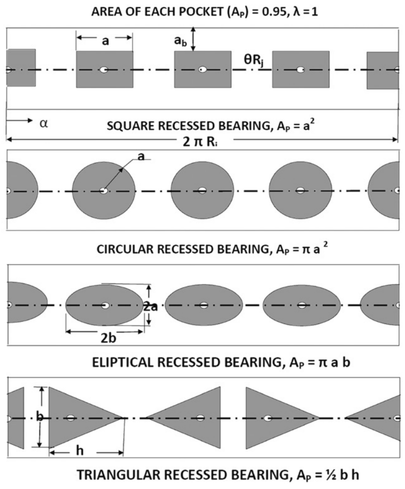 AREA OF EACH POCKET (Aₚ) = 0.95, λ = 1 a a_b θRⱼ α SQUARE RECESSED BEARING, Aₚ = a² 2 π Rⱼ a CIRCULAR RECESSED BEARING, Aₚ = π a² 2a 2b ELIPTICAL RECESSED BEARING, Aₚ = π a b b h TRIANGULAR RECESSED BEARING, Aₚ = ½ b h	Recess shape variations Hydrodynamic journal bearing [57]

	Keywords	Result	Research Topics
Fluid bearings	Aerostatic	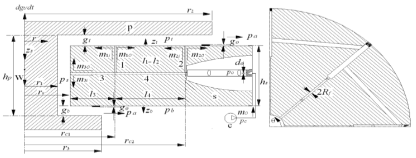	High load capacity Double pad [41]
	Elastic deformation Configurations	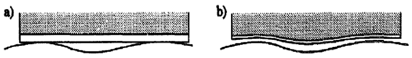	Rubber support thrust bearing Infinite length Computational analysis [12]
	Elastic support	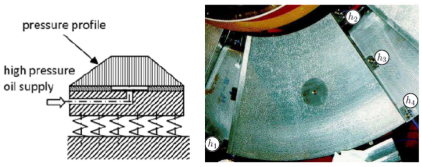 pressure profile high pressure oil supply h_1 h_2 h_3 h_4	Thermal-elastic deformation Hydrodynamic bearing [35]
	Spring supported	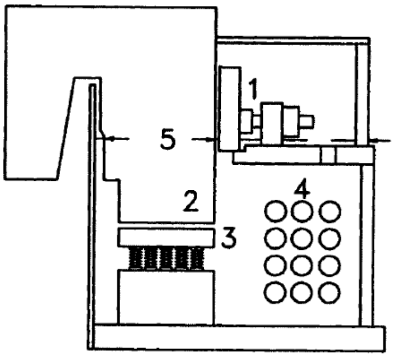 1 guide bearing 2 rotor 3 thrust pad 4 cooler 5 oil level	Thrust bearings Effects of Viscosity [21]

Table 2: A few support structures found

<table>
<tr><th></th><th>Keywords</th><th>Result</th><th>Research Topics</th></tr>
<tr><td>Support structures</td><td>Force balance</td><td>
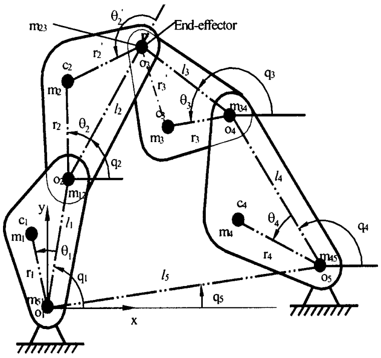

</td><td>Four bar linkage
Robotic mechanism
Real-time controllable
[48]</td></tr>
<tr><td></td><td>Rocker-bogie suspension</td><td>
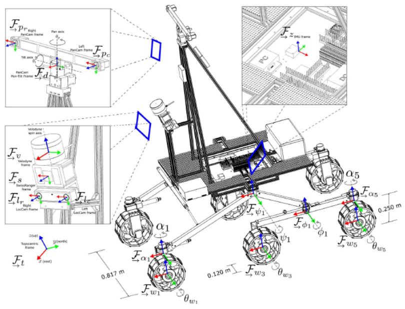

</td><td>Mars Rover
Experimental test set-up
[31]</td></tr>
<tr><td></td><td>Force balance</td><td>
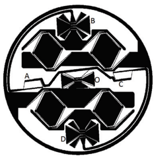

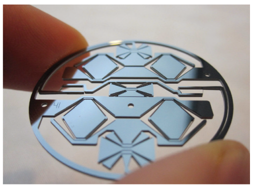
</td><td>Monolithic oscillator
[68]</td></tr>
<tr><td></td><td>Whiffle-Tree</td><td>
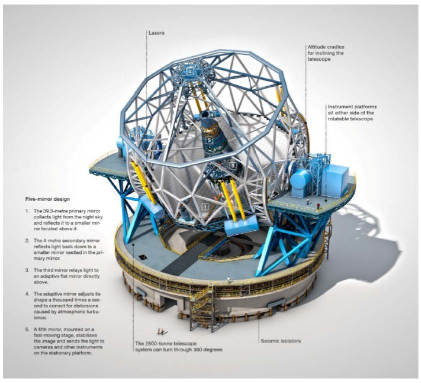

Lasers
Altitude cradles for inclining the telescope
Instrument platforms sit either side of the rotatable telescope
1
2
3
4
5
The 2800-tonne telescope system can turn through 360 degrees
Seismic isolators

Five-mirror design
1. The 39.3-metre primary mirror collects light from the night sky and reflects it to a smaller mirror located above it.
2. The 4-metre secondary mirror reflects light back down to a smaller mirror nestled in the primary mirror.
3. The third mirror relays light to an adaptive flat mirror directly above.
4. The adaptive mirror adjusts its shape a thousand times a second to correct for distorsions caused by atmospheric turbulence.
5. A fifth mirror, mounted on a fast-moving stage, stabilises the image and sends the light to cameras and other instruments on the stationary platform.
</td><td>Extremely large telescope
Mirror support
[4]</td></tr>
</table>

Table 3: Patents found on deforming hydrostatic bearings

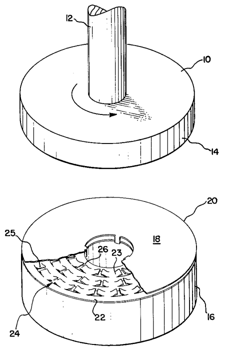	Compliant Hydrodynamic bearing [69]	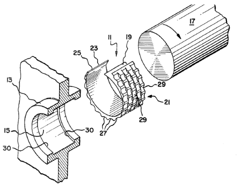	Compliant Hydrodynamic bearing [40]
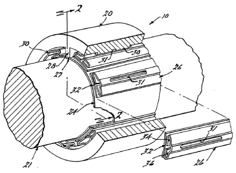	Compliant Hydrodynamic gas lubricated bearing [49]	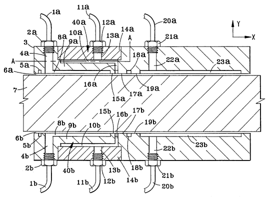	Elastic supported self compensating flow-restrictors [62]
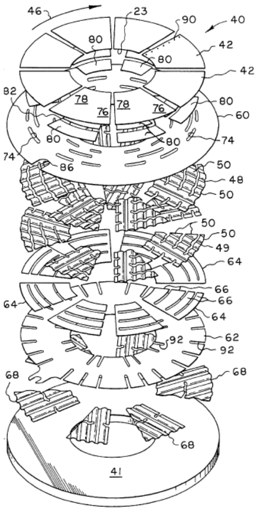	Compliant Foil Hydrodynamic Thrust Bearing [30]	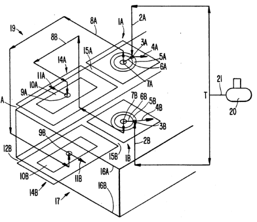	Self-Compensating Hydrostatic linear motion bearing [60]
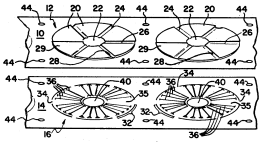	Compliant Foil Hydrodynamic Thrust Bearing [25]	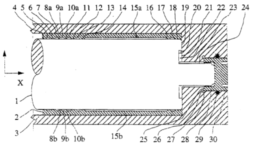	Low profile self-compensated hydrostatic thrust bearing [61]

Bibliography

[1] Comsol multiphysics® v. 5.2. www.comsol.com. comsol ab, stockholm, sweden.

[2] Matlab v. r2017a https://www.mathworks.com/products/matlab.html, mathworks, natick, massachusetts, united states.

[3] Engineering toolbox, (2011). steels - endurance limits and fatigue stress - accessed 19 april 2019. URL `https://www.engineeringtoolbox.com/steel-endurance-limit-d_1781.html`.

[4] The adaptive mirror for the E-ELT. *3rd AO4ELT Conference - Adaptive Optics for Extremely Large Telescopes*, (May), 2013. doi: 10.12839/AO4ELT3.13431.

[5] Hagglunds, 2019. URL `https://www.boschrexroth.com/en/us/products/product-groups/industrial-hydraulics/topics/motors/hagglunds-radial-piston-motors/index`.

[6] Hembrug, 2019. URL `https://www.hembrug.com/about-hembrug/history/`.

[7] Schaeffler, 2019. URL `https://www.schaeffler.de/content.schaeffler.de/en/products-and-solutions/industrial/x_life/index.jsp`.

[8] Zollern, 2019. URL `https://www.zollern.com/fileadmin/Upload_Konzernseite/Downloads/Brochueren/Antriebstechnik/ZOLLERN-Broschuere_Hydrostatik_ENG.pdf`.

[9] Gin L. Agrawal. Foil air/gas bearing technology - an overview. 1997. doi: 10.1115/97-GT-347.

[10] N.M.A.E. Ashour, K. Athre, Y. Nath, and S. Biswas. Distortion analysis of large thrust bearing on elastic support. *Wear*, 147(2):421–430, July 1991. doi: 10.1016/0043-1648(91)90196-2. URL `https://doi.org/10.1016/0043-1648(91)90196-2`.

[11] European Wind Energy Association. Pure power wind energy scenarios up to 2030. 2015. URL `http://www.ewea.org/fileadmin/ewea_documents/documents/00_POLICY_document/PP.pdf`.

[12] Antoon Van Beek and Lubor Lepic. Rubber supported hydrostatic thrust bearings with elastic bearing surfaces of infinite length. 201:45–50, 1996.

[13] D. A. Boffey and G. M. Alder. Paper XVII(iii) An experimental investigation of the steady-state performance of a compliant surface aerostatic thrust bearing. *Tribology Series*, 11(C):533–538, 1987. ISSN 01678922. doi: 10.1016/S0167-8922(08)70986-6.

[14] Michael Branagan, David Griffin, Christopher Goyne, and Alexandrina Untaroiu. Compliant Gas Foil Bearings and Analysis Tools. *Journal of Engineering for Gas Turbines and Power*, 138(5):054001, 2015. ISSN 0742-4795. doi: 10.1115/1.4031628. URL `http://gasturbinespower.asmedigitalcollection.asme.org/article.aspx?doi=10.1115/1.4031628`.

[15] C J Butler. The 15-inch Equatorial Reflector by Thomas Grubb at Armagh Observatory. 129, 2016.

[16] Dara Childs and Keith Hale. A test apparatus and facility to identify the rotordynamic coefficients of high-speed hydrostatic bearings. *Journal of Tribology*, 116(2):337, 1994. doi: 10.1115/1.2927226. URL `https://doi.org/10.1115/1.2927226`.

[17] Neils Frederik Boudewijn Diepeveen. Seawater-Based Hydraulics for Offshore Wind Turbines. *We-At-Sea.Org*, 2004. URL `http://www.we-at-sea.org/leden/docs/reports/RL1-42004-012CDelftOffshoreTurbine.pdf`.

[18] Niels Diepeveen. Design considerations for a wind-powered seawater pump. 06 2019. URL `https://www.researchgate.net/publication/266884842_Design_Considerations_for_a_Wind-Powered_Seawater_Pump`.

[19] Vijay Kumar Dwivedi, Satish Chand, and K.N. Pandey. Effect of number and size of recess on the performance of hybrid (hydrostatic/hydrodynamic) journal bearing. *Procedia Engineering*, 51:810–817, 2013. doi: 10.1016/j.proeng.2013.01.116.

[20] Bugra H. Ertas. Compliant hybrid journal bearings using integral wire mesh dampers. *Journal of Engineering for Gas Turbines and Power*, 131(2):022503, 2009. doi: 10.1115/1.2967476. URL https://doi.org/10.1115/1.2967476.

[21] J H Ferguson, J H Yuan, and J B Medley. *Spring-Supported Thrust Bearings For Hydroelectric Generators: Influence of Oil Viscosity on Power Loss*, volume 34. Elsevier Masson SAS, 1998. doi: 10.1016/S0167-8922(98)80073-4. URL http://dx.doi.org/10.1016/S0167-8922(98)80073-4.

[22] M. K. Ghosh and B. C. Majumdar. Design of multirecess hydrostatic oil journal bearings. *Tribology International*, 13(2):73–78, 1980. ISSN 0301679X. doi: 10.1016/0301-679X(80)90017-1.

[23] Louis-Dominique Girard. *Hydraulique appliquée. Nouveau système de locomotion sur les chemins de fer.* 1852. URL https://books.google.nl/books?id=4CtWAAAAcAAJ.

[24] S.B. Glavatskih. Tilting pad thrust bearings. In *Tribology Series*, pages 379–390. Elsevier, 2003. doi: 10.1016/s0167-8922(03)80151-7. URL https://doi.org/10.1016/s0167-8922(03)80151-7.

[25] Stanley Gray. Hydrodynamic compliant thrust bearing and method of making, 1978.

[26] Bernard J Hamrock, Steven R Schmid, and Bo O Jacobson. *Fundamentals of fluid film lubrication.* CRC press, 2004.

[27] J. A. Haringx. The cross-spring pivot as a constructional element. *Flow, Turbulence and Combustion*, 1(1), December 1949. doi: 10.1007/bf02120338. URL https://doi.org/10.1007/bf02120338.

[28] K. Hayashi and K. Hirasata. Paper XVII(ii) comparison of theoretical characteristics of two types of externally pressurized, gas lubricated, compliant surface thrust bearings. In *Tribology Series*, pages 525–532. Elsevier, 1987. doi: 10.1016/s0167-8922(08)70985-4. URL https://doi.org/10.1016/s0167-8922(08)70985-4.

[29] Niels Heinrichson. On the design of tilting-pad thrust bearings. 2007. URL https://findit.dtu.dk/en/catalog/2389469376.

[30] Hooshang Heshmat. High load capacity compliant foil hydrodynamic thrust bearing, 1997.

[31] Robert A Hewitt, Evangelos Boukas, Martin Azkarate, Marco Pagnamenta, Joshua A Marshall, Antonios Gasteratos, and Gianfranco Visentin. The katwijk beach planetary rover dataset. *The International Journal of Robotics Research*, 37(1):3–12, dec 2017. doi: 10.1177/0278364917737153.

[32] Larry L. Howell, Spencer P. Magleby, and Brian M. Olsen, editors. *Handbook of Compliant Mechanisms.* John Wiley & Sons Ltd, February 2013. doi: 10.1002/9781118516485. URL https://doi.org/10.1002/9781118516485.

[33] H. Iliev. Failure analysis of hydro-generator thrust bearing. *Wear*, 225-229:913–917, April 1999. doi: 10.1016/s0043-1648(98)00410-4. URL https://doi.org/10.1016/s0043-1648(98)00410-4.

[34] N. R. Kane, J. Sihler, and A. H. Slocum. A hydrostatic rotary bearing with angled surface self-compensation. *Precision Engineering*, 27(2):125–139, 2003. ISSN 01416359. doi: 10.1016/S0141-6359(02)00194-0.

[35] Zhai Liming, Luo Yongyao, Wang Zhengwei, Liu Xin, and Xiao Yexiang. A review on the large tilting pad thrust bearings in the hydropower units. *Renewable and Sustainable Energy Reviews*, 69:1182–1198, March 2017. doi: 10.1016/j.rser.2016.09.140. URL https://doi.org/10.1016/j.rser.2016.09.140.

[36] Zhifeng Liu, Yumo Wang, Ligang Cai, Yongsheng Zhao, Qiang Cheng, and Xiangmin Dong. A review of hydrostatic bearing system: Researches and applications. *Advances in Mechanical Engineering*, 9(10): 168781401773053, October 2017. doi: 10.1177/1687814017730536. URL https://doi.org/10.1177/1687814017730536.

[37] Nicolae Lobontiu. *Compliant Mechanisms.* CRC Press, December 2002. doi: 10.1201/9781420040272. URL https://doi.org/10.1201/9781420040272.

[38] D. Farhadi Machekposhti, N. Tolou, and J. L. Herder. A review on compliant joints and rigid-body constant velocity universal joints toward the design of compliant homokinetic couplings. *Journal of Mechanical Design*, 137(3):032301, jan 2015. doi: 10.1115/1.4029318. URL https://doi.org/10.1115/1.4029318.

[39] K. J. Metman, E. A. Muijderman, G. J J van Heijningen, and D. M. Halemane. Load capacity of multi-recess hydrostatic journal bearings at high eccentricities. *Tribology International*, 19(1):29–34, 1986. ISSN 0301679X. doi: 10.1016/0301-679X(86)90092-7.

[40] William H. Miller. Compliant and hydrodynamic fluid and bearing with and reslient support, 1975.

[41] Nripen Mondal, Rana Saha, and Dipankar Sanyal. Modeling and performance analysis of aerostatic bearings for lifting heavy payload. *Procedia Engineering*, 90:123–128, 2014. ISSN 18777058. doi: 10.1016/j.proeng.2014.11.824. URL `http://dx.doi.org/10.1016/j.proeng.2014.11.824`.

[42] Zolton N Nemeth and Wizziam J Anderson. NASA TECHNICAL NOTE DYNAMIC BEHAVIOR OF AIR LUBRICATED PIVOTED-PAD I - Effects of Mount Stiffness and Damping. 2018.

[43] A. Benali; A. Bonifacie; D. Nicolas. Dynamic analysis of tilting pad thrust bearings.

[44] Joep Nijssen and Ron van Ostayen. Open form pressure balancing for compliant hydrostatic thrust bearings. In *Advances in Mechanism and Machine Science*, pages 3965–3974. Springer International Publishing, 2019. doi: 10.1007/978-3-030-20131-9_395. URL `https://doi.org/10.1007/978-3-030-20131-9_395`.

[45] Joep Nijssen, Niels Diepeveen, and Anton Kempenaar. Development of an interface between a plunger and an eccentric running track for a low-speed seawater pump. 06 2018. URL `https://www.researchgate.net/publication/325995634_Development_of_an_interface_between_a_plunger_and_an_eccentric_running_track_for_a_low-speed_seawater_pump`.

[46] Ron Van Ostayen. *The Hydro–Support: An Elasto–Hydrostatic Thrust Bearing with Mixed Lubrication.* 2002.

[47] F Osterle and E Saibel. The spring supported thrust bearing. *Trans ASME*, 79:351–359, 1957.

[48] P. R. Ouyang and W. J. Zhang. Force Balancing of Robotic Mechanisms Based on Adjustment of Kinematic Parameters. *Journal of Mechanical Design*, 127(3):433, 2005. ISSN 10500472. doi: 10.1115/1.1864116. URL `http://mechanicaldesign.asmedigitalcollection.asme.org/article.aspx?articleid=1448482`.

[49] Guisuppe Paletta; Angelo D. Paletta;. Compliant hydrodynamic gas lubricated bearing, 1987.

[50] Eric Ponslet, Dan Blanco, Myung Cho, Terry Mast, Jerry Nelson, R J. Ponchione, Mark Sirota, Vince Stephens, Larry Stepp, Alan Tubb, and Eric. C. Williams. Development of the primary mirror segment support assemblies for the thirty meter telescope - art. no. 627319. proc spie. 6273. 2006. doi: 10.1117/12.670604. URL `https://doi.org/10.1117/12.670604`.

[51] Enbing Qi, Zhenyong Fang, Tao Sun, Jianchao Chen, Changzai Liu, and Jian Wang. A method for predicting hydrostatic guide error averaging effects based on three-dimensional profile error. *Tribology International*, 95: 279–289, March 2016. doi: 10.1016/j.triboint.2015.11.032. URL `https://doi.org/10.1016/j.triboint.2015.11.032`.

[52] J. M. Reddecliff and J. H. Vohr. Hydrostatic bearings for cryogenic rocket engine turbopumps. *Journal of Lubrication Technology*, 91(3):557, 1969. doi: 10.1115/1.3554989. URL `https://doi.org/10.1115/1.3554989`.

[53] W B Rowe, S X Xu, F S Chong, and W Weston. Hybrid journal bearings. *Tribology International*, 15(6):339–348, 1982.

[54] W. Brian Rowe. Grinding machine developments. In *Principles of Modern Grinding Technology*, pages 163–210. Elsevier, 2009. doi: 10.1016/b978-0-8155-2018-4.50016-1. URL `https://doi.org/10.1016/b978-0-8155-2018-4.50016-1`.

[55] W. Brian Rowe. *Hydrostatic, Aerostatic and Hybrid Bearing Design.* Butterworth-Heinemann, 2012. ISBN 978-0-12-396994-1. doi: 10.1016/c2011-0-07331-3. URL `https://doi.org/10.1016/c2011-0-07331-3`.

[56] Luis San Andres. Effects of Misalignment on Turbulent Flow Hybrid Thrust Bearings. *Journal of Tribology*, 124 (1):212, 2002. ISSN 07424787. doi: 10.1115/1.1400997. URL `http://tribology.asmedigitalcollection.asme.org/article.aspx?articleid=1466608`.

[57] E. Rajasekhar Nicodemus; Satish C. Sharma. Orifice compensated multirecess hydrostatic/hybridjournal bearing system of various geometric shapes of recess operating with micro polar lubricant. 2011. doi: 10.1.

[58] Satish C. Sharma and Arvind K. Rajput. Effect of geometric imperfections of journal on the performance of micropolar lubricated 4-pocket hybrid journal bearing. *Tribology International*, 60:156–168, 2013. ISSN 0301679X. doi: 10.1016/j.triboint.2012.10.017. URL `http://dx.doi.org/10.1016/j.triboint.2012.10.017`.

[59] Narendra Singh, Satish C. Sharma, S. C. Jain, and S. Sanjeeva Reddy. Performance of membrane compensated multirecess hydrostatic/hybrid flexible journal bearing system considering various recess shapes. *Tribology International*, 37(1):11–24, 2004. ISSN 0301679X. doi: 10.1016/S0301-679X(03)00110-5.

[60] Alexander H. Slocum. Self-compensating hydrostatic linear motion bearing, 1992.

[61] Alexander H. Slocum. Low profile self-compensated hydrostatic thrust bearing, 1996.

[62] Nathan R. Kane; Alexander H. Slocum. Elastically supported self-compensating flow restritor, 1994.

[63] Stuart T. Smith. *Flexures*. CRC Press, apr 2014. doi: 10.1201/9781482282962. URL `https://doi.org/10.1201/9781482282962`.

[64] Kim Thomsen and Peder Klit. Improvement of journal bearing operation at heavy misalignment using bearing flexibility and compliant liners. *Proceedings of the Institution of Mechanical Engineers, Part J: Journal of Engineering Tribology*, 226(8):651–660, 2012. ISSN 13506501. doi: 10.1177/1350650112439372.

[65] Antoon van Beek and Lubor Lepic. Rubber supported hydrostatic thrust bearings with elastic bearing surfaces of infinite length. *Wear*, 201(1-2):45–50, dec 1996. doi: 10.1016/s0043-1648(96)06987-6. URL `https://doi.org/10.1016/s0043-1648(96)06987-6`.

[66] Ron A.J. van Ostayen, Anton van Beek, and Mink Ros. A mathematical model of the hydro-support: an elasto-hydrostatic thrust bearing with mixed lubrication. *Tribology International*, 37(8):607–616, aug 2004. doi: 10.1016/j.triboint.2004.01.008. URL `https://doi.org/10.1016/j.triboint.2004.01.008`.

[67] X. Wang and A. Yamaguchi. Characteristics of hydrostatic bearing/seal parts for water hydraulic pumps and motors. Part 1: Experiment and theory. *Tribology International*, 35(7):425–433, 2002. ISSN 0301679X. doi: 10.1016/S0301-679X(02)00023-3.

[68] Sybren L. Weeke, Nima Tolou, Guy Semon, and Just L. Herder. A Monolithic Force-Balanced Oscillator. *Journal of Mechanisms and Robotics*, 9(2):021004, 2017. ISSN 1942-4302. doi: 10.1115/1.4035544. URL `http://mechanismsrobotics.asmedigitalcollection.asme.org/article.aspx?doi=10.1115/1.4035544`.

[69] Donald F. Wilcock. Compliant gas thrust bearing with profiled and a pertured thrust runner, 1978.